SMC Bulletin

A Publication of the Society for Materials Chemistry

Volume 3 No. 3 December 2012

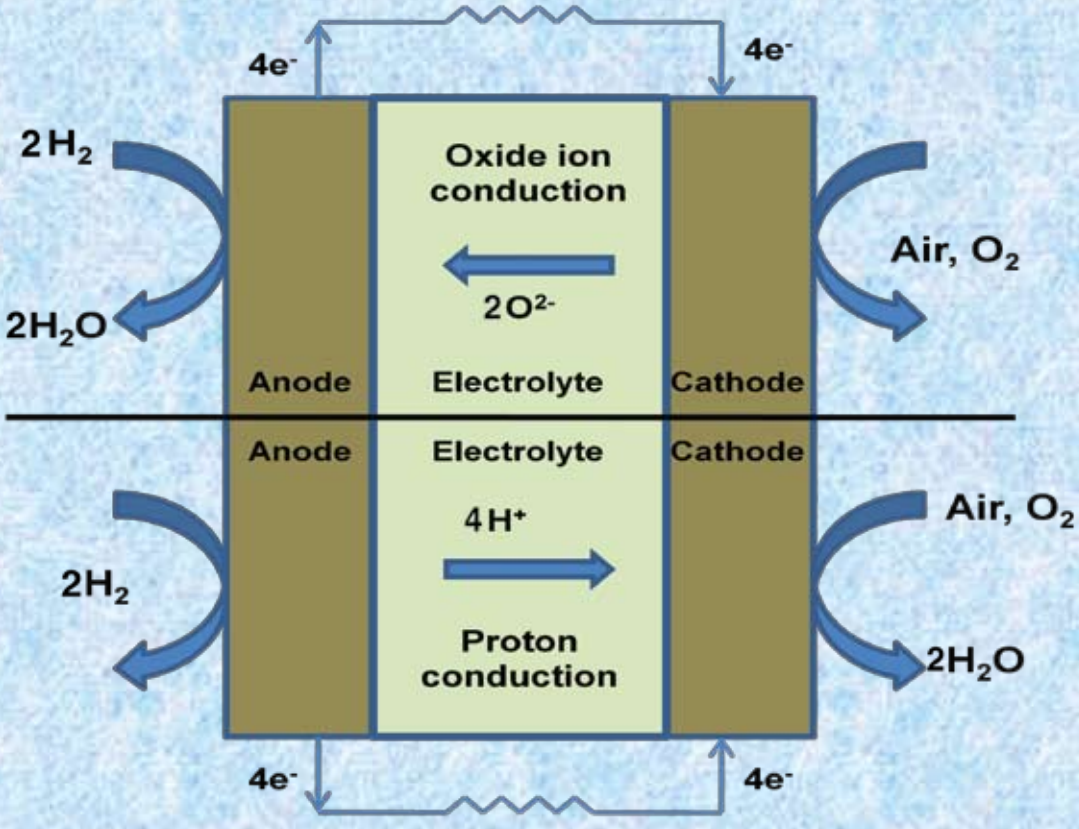

SOCIETY FOR MATERIALS CHEMISTRY

Society for Materials Chemistry

Society for Materials Chemistry was mooted in 2007 with following aims and objectives:

(a) to help the advancement, dissemination and application of the knowledge in the field of materials chemistry,

(b) to promote active interaction among all material scientists, bodies, institutions and industries interested in achieving the advancement, dissemination and application of the knowledge of materials chemistry,

(c) to disseminate information in the field of materials chemistry by publication of bulletins, reports, newsletters, journals.

(d) to provide a common platform to young researchers and active scientists by arranging seminars, lectures, workshops, conferences on current research topics in the area of materials chemistry,

(e) to provide financial and other assistance to needy deserving researchers for participation to present their work in symposia, conference, etc.

(f) to provide an incentive by way of cash awards to researchers for best thesis, best paper published in journal/national/international conferences for the advancement of materials chemistry,

(g) to undertake and execute all other acts as mentioned in the constitution of SMC.

Executive Committee

Contact address
Society for Materials Chemistry
C/o Chemistry Division
Bhabha Atomic Research Centre, Trombay, Mumbai, 400 085, India
Tel: +91-22-25592001, E-mail: socmatchem@gmail.com

SMC Bulletin

A Publication of the Society for Materials Chemistry

Volume 3 **No. 3** **December 2012**

SOCIETY FOR MATERIALS CHEMISTRY

SMC Bulletin

Vol. 3, **No. 3** **December 2012**

Guest Editors

Dr. B.N. Wani
Chemistry Division
Bhabha Atomic Research Centre
Trombay, Mumbai, 400 085
e-mail: bnwani@barc.gov.in

Dr. Shyamala Bharadwaj
Chemistry Division
Bhabha Atomic Research Centre
Trombay, Mumbai, 400 085
e-mail: shyamala@barc.gov.in

Editorial Board

Published by
Society for Materials Chemistry
C/o. Chemistry Division
Bhabha Atomic Research Centre, Trombay, Mumbai, 400 085
E-mail: socmatchem@gmail.com,
Tel: +91-22-25592001

Front cover shows a schematic diagram displaying the operation of oxide ion conducting and proton conducting SOFCs

Guest Editorial

Bina Wani

Shyamala Bharadwaj

Heavy dependence on fossil fuels as our major source of energy has caused serious energy crisis in the world. Combustion of fossil fuels for power generation poses unresolved impact on the climate. In order to mitigate these two problems, there is urgent need to explore and utilize clean and renewable energy sources. In response to the escalating energy crisis and related pollution problems, new technologies that utilize renewable energy sources in an efficient and environmentally friendly manner are the need of the hour. Fuel cell has been identified as one of the most promising technologies for the future clean energy industry. It converts the energy chemically stored in a fuel, such as hydrogen, into an electrical energy output by electrochemical reactions. The fuel cell operation is efficient, clean, and silent. Fuel cell can be applied to large-scale stationary systems for distributed power generation as well as small-scale portable power supply devices for micro-electronic equipment and auxiliary power units in vehicles.

Out of the five major fuel cell types, alkaline fuel cell (AFC), molten carbonate fuel cell (MCFC), phosphoric acid fuel cell (PCFC), polymer electrolyte fuel cell (PEMFC) and solid oxide fuel cell (SOFC), the last two are pursued more intensively worldwide for their respective potentials in transportation applications using hydrogen as fuel and stationary power generation using hydrogen, natural gas and hydrocarbon fuels with high fuel utilization efficiency (50 – 80 %). Continuous improvement in materials, cell design and manufacturing processing has resulted in high level of technical refinement in SOFCs. Successful commercialization of traditional SOFC technology, however, has been precluded by a number of factors including: high cost of cell materials; unreliable cell sealing; susceptibility of the cell to failure due to rapid thermal transients, mechanical shock, or oxidation of the anode; and, manufacturing issues associated with production of large, complex ceramic parts. SOFC in the reverse mode of operation results in solid oxide electrolysis cell (SOEC), which is a promising technology for hydrogen generation from water in large scale.

Fuel cell can also work with biomass for renewable electricity supply. Biomass is renewable, clean, carbon neutral, and widely available. Microbial fuel cells (MFCs) have gained a lot of attention in recent years as a mode of converting organic waste including low-strength wastewaters and lignocellulosic biomass into electricity. Microbial production of electricity may become an important form of bioenergy in future because MFCs offer the possibility of extracting electric current from a wide range of soluble or dissolved complex organic wastes and renewable biomass.

In this thematic issue of SMC Bulletin on "Fuel Cells", we have articles focusing on the various materials and micro structure aspects of fuel cell components such as electrodes, electrolytes etc. for SOFC/SOEC and direct methanol fuel cell (DMFC) applications. An article on biofuel cells has also been included as this type of fuel cell holds promise for future energy conversion from waste biomass.

We gratefully acknowledge the efforts of the authors who have contributed to this issue. We would also like to thank the editorial committee of SMC bulletin for inviting us to be guest editors for this theme based issue.

Editorial Note

We are happy to present the thematic issue of the SMC bulletin on "Fuel Cells Materials" where in the materials challenges faced by scientists working in the field of fuel cells have been highlighted. There are six research articles in this issue, two of them focussing on cathode materials for Solid Oxide Fuel Cells (SOFCs). The other articles deal with proton conducting SOFCs, spray pyrolysis as a processing method for obtaining thin films for ITSOFCs (intermediate temperature solid oxide fuel cells) and efficient anode catalysts for DMFCs (direct methanol fuel cells). There is an interesting article on biofuel cells that hold promise for future energy generation from biological wastes. We hope that this thematic issue will encourage our young members to take up the challenges for materials research for fuel cells and come up with environmental friendly energy conversion devices. The next issue of the bulletin is proposed to be on the following theme: 'Thorium based Nuclear Fuels'. Readers are encouraged to send their feedbacks so that we will enable us to improve the SMC bulletin.

Editors

From the President's Desk

Dear Fellow Members,

It gives me great pleasure to inform you that the Society for Materials Chemistry (SMC) has been quite successful in promoting interactions among material scientists both at national and international level through organization of various scientific events on a regular basis. Last year, we have successfully organised a National Workshop on Materials Chemistry: Functional Materials, NWMC-2011 (FUN-MAT) while this year we are looking forward towards a successful organization of the DAE-BRNS 4th Interdisciplinary Symposium on Materials Chemistry (ISMC-2012) during December 11-15, 2012. The response to ISMC-2012, a popular biennial event of our society, has been very impressive this year, both in terms of number and quality of abstracts received. It is quite reassuring to note that the participation from our members in this event has increased with time.

I am happy to know that the frequency of SMC bulletin brought out by the society has been increased to three per year. Please do send your feedback to improve it further. I also request all memberes to contribute towards the SMC bulletin which is publishing articles on various themes. I expect that the bulletin will continue to provide a platform to highlight the advances made in the field of materials chemistry and hope that the members will enrich it further with their contributions.

T. Mukherjee

CONTENTS

Processing of Lanthanum Strontium Manganite ($La_{0.85}Sr_{0.15}MnO_3$ – LSM) Cathode for SOFC studies

S. Ramanathan[a*], M. B. Kakade[a] and D.Das[b]

[a]- Glass & Advanced Ceramics Division; [b]- Chemistry Division
Bhabha Atomic Research Centre, Mumbai -400085
**-E-mail: srama@barc.gov.in*

Abstract

Ceramic processing of lanthanum strontium manganite ($La_{0.85}Sr_{0.15}MnO_3$ – LSM) cathode for SOFC application was studied. The conditions for preparation of powder by gel combustion technique using metal nitrates as oxidizer and citric acid as fuel were optimized through a detailed study using TG-DTA, FTIR and XRD. A study of the role of calcination treatment on the powder characteristics and sintering behaviour was studied and the results exhibited the need for incorporation of a pore former to obtain the required level of porosity (35 to 40%) in the sintered cathode. A study of the role of porosity on the thermal expansion coefficient, electrical conductivity and microstructure was carried out. Conditions for formation of sintered one end closed tubes (~2mm wall thickness & ~200 mm length) by slip casting and self standing thick films (0.2 to 0.8mm thick & ~50mm diameter) by tape casting were optimized.

Introduction

Solid oxide fuel cell (SOFC) is one of the most efficient and environmental-friendly technologies available for generating power from hydrogen, natural gas, and other renewable fuels and has been extensively reviewed [1-4]. Large-scale SOFC power generation systems have reached pilot-scale demonstration stages in the US, Europe, and in Japan while SOFC systems in small-scale are used for military, transportation and space applications.

SOFC technology is the most demanding from materials standpoint and is developed for its potential market competitiveness arising from efficiency, flexibility of fuel (hydrogen, natural gas, hydrocarbons, etc,); do not require costly noble metals, very low emission of exhaust gases etc. It uses a solid ceramic as the electrolyte and operates at high temperatures (800–1000^{0}C). This high operating temperature allows internal reforming, promotes rapid electro catalysis with non-precious metals, and produces high quality by product heat for co-generation. Efficiencies for this type of fuel cell can reach up to 70%.

The schematic of the unit cell and the electrode reactions are described in Fig.1. The cathode catalyses the reaction of conversion of oxygen to oxide ion at the point of contact of the triple junction boundary (i.e., cathode, electrolyte and gaseous oxygen) while the anode catalyses the reaction of oxide ion (that diffused through the impervious electrolyte film from cathode to anode side) with the fuel hydrogen at the triple junction boundary of electrolyte, anode and gaseous hydrogen.

a) Reaction at cathode: $\frac{1}{2}O_2 + 2e^- \rightarrow O^{2-}$

b) Reaction at anode: $H_2 + O^{2-} \rightarrow H_2O + 2e^-$ or $CO + O^{2-} \rightarrow CO_2 + 2e^-$

c) Net cell reaction: $H_2 + 1/2O_2 \rightarrow H_2O$, or $CO + \frac{1}{2} O_2 \rightarrow CO_2$

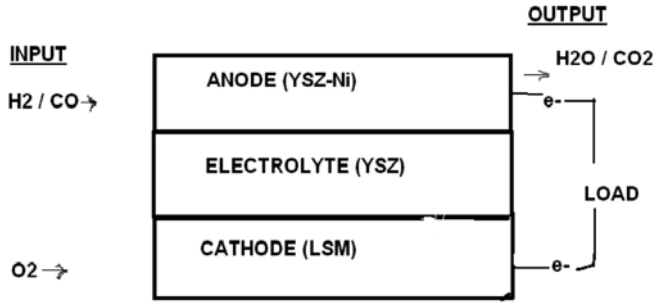

Fig.1. Schematic diagram of SOFC

The open circuit or reversible e.m.f. of the cell is given by the free energy change of the above redox reaction (E_{ocv} =ΔG/-2F) and is ~1V at 1000^{0}C. However, under load condition, the e.m.f. decreases to 0.7V while current density attains to the value of 800mA/cm^2. The cells are connected in series and parallel through interconnect and glass sealant to form the battery that yields the required voltage and power for applications. Among the various designs of SOFC studied world over, the tubular and planar type are the proven ones. The tubular design has the advantage of not requiring any sealant and it is easy to repair while the planner design is compact and has higher power density [5]. Among the various systems being explored world over, the proven systems are yttria stabilized zirconia (YSZ) as electrolyte, lanthanum strontium chromite ($LaSrCrO_3$)as interconnect and lanthanum boro-alumino-silicates

based glass as sealant, nickel-yttria stabilized zirconia (Ni-YSZ) as anode and lanthanum strontium manganite ($La_{0.85}Sr_{0.15}MnO_3$ – LSM) as cathode.

These materials need to have desired properties such as electrical conductivity, matching thermal expansion coefficient (~10-12 ppm/^{0}C) to avoid deterioration during thermal cycling, compatibility during processing and operating conditions. The electrodes (anode and cathode) should have sufficient porosity to allow the oxidant and fuel gases to easily diffuse in to the point of triple junction boundaries (electrode, electrolyte, gaseous fuel/oxidant) where the reaction occurs and also allow diffusing out of water vapour formed. They must have higher electronic conductivities to avoid polarisation which reduces the power output of the cell. Also they must be thermodynamically stable (i.e., compatible) in the environments with the electrolyte during co-processing and operating conditions of the cell.

In both tubular and planar designs, for the formation of single cell, the electrodes are used as mechanical supports for the electrolyte as the electrolyte needs to be much thinner due to its least oxide ion conductivity. Thus for single cell studies, the electrode (anode or cathode) is needed in the form of one end closed tubes or thick wafers. Tubes are processed through ceramic processes such as slip casting, cold isostatic pressing and extrusion. The self standing films are processed through tape casting technique [6-8]. Extensive investigations on lanthanum strontium manganite ($La_{0.85}Sr_{0.15}MnO_3$) cathode system have been carried out in our laboratory on aspects such as powder synthesis by gel combustion, phase evolution behaviour by TG-DTA, FTIR and XRD studies, role of powder calcination on its characteristics and sintering behaviour, formation of sintered porous bodies incorporating carbon pore former and their characterization (electrical conductivity, thermal expansion coefficient, microstructure), fabrication of tubes and self standing thick films by aqueous slurry based slip casting and tape casting [9-15]. A comprehensive review of all these aspects of work is presented in this paper.

Powder synthesis

There are various methods reported for the synthesis of powders such as solid state reaction, sol-gel, decomposition of mixed nitrates, co- precipitation, solution combustion etc. [16-26]. Formation of powders by solid-state reaction requires high temperature of the order of 1400^{0}C (for LSM) and long duration of heat treatment for compound formation. The solution based methods reported are environment friendly (such as co-precipitation and solution combustion). In the later processes, the product phase forms at a much lower temperature due to mixing of the reactants in molecular scale in solutions. In co-precipitation different metal ions are precipitated together resulting in compositional homogeneity or mixing in molecular level. However, due to solubility of hydroxides of strontium in ammonia solution, gel combustion technique is preferred for the synthesis of powders of LSM.

Gel combustion is a versatile technique in which the product phase is formed by the reaction between a fuel and an oxidizer accompanied by heat evolution. However, the exothermicity, fast reaction kinetics and evolution of large amount of gases make the reaction violent and pose problems in scaling up of the process. One way of exercising control over the reaction kinetics is by way of using the fuel for which the heat of combustion is sufficient but not excessively too high. The exothermicity of the reaction changes with the nature of the fuel and it decreases in the order urea > glycine > citric acid. The fuel need to be chosen such that the combustion reaction is not violent (i.e., smooth) so that it can yield product of larger batch size of compositionally homogeneous softer agglomerates of nano-crystalline powder. For LSM formation, the ideal fuel to be used was found to be citric acid.

Formation of metal oxide using metal nitrate – citric acid combustion reaction in general for a mono-valent metal can be written as [27]

$$18\ MNO_3 + 5\ C_6H_8O_7 \rightarrow 9\ M_2O + 30CO_2 + 9N_2 + 20\ H_2O \quad .....(1)$$

In particular for LSM formation, the reaction is

$$0.84La(NO_3)_3 + 0.16Sr(NO_3)_2 + Mn(NO_3)_2 + 1.28C_6H_8O_7 \rightarrow$$

$$La_{0.84}Sr_{0.16}MnO_3 + 7.68CO_2 + 2.42N_2 + 5.12H_2O \ldots\ldots\ldots\ldots\ldots\ldots(2)$$

Thus the stoichiometric molar ratio of (citric acid / nitrate ion) required is 0.28.

Phase evolution by TG-DTA, XRD and FTIR

The combustion temperature and calcination condition to form into chemically and phase pure powder from the gel is an important aspect for powder preparation and is obtained through a study of the thermal decomposition and phase evolution behavior by TG-DTA, XRD and FTIR. For these studies, the gel was prepared from the stock solutions by evaporation of the aqueous mixed nitrate solution containing the fuel (amount calculated as per equation 2) on a heater to form into a viscous gel followed by drying it into granules in a laboratory air oven at 80^{0}C.

The TG-DTA pattern of the oven-dried gel is shown in Figure.2. The DTA of gel exhibits a shallow endotherm accompanied by a weight loss of about 8% in the range of 25 to 195^{0}C attributing to the loss of absorbed moisture. A

sharp and intense exothermic peak accompanied by about 80% loss in weight was observed around 200°C which could be attributed to the exothermic combustion reaction (2). Even though there was no detectable heat effect after this temperature, a keen analysis of the TG plot exhibits about 1.5% loss in weight in the range of 200 to 700°C, which could be due to the decomposition of un-reacted material and intermediates left behind possibly due to the quickness of the combustion reaction. In our previous study, the precursor formed after combustion has been found to exhibit an equivalent amount of weight loss, which is in agreement with this observation. [10].This indicates that as formed crystalline LSM is not chemically pure and it requires to be calcined above 700°C.

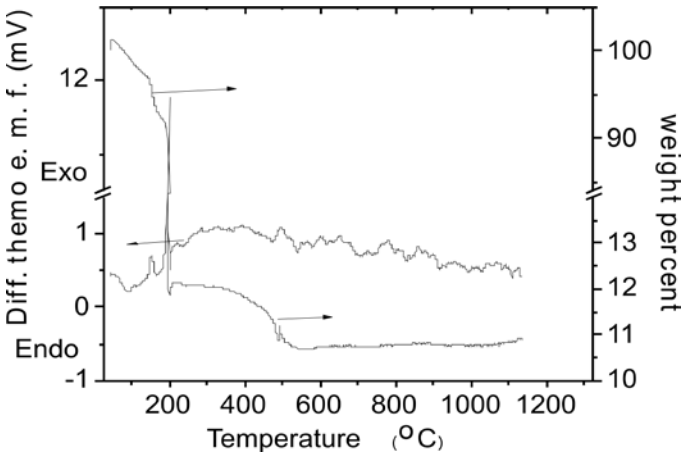

Fig.2. TG-DTA pattern for dried LSM-citric acid gel

Chemical and structural changes that take place during combustion of the gel can be monitored by FTIR spectra, which exhibit the presence of certain functional groups and metal – oxygen bonds. The FTIR spectra of the oven dried gel heated to different temperatures (as decided from the TG-DTA pattern) are shown in Fig.3a. The oven dried gel and that heated to 190° C exhibited absorption bands with peak positions at 1380 and 1614 cm^{-1} characteristic of carboxylate in citric acid and at 1442cm^{-1} characteristic of nitrate group.

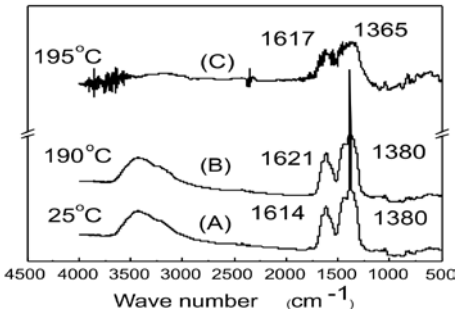

Fig.3a. FTIR spectra of gel heated to 25, 190 & 195°C

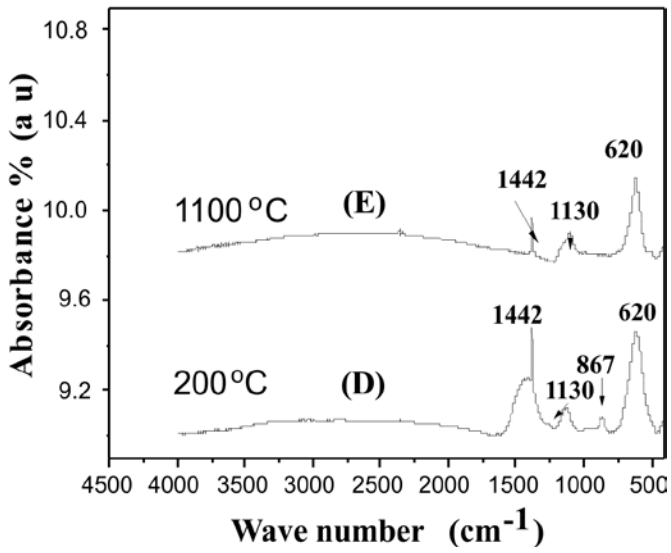

Fig. 3b. FTIR spectra of gel heated to 200 & 1100°C

The band in the range of 3200 to 3700cm^{-1} is due to the presence of absorbed moisture. The spectra of the gel heated to 195°C exhibit a drastic reduction in the intensity of the above mentioned bands. This indicates once combustion takes place, most of the carboxylate and nitrate are eliminated. An additional low intensity band around 620$cm.^{-1}$ was observed in this precursor which has been reported to be characteristic of a lattice mode of vibration of metal – oxygen bond in LSM [28]. Thus at this stage the combustion has set in with the loss of volatiles. The spectra of the gel heated to 200°C and that heated to 1100°C are shown in Fig. 3b. The gel heated to 200°C has exhibited an increase in the intensity of the band with a sharp peak around 620 cm^{-1} characteristic of crystallization of LSM and a major decrease in the intensity of the band around 1442 and 1382 cm^{-1} characteristic of reduced amount of citrate and nitrate due to combustion. Also there was a small intensity absorption band centered around 867 cm^{-1} which is characteristic of carbonate. Formation of carbonate as an intermediate in combustion process of citrates has been reported for many systems in general and for this system in particular [28]. The peaks corresponding to nitrate and citrate/carbonate further reduced drastically while that due to metal – oxygen bond remained essentially the same for the sample heated to 1100°C.

The XRD pattern of the gel, that heated to 190°C and 200°C are shown in Fig.4. The gel and that heated to 190°C are amorphous while that heated to 200° C are crystalline LSM compound (pc-pdf win no. #401100). However, the TG and FTIR data of the product after combustion exhibit it to be chemically impure and need to be calcined to a temperature above 700°C. Thus nitrate – citrate combustion reaction to form LSM takes place around 200°C.

The average crystallite size of the as-prepared precursor was 90 Å and it increased to 130 Å for 700° C calcined powder.

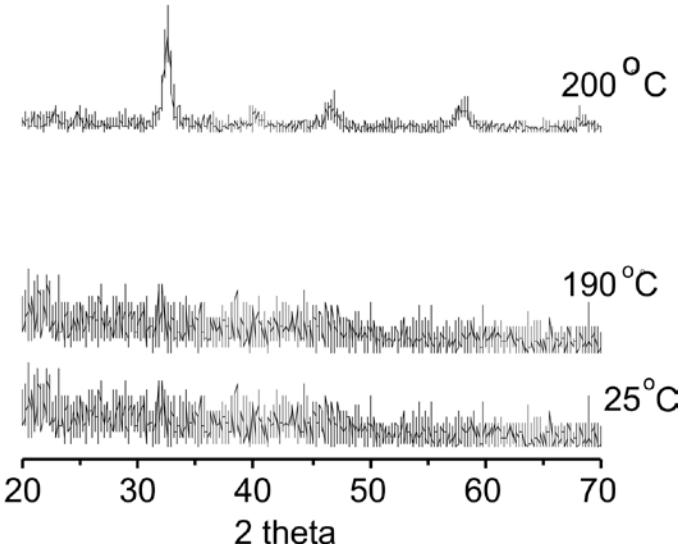

Fig.4. XRD pattern for the as formed gel that heated to 190 & 200°C

Thus the amorphous oven dried gel, upon heating, undergoes dehydration, combustion reaction and directly transforms into a single phase LSM powder with nano-sized crystallites (90Å). The weight loss occurred in three stages due to dehydration, combustion and elimination of a little amount of left behind nitrate – citrate complex. The FTIR analysis revealed the combustion product to contain some amount of nitrate, citrate and carbonate, which was eliminated during calcination at 700^{0}C thereby establishing it to be the minimum temperature required to form pure powder.

The combustion of the bulk of the gel (for a 250g batch size) was carried out on a laboratory heater using a stainless steel vessel by continuing heat treatment of the oven dried or viscous gel till smooth combustion occurs forming into a foam-like product mass. The progress of combustion reaction from oven dried gel as seen visually is shown in (Fig5). The precursor powder formed was crushed and heated to 700^{0}C to form into chemical and phase pure powder as obtained through this study.

Powder calcination treatment on its characteristics and sintering behaviour

Powder characteristics such as crystallite size, specific surface area, agglomerate size and green density decide the thermodynamics and kinetics of sintering. The results of such study really help to optimize calcination treatment. Larger crystallite size and lesser specific surface area contribute to poorer driving force for sintering. The variation of crystallite size with calcination temperature is shown in Fig. 6.

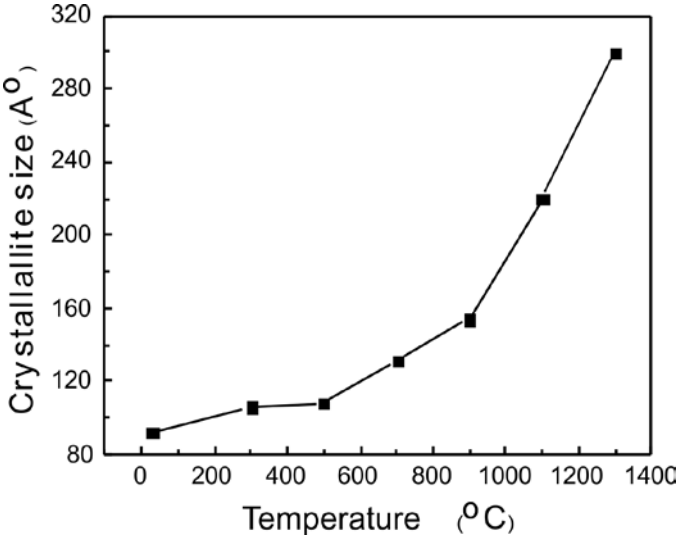

Fig.6. Variation of crystallite size of LSM powder with calcination temperature

The size increases from 9.0 nm for as formed product to 30 nm for 1300°C calcined powder. It is obvious that the kinetics of growth of crystallite is enhanced above 900^{0}C and such an observation has been reported for other systems also [29]. The specific surface area value decreased from 11.6 to 2.21m^2/g with increasing calcination temperature to 1300^{0}C. Thus the sinterability is expected to decrease with increasing calcination temperature,

Oven Dried Gel | Setting in of combustion | Completion of combustion

Fig.5. Sequential photograph for the process of combustion of nitrate-citrate dried gel of LSM

an aspect important for preparation of porous cathode bodies. The morphology of the as formed powder and that calcined at 1300^{0}C by SEM and TEM are shown in Fig.7a & 7b. The SEM morphologies exhibit the porous nature of the agglomerates of nano-particles that become compact upon calcination. The TEM data, in addition to bringing out the same features (Fig.7b –A & C), clearly indicated the improvement in crystallinity of the powder upon calcination as shown by the selected area diffraction patterns (Fig.7b.-B & D). Thus well crystallized dense particle forms after calcinations at 1300^{0}C.

De-agglomeration is an important aspect in obtaining quality products during ceramic processing as presence of agglomerates generate micro-structural heterogeneity in the green bodies which lead to poorer quality product. It is achieved by dry and wet grinding. Dry grinding is limited by the formation of cake along the wall of the pot in the mill while further de-agglomeration is achieved by wet grinding. The factors influencing the wet grinding of slurries is discussed in detail by Houivet etal [30].

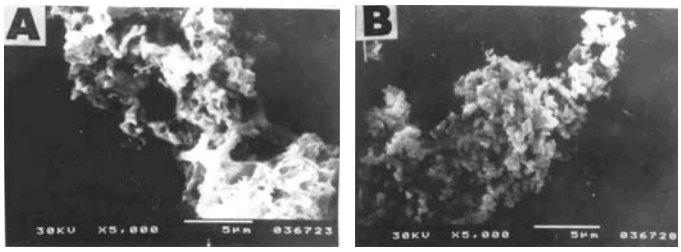

Fig.7a. SEM morphology of the typical agglomerate of LSM precursor (A) and that calcined at 1100°C (B)

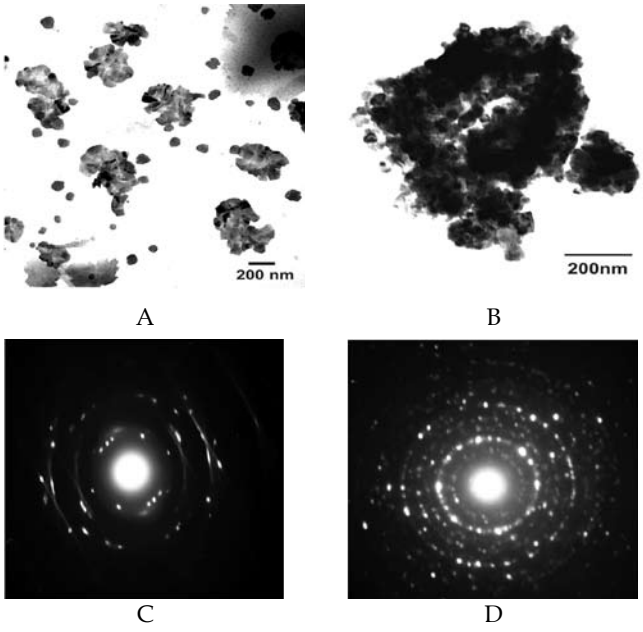

Fig.7b. Powder morphology by TEM of Ground LSM powders (A, B- as formed powder; C, D –1300°C calcined powder) (B, D- exhibits the improvement in crystallinity upon calcination)

Dispersion of the particle being ground and that formed during grinding is essential for effective wet grinding and is achieved by charging the surface of the particle in the slip. Zeta potential is the quantitative parameter that throws light on the extent of surface charge in the slip. It is maximum for the LSM slip in alkaline pH of 10 (Fig.8). It appears that in acidic range the surface chemistry of the LSM particle is such that there it is not much charging (maximum positive zeta potential is ~9mV). Thus dispersion of LSM powder in aqueous medium is elecrtostatically stabilized only in alkaline medium and the particles, as expected, are negatively charged. Hence the slip for grinding was formulated at this pH. For effective wet grinding the slip should exhibit near

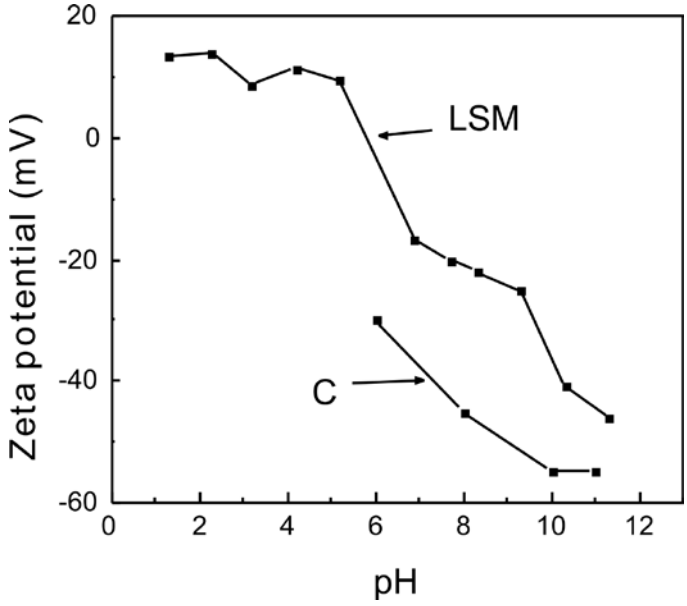

Fig.8. Zeta-potential variation for aqueous suspensions of LSM, carbon powders with pH

Newtonian flow behaviour under the milling conditions, indicate absence of any flocculates. Generally, the flow behaviour becomes Newtonian with decreasing solid content and hence a dilute slip (20wt% solid content) at a pH of 10 was used for wet grinding for an hour. The particle size distribution of the powder calcined upto 1300^{o}C followed by wet grinding for 1 hour are shown in Fig.9. The powders were found to possess almost same particle size with a D_{50} in the range of 3 to 5µm. This is expected to result in no change in sinterability. Thus the increase in crystallite size and no change in the particle size distribution during calcination is expected to reduce the sinterability.

An investigation of the role of compaction pressure on the quality of the compacts formed revealed that both the low calcined powder and the one containing carbon pore

former develop laminations above a compaction pressure of 60MPa.

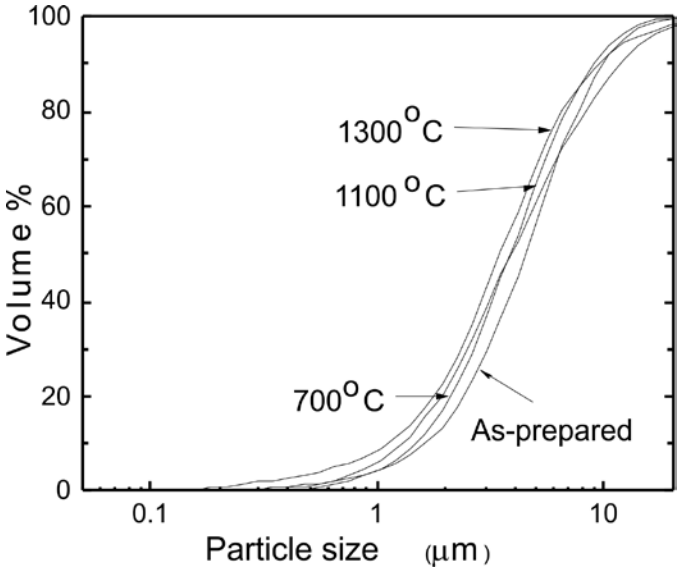

Fig.9a. Particle size distribution of LSM powder calcined at various temperatures (after wet grinding)

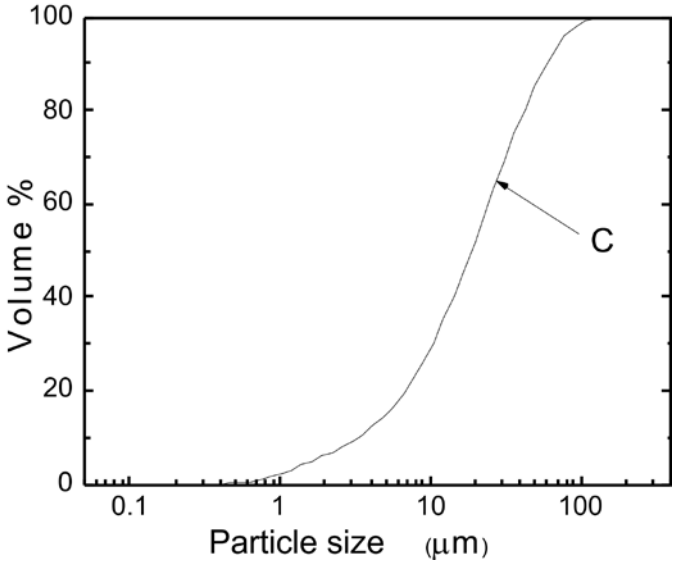

Fig.9b. Particle size distribution of carbon (pore former)

Hence pellets were formed at a pressure of 60 MPa for the study. The change in green density, sintered density, porosity, percentage of increase in density and linear shrinkage for compacts as a function of calcination temperature are given in Table.1. The sintering was done at 1400^{0}C for 5 minutes. The green density of the compacts increased with increasing calcination temperature from 38 to 52% T.D. This can be attributed to the increase in the particle density due to intera-agglomerate sintering of the particles upon calcination that leads to decrease in specific surface area.

Table.1. Variation of green density (G.D.), sintered density (S.D.), open porosity (O.P.), % increase in density (ΔD/D), % linear shrinkage (L.S.) for LSM powder prepared by gel combustion method and calcined at varying temperature (Tc)

S. No.	T_c (°C)	%G.D.	%S.D.	O.P.	%(ΔD/D)	% L.S.
1	25	38	80.5	19.5	42.0	26.5
2	700	42	81.5	18.5	39.5	22.0
3	1100	48	82	18.0	34.0	16.0
4	1300	52	78	22.0	25	12.0

Thus increase in green density is expected to result in higher sintered density. The resultant of contributions from crystallite size, surface area, particle size and green density decides the final sintered density and is an aspect difficult to be predicted but could be understood easily through experimental results. The sintered density of the compacts exhibited a marginal increase with increasing calcination temperature up to 1100^{0}C followed by a decrease even though the green density increased continuously. However, the percent increase in density and linear shrinkage decreased with increasing calcination temperature. This is an aspect worthy of importance in fabrication of larger shapes as better control over the dimensional precision can be exercised only if the shrinkage is lesser. Hence green body specimens required for further studies were formed using 1300^{0}C calcined powder. However upon soaking at1400^{0}C for 1 hour, densification to ~92% occurred and no further densification was observed for subsequent 6 hours of soak. Thus upon soaking the densification proceeded and the required porous structure (35% porous) could not be formed which necessitated the study on incorporation of a carbon fugitive in the green bodies.

Formation of sintered porous bodies and their characterization

As discussed in the introduction section, the LSM cathode material must possesses about 30 to 40% open porosity (pore size ~10 to 20micron) after sintering and the porous structure should be stable upon further soaking at 1400^{0}C. As the maximum porosity that could be obtained is only 8 %, further increase in porosity with size in the desired range could be possible only by incorporation of a carbon pore former (fugitive). It is essential to burn away the carbon pore former under controlled condition to avoid formation of defects in the sintered body and hence its decomposition behaviour was studied by TG-

DTA (Fig.10).

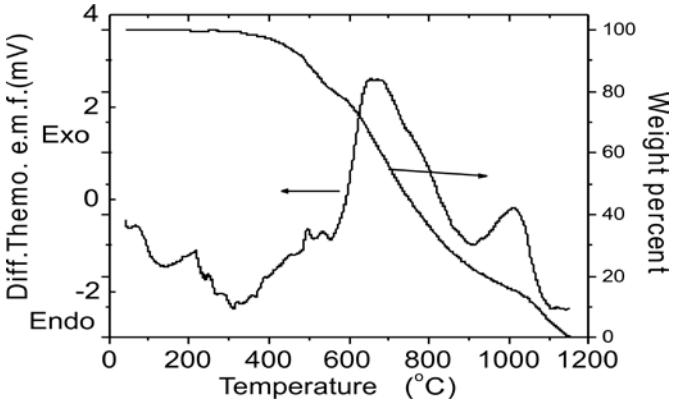

Fig.10. TG-DTA pattern for the pore former

As the combustion of the pore former completed at 1100^{0}C, the samples were heated slowly up to 1100^{0}C (0.5^{0}C/minute) followed by normal rate of heating (5^{0}C/minute) up to 1400^{0}C for sintering. A study on the variation of the amount of carbon pore former (D_{50}~ 15micron) on the open porosity of 1400^{0}C sintered LSM pellets has shown about 20wt % petroleum coke is needed to yield 45 % open porosity. The porosity remained constant for further soaking at 1400^{0}C up to 10hrs establishing the stability of the porous structure for further processing of formation electrolyte coating etc.

Hence bar specimens were prepared using the pore former under the above sintering conditions for further characterization studies such as thermal expansion coefficient, electrical conductivity and microstructure. The variation of thermal expansion coefficient (TEC) in the temperature range of 100 to1000^{o}C for the porous sample as determined by dilatometry is shown in Fig.11. It is obvious that the increasing porosity decreases while increasing temperature increases TEC even though the effect was marginal.

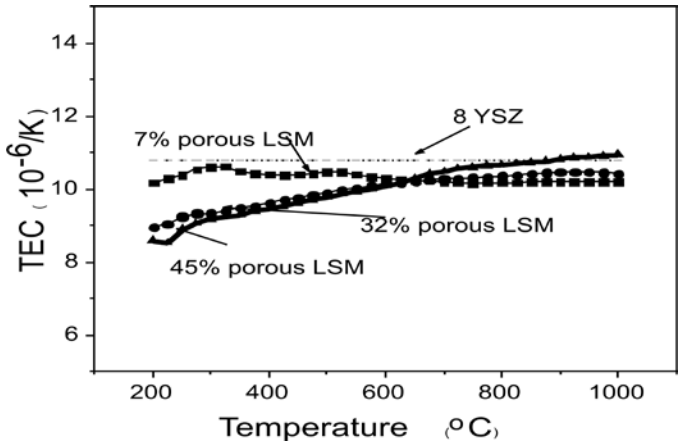

Fig.11. Variation of thermal expansion coefficient with temperature for LSM samples with graded porosity

The variation was in the range of 9.5 to 11 ppm /^{o}C for all samples which is close to the value reported for YSZ and is a requirement for cathode material for SOFC. The electrical conductivity decreased with increasing porosity and increased with temperature (semiconducting behaviour). The Arrhenius plot of variation of electrical conductivity with temperature for the samples (Fig.12) exhibits characteristic activation energy of 0.1376 eV for electronic conduction and is in agreement with that reported in literature [31]. Even though the conductivity decreased with porosity the activation energy remained essentially the same as expected. The micro-structural investigation of the sample exhibits the desired interconnected porous structure containing well sintered LSM grain (Fig.13).

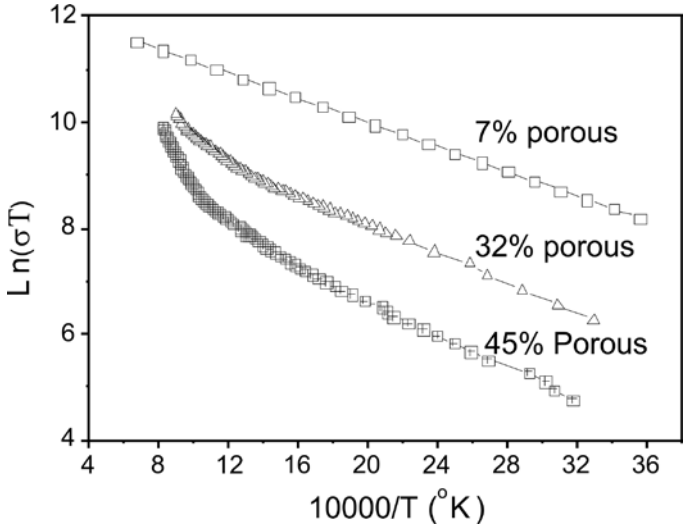

Fig.12. Variation of electrical conductivity with temperature for LSM samples with graded porosity

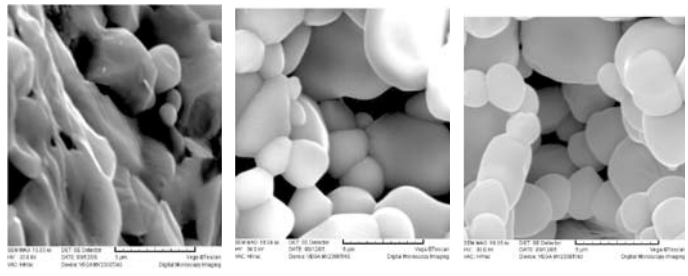

A- 7% B-32% C-45%

Fig.13. SEM microstructure of LSM with graded porosity (7, 32 and 45% open porosity)

As mentioned previously porous LSM tubes and thick self standing films (200 to 500 micron) find application in developmental studies such as formation of the test cells for obtaining current – voltage and polarization characteristics, thermal cycling behaviour etc. [32-33]. Hence, formation of tubular specimens and self standing thick films of LSM by aqueous slurry based slip casting and tape casting techniques was studied.

Aqueous slip casting of tube

Slip casting is the most versatile technique and possess capability to fabricate products with complex shapes and homogeneous cast composition. The slip characteristics need to be tailored to ensure formation of proper dispersion and is measured by zeta-potential and viscosity studies. Also the slip characteristics should be optimized to make easier the process of exercising control over formation of desired dimensions of the shape. The role of process conditions on the dispersion characteristics of the slip and its casting behaviour has been extensively described by Robert Fries and Brian Rand [34]. For materials with higher density (eg. LSM ~6g/cc), under a given set of dispersion conditions (i.e., pH and solid concentration), lowering the particle size increases the stability of the slip towards segregation (desirable for producing homogeneous green microstructure). In dry processing, as seen in the above study, formation of porous LSM requires incorporation of a carbon fugitive. In liquid based ceramic fabrication techniques, engineered porosity is introduced in the products by incorporating less dense coarser particles of pore former, like carbon in the slurry [35] and hence has been used.

A detailed investigation on the role of process conditions on the dispersion characteristics (zeta-potential and rheology) of the slip of powder mixture of LSM and carbon pore former, cast formation and the sintering behaviour of the bodies formed was carried out. A powder mixture of LSM and carbon pore former was used for formulation of aqueous slips with varying solid content and was evaluated for their zeta potential and rheological behaviour. The zeta-potential variation with pH for the aqueous suspensions of carbon powder along with that of LSM is shown in Fig. 8. The zeta-potential variation for the carbon powder suspensions in the pH range of 8 to 11 also exhibited negative charge (maximum value of -55 mV at a pH ~ 10). Thus at a pH of 10, both LSM and carbon pore former particles are sufficiently like-charged indicating the optimum pH window for their co-dispersion. Hence slips with varying solid content were prepared at a pH of ~10. The particle size distribution of the LSM and carbon pore former exhibited a D_{50} of 3 and 15microns respectively (Fig.9).

Even at the pH of maximum zeta-potential, flocculates are said to be present in the slurries with higher solid loading [36, 37] which is exhibited in their rheological behaviour. Obtaining a homogeneous green body microstructure is a precondition for formation of a quality and defect free sintered product. In slip casting, heterogeneity in microstructure results due to segregation and clogging phenomena which occur during liquid removal [38]. Segregation occurs due to higher rates of settling down of particles with larger size and density under the effect of gravity. Clogging effect occurs due to faster moving of finer particles along with suspending medium and it occurs in the direction parallel to that of liquid flow. As the liquid is removed into the pores present in the mould, the particles are dragged into its wall. The finer and lighter ones move faster towards the wall due to lesser inertia while the coarser ones form the subsequent layers of the wall, resulting in heterogeneous microstructure. These problems can be minimized by increasing the viscosity of the slurries using higher solid content in the slips and increasing the rate of cast formation i.e, reducing casting time. However, higher viscosity of the slip could result in improper mixing of the components during slip formulation, entrapment of air bubbles in the cast and formation of non-uniform cast thickness. Non-uniform wall thickness of the tube from bottom to top can result due to reduced time of casting compared to the time taken for filling and draining of the mould in case of very concentrated slips. Also defects get introduced due to improper flow of the slip in to the interior details of the mould. Thus it is essential to optimize the rheological parameters of the slurry to form quality casts with homogeneous microstructure and it varies with product dimensions. For long one end closed tubular specimens, it is done from the following points of view: i). the slip should easily flow in to and drain out the mould, and the time taken for the above should be much less compared to the time of casting to ensure uniform wall thickness, ii). avoid segregation of particles due to gravity and clogging effects during the course of the process. Also during casting viscosity should be large enough to provide desired degree of colloidal stability to avoid segregation.

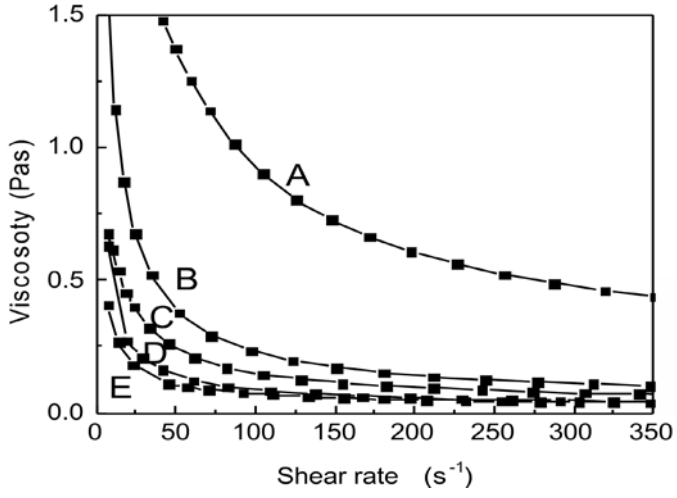

Fig.14. Viscosity variation with shear rate plots for slips of (LSM + carbon) A, B, C, D, E – slips with of 65, 60, 55, 50 and 45 weight percent solid content in water at a pH of ~10

The viscosity versus shear rate plots for the slips with varying solid contents (mixture of LSM and carbon pore former containing 1 wt % PEG binder) is shown in Fig.14. For all the slips, with increasing shear rate, the viscosity decreased gradually and attained a constant value above a critical shear rate (i.e., shear thinning behaviour – pseudo-plasticity) which is attributed to the breaking away of the flocculates present in slips upon shearing [36].

With decreasing solid content in the slip, the viscosity decreased and the critical shear rate above which viscosity becomes constant also decreased, indicating the flocculates becoming weaker with dilution. Also it is interesting to note that the decrease in viscosity becomes less significant with decreasing solid content in the slip. Pseudo-plasticity of the slurry is desirable for casting as less viscosity under shearing makes the slip to flow easily into the intricate details of the mould to yield quality cast of the complex shape and removal during draining. Increased viscosity with decrease of shear improves colloidal stability of the slip during casting to yield uniform wall thickness.

The casting behaviour was evaluated in plaster of Paris moulds using slips with varying solid concentration. The time taken for casting to a wall thickness of 2 mm was optimised such that the time of casting is an order of magnitude higher than the time taken for the slip to fill in and drain out of the mould. A slip with a solid content of 50 weight percent at a pH of 10 was found to exhibit enough viscosity to suppress segregation (leading to homogeneous microstructure) and still this solid concentration was low enough to exercise easy control over formation of desired thickness. Quality tubes of about 200mm long and wall thickness of 2 mm could be formed in about ten minutes.

The bodies after drain casting were dried in the mould for about 2 hours to form into a rigid shape, which could subsequently come out of the mould easily. These bodies were air dried for 48 hours in ambient atmosphere for slow evaporation of residual moisture to avoid introduction of cracks. Use of 1 weight percent of polyethylene glycol as binder in the starting powder mixture of LSM and carbon pore former improved markedly the strength of the dried cast. As the TG-DTA results of the carbon pore former in air exhibited combustion in the range of 400 to 1100^{0}C, the dried cast tubes were subjected to control burning out of the carbon pore former by heating at a rate of 0.5^{o}C/ minute up to 1100^{o}C. Controlled rate of heating enabled slow evolution of gases results in formation of crack-free bodies. These bodies sintered at 1400^{o}C from 1 to 8 hours exhibited same bulk density and open porosity (65% T.D. and 35% open porosity) as estimated by the water immersion technique. The photograph of the slip cast LSM tubes sintered at 1400^{o}C is shown in Fig.15. The wall thickness and density/porosity data of the sintered bodies cut at different lengths exhibited little variation (<5%) showing the absence of heterogeneity due to segregation of particles.

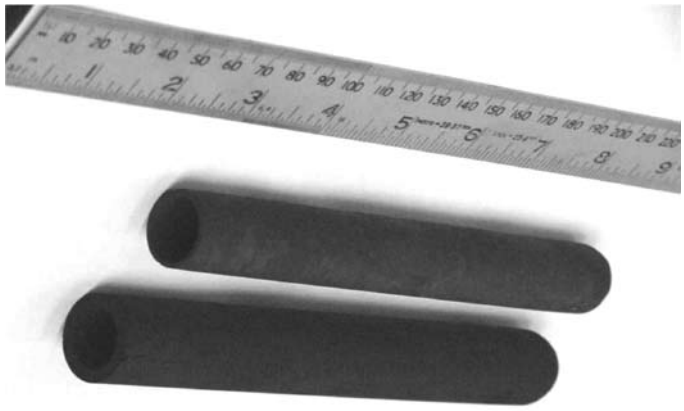

Fig.15. Porous slip cast LSM tubes sintered at 1400°C

The porous morphology of the sintered porous tube as shown in Fig.16 exhibits bigger voids created by the burning away of the carbon particles (pore former). As the pores are very big they are not expected to be eliminated by repeated sintering at 1400^{o}C, exhibiting the stability of the porous structure which is a prerequisite for the formation of a dense coating of YSZ by the various techniques (eg. EVD, EPD, dip coating).

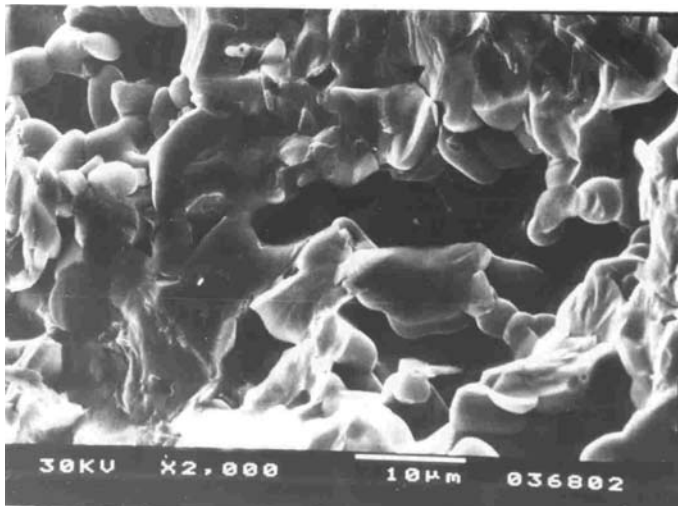

Fig.16. SEM micrograph of the porous LSM slip cast tube sintered at 1400°C

It involves repeated heat treatment of the coated tubes at a temperature around 1400^{o}C, as YSZ and LSM are reported to undergo reactivity above 1400^{o}C. As the maximum and safe sintering temperature for the YSZ coating on LSM has to be restricted to temperature less than 1400^{o}C, the tubes formed in this work can act as a potential electrolyte support for formation of SOFCs.

Aqueous tape casting of self standing film

In this process, as the shape is a wafer (0.2 to 0.5 mm thick), the green body formed would be very week and improvement in its strength is achieved by incorporating an additional constituent called binder/plasticizer in the slip. It imparts flexibility to the body so that it can be easily peeled off, punched to required size. The slurry dispersion is again an important aspect and the slip of LSM powder and carbon pore former is formed at a pH of 10 (point of maximum zeta-potential). The slurry is formulated and cast on Mylar or polythene sheets using a locally assembled tape casting facility which uses a blade with desired amount of gap between flat top surface of a table and the blade. The blade can be moved at varying speed horizontally to cast the slurry. By varying the gap between the blade and the surface of the table, it is possible to cast tapes with required thickness. The process parameters are optimised through a detailed investigation comprising of studies on dispersion conditions (i.e., zeta potential and rheology), and binder content. A preliminary study is required to find out the optimum composition of the slip (binder/plasticizer, powder and water) to form a flexible tape that can be easily peeled off and handled before sintering. The cast tapes after drying overnight in ambient conditions were punched to desired diameter and subjected to slow heating to eliminate the binder, plasticizer and pore former without introduction of defects in the sintered bodies (0.5^0C/minute up to 1100^0C) followed by fast heating to sinter at 1400^0C. It was essential to sand witch the tapes in between flat thermal insulation fibreboard to obtain flat sintered tapes which can be used for further processing with formation of electrolyte layer for formation of single test cell for studies.

To bring out the importance of rheological study in processing the films, the results on LSM-15wt% carbon pore former system is presented here. A pH of 10 was chosen for slurry formulation due to presence of sufficient amount of charge on the particles (LSM: -35mV, Carbon pore former:-50mV) at this pH. The viscosity variation with shear rate plot (Fig.17D) for the slurry containing 35wt% solid content (LSM -15wt% Carbon pore former) without binder exhibited moderate amount of pseudoplasticity i.e., decrease in viscosity with increase in shear rate. Pseudo-plasticity generally indicates presence of flocculates which entrap the water and make it immobile leading to higher viscosity. As they are broken upon shearing, the water becomes available for reducing the viscosity. Thus with increasing shear rate, the viscosity decreases but the effect was lesser compared to the slurries containing the binder. Similar behaviour was exhibited for YSZ and YSZ-NiO slurries also [25, 39]. A detailed study of the tapes formed with (LSM-C) slurries containing varying amounts of powder, polyvinyl alcohol (binder), glycerol (plasticizer) and water exhibited the composition in which the weight ratio has to be (89-x) : 10 : 1 : x for formation of flexible tapes that could be easily peeled off without breaking.

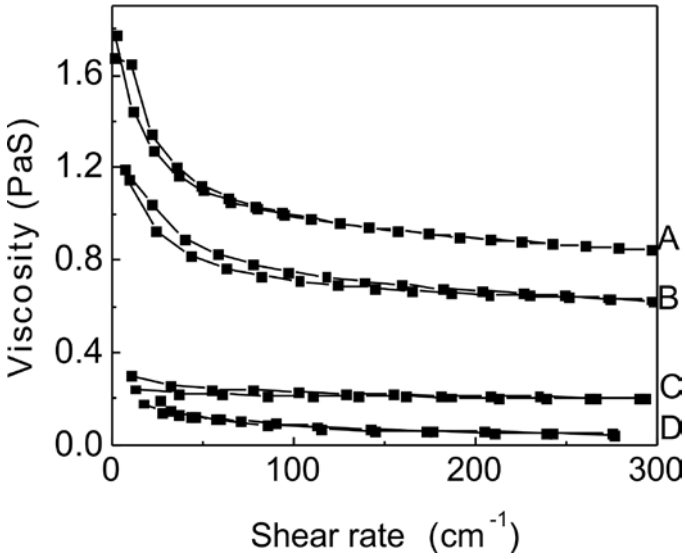

Fig.17. Typical rheology plots for tape cast slurry containing LSM with 15% pore former, dispersant, binder & varying amount of water (D-slurry with 35 wt.% powder mixture without binder in water, C, B, A – slurry containing binder & plasticizer with 22, 24 & 26 wt% powder mixture in water)

Hence rheological behaviour of slurries containing above-mentioned amount of powder-binder-plasticizer combination with varying amount of water (x -22, 24, 26 wt% solid content) was studied and the results are given in Fig 17(C, B, A). All the slurries exhibited shear thinning (i.e., decrease of viscosity with increasing shear rate) flow behaviour. Even though solid loading decreased from 35 to 22% with addition of binder solution, the viscosity of the slurries with binder solution were found to be higher Fig.17 (C, B, A) compared to that without binder solution (Fig.17D). This is attributed to the presence of binder-powder-water interaction in the slurries. The viscosity variation with shear rate plots for all slurries exhibited pseudo-plasticity. However, with slight increase in solid content (~ 2wt %), the viscosity increased drastically. Slurries-A (26wt. % solid content) and B (24wt. % solid content) exhibited time dependent flow behaviour (thixotropy) while slurry-C (22wt. % solid content) exhibited time independent variation in viscosity during increase and decrease of shear rate. Time dependent variation of viscosity in slurries (thixotrpoy) is not desirable for formation of quality casting as flow characteristics vary during the time of casting. In addition, at this stage, it is difficult to mix and de-air the slurry. Uncontrolled flow of slurry occurs with slip of lower solid contents (slurries with

solid content lesser than that corresponding to 'C'). The slurry-C was found to be the optimum one for formation of quality casts i.e., exhibits flow under the shear of the blade but rigid after shear to avoid back flow leading to formation of desired thickness. The viscosity was high enough to avoid sedimentation of particles during drying of the wet tapes and still low enough for easy removal of air bubbles.

The role of rheology on the characteristics of tape casting has been discussed by Bernd Bitterlich etal [40]. During tape casting the viscosity of the slurry reduces due to shearing by the blade and it should increase rapidly to control the uncontrolled flow of the slip and sedimentation of the powder particles. Thus the increased viscosity and pseudo-plasticity help in obtaining quality cast tapes. The water, binder and plasticizer have to be as much as possible minimum to allow fast drying. However increase of viscosity makes difficult both mixing and homogeneous mass flow during casting. The optimum composition of the slurry was obtained by considering all the above factors.

The tapes were cast with wet slurry thickness varying from 200 to 800 μm which yielded tapes with dried thickness in the range of 100 to 500 μm. The green density of the tape was determined from geometrical measurements after correcting for the binder (volatile) weight and was found to be 45 percent of the theoretical value. As the binder and carbon pore former burned in the temperature range of ambient to 1100^0C, tapes were heated at a slower rate of heating (0.5^0C per minute) up to 1100^0C to avoid formation of cracks due to evolution of gases. Further heating was done at a faster rate (5^0C per minute till 1400^0C and soaked for 2 hours). The densities of the sintered tapes obtained by water immersion technique (Archimedes method) were 65 percent with an open porosity values of 35 percent. The tapes possessed adequate mechanical strength. Also tapes were formed without carbon pore former and were found to possess 20% porosity which could be attributed to larger amount of organic binder used in forming flexible tapes.

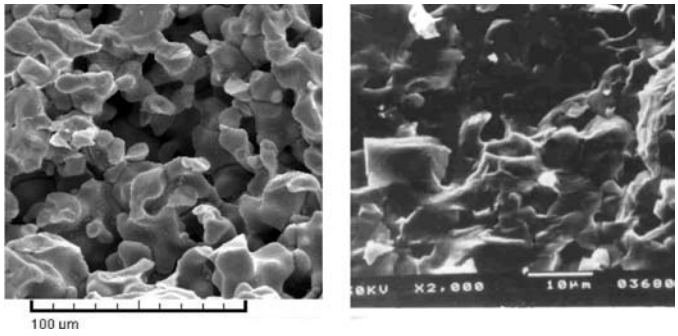

Fig.18. SEM micrograph of the fractured surface of LSM sintered tapes (A, B – with & without pore former)

The typical scanning electron microscopic fractograph of the sintered tapes showed presence of colony of open pores in the sintered body (Fig.18A, B). The tapes were found to be very flat as shown by the front and cross-sectional views in Fig.19 (A, B, C).These self standing tapes find application in formation of supported electrolyte and anode coatings to carry out single cell investigations.

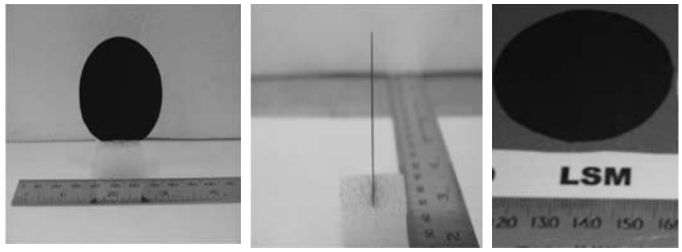

A- Front view *A- Cross-sectional view* *B- Front view*

Fig.19. Sintered LSM tape specimens (A, B -prepared without & with pore former respectively)

Summary

Combustion reaction of nitrate – citrate gel is not violent / explosive so that powder of large batch sizes can be easily prepared. However, chemically and phase pure LSM forms at 700^0C. Increasing calcination temperature to 1300^0C led to sinter-inactivity in the powder but the sintered bodies at 1400^0C did not retain the desired amount of porosity (35 to 45% open porosity) indicating the needs for incorporation of a carbon pore former. Sintered bodies exhibited decrease in electrical conductivity and a little decrease in thermal expansion coefficient with increasing porosity and was correlated to the microstructure. Processing conditions were optimized for fabrication of one end closed tubes by slip casting and self standing films by tape casting techniques. These cathode shapes could be further processed for formation of composite structure of the single test cell.

Acknowledgements

The authors would like to thank Dr K. Bhattacharyya and Dr A.K. Tyagi of Chemistry Division, Dr.G.K. Dey of Materials Science Division, Dr A.K. Sahu of Glass & Advanced Ceramics Division, Mrs (Dr) Shyamala Bharadwaj of Chemistry Division and Dr S.K. Gupta of Technical Physics Division for their help in FTIR, XRD, TEM, Dilatometry, electrical conductivity, and SEM investigations respectively. Also the authors thank Dr G.P. Kothiyal, Head Glass & Advanced Ceramics Division and Dr A. K. Suri, Director, Materials Group for their keen interest in the work.

References

1. A.Boudghene Stambouli, E. Traversa, Renewable and Sustainable Energy Reviews, 6 (2002) 433.

2. N.Q. Minh, J. Am. Ceram. Soc., 76, (1993), 563.
3. J. Weissbart, R. Ruka,. J. Electrochem. Soc., 109, 8 (1962) 723.
4. S.C. Singhal, MRS Bull., 25, 3, (2000) 16.
5. Masashi Mori, Yoshiko Hiei, J. Am. Ceram. Soc (2001)84, 11: 2573.
6. Changjing Fu, Siew Hwa Chan , Qinglin Liu, Xiaoming Ge, G. Pasciak, International Journal of Hydrogen Energy 2010;35:301.
7. Basu R N, Das Sharma A, Atanu Dutta, Mukhopadhyay J. , International Journal of Hydrogen Energy; 33, (2008) 20:5748.
8. Shangquan Zhang, Lei Bi, Lei Zhang, Chunli Yang, Haiqian Wang, Wei Liu. International Journal of Hydrogen Energy; (2009) 34, 18:7789.
9. Kakade M B, Ramanathan S., De P K., British Ceramic Transaction (2003) 102 5:211.
10. Ramanathan S, Peeyush Kumar Singh, Kakade M B, De P K., Journal of Materials Science (2004) 39, 9, 3207.
11. A.S. Shankarnarayanan, B.B. Kalekar, S.Ramanathan & P.V. Ravindran, Proceedings of the symposium THERMANS-2004, pp.108.
12. M.B. Kakade, S. Ramanathan, D. Das, P.R. Singh, Proceedings of DAE - BRNS International Symposium on Materials Chemistry (ISMC), 2006, pp. 324.
13. M.B. Kakade, S.Ramanathan, G.K. Dey & D. Das, Advances in Applied Ceramics, 107, 2, (2008) 89.
14. M. B. Kakade, D. Das and S. Ramanathan, Ceramics International, 37,2011, 1789.
15. S. Ramanathan and M.B. Kakade, International Journal of Hydrogen Energy, 36 (2011) 14956.
16. Chick L.A., Pederson L.R., Maupin G.D., Bates J.L., Thomas L.E., Exarhos G.J., Mater. Lett. (1990)1: 6.
17. Zuoyan Peng and Meilin Liu, J. Am. Ceram. Soc., 84, 2 (2001) 283.
18. Chakraborthy A, Devi P.S, Roy S., Maiti H S., J. Mater. Res. 1994; 9:986.
19. Herle J V, Horita T, Kawada T, Sakoi N, Yokok H, Dokiya M. , Ceramics International, (1998) 24, 229.
20. Kim S J, Lee W, Lee W J, Park S D, Song J S, J. Mater. Res., 2001; 12 36:21-27.
21. Jingfeng Xue, Yu Shen, Qingjun Zhou, Tianmin He, Yanhong Han. , International Journal of Hydrogen Energy 2010; 35:294 – 300.
22. D.W. Johnson, P.K. Gallagher, F. Schrey and W.W. Rhodes, Am. Ceram. Soc. Bull., (1976) 55, 5, 520.
23. S. Bilger, E.Syskakis, A. Naumidis and H. Nickel, J. Am. Ceram. Soc. (1992) 75, 4,964.
24. S. Ramanathan, K.P. Krishna kumar, P.K. De and S. Banerjee , Bulletin of Materials Science, 28, 2 (2005) 100.
25. S. Ramanathan, K.P. Krishnakumar, P.K. De and S. Banerjee Journal of Materials Science, 39, 10 (2004) 3339.
26. M.B. Kakade, S.Ramanathan, & D. Das, Ceramic International, 37, (2011) 195.
27. Srikumar Roy, A. Das Sharma, S.N.Roy and H.S. Maiti, J. Mater. Res., 8, 11 (1993) 2761.
28. C.C. Chen, M.M. Naasrallah, H.U. Anderson, J. Electrochem. Soc.140 (1993) 12, 3555.
29. S. Ramanathan, N. C. Soni and Ramprasad, J. Mater. Sci. Letters 12 (1993) 122.
30. Grinding David Houivet, Jaffar El Fallah and Jean Marie Haussonne, J. Am. Ceram. Soc., (2002) 85, 2, 321.
31. P. Sujata Devi, A. Das Sharma and H. S. Maiti, Transactions of the Indian Ceramic Society Vol.63, No.2 (2004) 75.
32. S. C. Singhal and Kevin Kendall, "High Temperature Solid Oxide Fuel Cell: Fundamentals, Design and Applications," Elsevier Ltd, UK, (2003) pp. 210.
33. S. C. Singhal, Solid State Ionics, 152-153 (2002) 405.
34. R. W. Cahn, P. Haasen, E. J. Kramer, Science and Technology, Processing of Ceramics – Part I Vol. 17A, in: Robert Fries and Brian Rand, (Eds.), Slip casting and filter pressing, Materials VCH Publishers Inc., (1996) pp. 153.
35. Stephen F. Corbin, Joyee Lee, Xin Qiao, J. Am. Ceram. Soc. 84 (2001) 41.
36. J. S. Reed, Principles of Ceramic Processing, Wiley, New York, 1995.
37. S. Vallar, D.Houivet, J. EI Fallah, D. Kervadec, J. M. Haussome, J. Eur. Ceram. Soc. 19 (1999)1017.
38. S. M. Olhero, J. M. F. Ferreira, Ceram. Int. 28 (2002) 377-386.
39. S. Ramanathan, Advances in Solid oxide fuel cells VI, Proceedings, Ed. Prabhakar Singh, Narottam P. Bansal, Edrjay Mathur & Tatsuki Ohij Vol. 31, Issue 9, 2010 pp. 91.
40. Bernd Bitterlich, Christiane Lutz, Andreas Roosen, Ceramics International, 2002, 28, 675 – 683.

Dr S. Ramanathan *joined Metallurgy Division, BARC in 1976 and since then has specialized on processing of advanced ceramics. He has worked on the development of solid oxide electrolyte ceramics for oxygen sensor in liquid metals, silicon carbide ceramics and sol – gel processing for nano-powders, coating and monoliths. He has contributed in the development of aqueous solution based processing of nano-crystalline YAG phosphors and colloids of hematite, magnetite, ceria, titania and alumina through sol-gel and gel combustion techniques. His current interest is on the processing of oxide ceramics through aqueous solution-slurry based processing of monolithic shapes and self-standing films. He is also engaged in the processing and characterization of lithium based oxide compounds and nano-alumina with tailored microstructure for Fusion Reactor research. He has published these works in about 100 papers in national / international journals and Proceedings.*	
Dr. M. B. Kakade *joined BARC in 1984 and since then is working on solution based processing of oxide ceramics which include alumina, zirconia, YAG etc. He worked on the development of LSM cathode and Ni-YSZ composite anode materials for SOFC and obtained Ph D in chemistry from Mumbai University in 2010. At present he is working on the preparation and processing of nano-crystalline lithium based ceramics and alumina coating on metallic substrate for Fusion Reactor Research. He has about twenty-eight publications in Indian and International journals.*	
Dr D Das *did his post graduation in chemistry from the University of Calcutta and joined BARC Training School in 1974. After completion of the one year course of Training school he began his research career in the field of high temperature thermochemistry studying the thermodynamic properties of uranium and its alloys and addressing to containment problems in uranium vapour processing. He obtained his PhD from University of Mumbai in 1984. He was deputed to KFA Julich, Germany for 15 months during 1993-94. With his expertise in materials chemistry at high temperature, Dr. Das worked for sometime in the development of high power electron guns for evaporation purpose, and in the thermodynamic analysis of cell components in High Temperature Solid Oxide Fuel Cell. In the last few years, Dr Das has focused his efforts on thermochemical characterization of thoria based fuels for the Advanced Heavy Water Reactors. He has large number of research publications in refereed journals. Presently, he is serving as Head, Chemistry Division, BARC, and looks after a number of activities in the field of materials chemistry.*	

Novel materials for air/oxygen electrode applications in Solid Oxide Cells

P.K. Patro*, R.K. Lenka, T. Mahata and P.K. Sinha

Energy Conversion Materials Section,
Materials Group, Bhabha Atomic Research Centre,
Vashi Complex, Navi Mumbai-400703
E-mail: pankajpatro@gmail.com

Abstract

One of the driving forces for the research in the field of solid oxide cells (SOFCs/SOECs) is to lower the operating temperature. Lowering the operating temperature can suppress degradation of components and extend the range of acceptable material selection. This will also improve cell durability hence prolonged service will result in reducing the effective cost. However, lowering in operating temperature increases the ohmic resistance, decreases the electrode kinetics and increases the electrode-electrolyte interface resistance. When the ohmic losses from the electrolytes are minimized by decreasing the electrolyte thickness or by using materials of higher ionic conductivity, the overall cell resistance is dominated by the electrode polarization resistance. It becomes important to develop new electrode materials or suitably modify the microstructure of the existing electrode materials to decrease the polarization resistance. For application as oxygen/air electrode (cathode in SOFC mode and anode in SOEC mode), novel materials such as Co and Co-Fe based Perovskites, spinels and Ruddlesden – Popper series materials in particular $Ln_2NiO_{4+\delta}$ have gained much attention in these days. In the present manuscript the microstructural development to reduce the interface polarization resistance of selected materials from the above mentioned series will be discussed.

Introduction

Conversion of the conventional fossil fuels to useful form of energy in the most efficient manner with the minimal environmental impact is the theme of future energy development. Fuel Cells and in particular solid oxide fuel cells (SOFCs) is in the forefront of the power generation systems due to its high conversion efficiency, fuel flexibility and environment impact. The current efficiency of different power systems are shown in Fig.1. SOFCs are in a position to offer clean and efficient power generation [1,2]. These systems find application in stationary, remote and distributed power generation due to its compactness, modular, durability and to extent fuel flexibility. Another application of this technology is as Solid Oxide Electrolysis Cell (SOEC), a reverse mode application of SOFC. It is so far the most practical and promising technology for large-scale renewable hydrogen production and further, being operated at high temperature it is expected to consume less electrical energy as compared to electrolysis at low temperature [3-5]. When the heat and electricity are from relatively green non oil sources, as in of nuclear processes, SOEC has always an edge over other conventional processes of hydrogen productions [6,7]. SOFC and SOEC in combinations are termed as Solid Oxide Cells (SOCs). Schematics of both the process are given in Fig. 2.

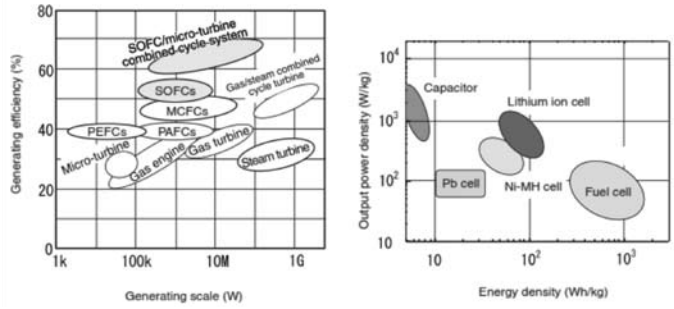

Fig.1. Current efficiency of various power systems and comparison of output power performance between various power generation systems [1].

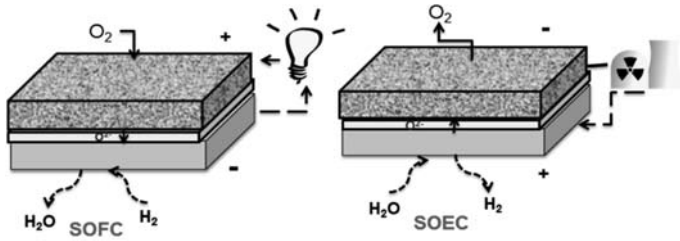

Fig.2. Schematic of Solid Oxide Fuel Cell (SOFC) and Solid Oxide Electrolysis Cell (SOEC).

Regardless the promise of SOCs, it has to overcome many hurdles e.g. the cost and reliability, the two foremost among the few, in order to being commercialized. Both the above obstacles are essentially the outcome of high

operating temperature, a unique character of SOFCs which has both pros and cons. The high operating temperature activates the fuel reforming and oxidation reactions and avoids the CO poisioning at the electrodes which normally occurs in the low temperature fuel cells. The high temperature also permits the excessive heat in the exhaust to be further reutilized as the primary heat for secondary electricity production. On the contrary, the high temperature operations restricts to only the use of materials with exceptional properties [8].

Present challenge in the research of development of SOFC/SOEC is to explore the possibilities in lowering the operating temperature to the range of 600-800°C [9]. This will not only reduce the degradation of the cell and stack components but also broadens the scope of possibility of wide range of materials. Decreasing operating temperature also reduces electrolyte conductivity and electrode kinetics.

The overall cell reaction in SOFC and SOEC are as follows

SOFC Mode	**SOEC Mode**
Anodic reaction: $H_2 + O^{2-} \rightarrow H_2O + 2e^-$	Cathodic reaction: $H_2O + 2e^- \rightarrow H_2 + O^{2-}$
Cathodic reaction: $½\ O_2 + 2e^- \rightarrow O^{2-}$	Anodic reaction: $O^{2-} \rightarrow ½\ O_2 + 2e^-$
Overall reaction: $H_2 + ½\ O_2 \rightarrow H_2O$	Overall reaction: $H_2O \rightarrow H_2 + ½\ O_2$

The cathodic reaction in SOFC and the anodic reaction in SOEC, involves oxygen reduction or oxide ion oxidation. Since both involve the oxygen species, for simplicity to represent this in both the systems, it is also termed as the oxygen/air electrode. Similarly the anode in SOFC and cathode in SOEC, involves reactions with hydrogen, it is also termed is hydrogen/fuel electrode for both the systems.

The oxygen electrode acts as the site for oxygen reduction/oxide oxidation in SOFC/SOEC mode. The mechanism of the same involves several intermediate steps [10]. This is explained considering the SOFC mode where the Oxygen reduction reaction (ORR) takes place. The primary requirements of cathode are:

a) It should have high electronic conductivity (Preferably > 100 S/cm at the operating temperature in oxidizing atmosphere).

b) Chemical compatibility with the electrolyte material (if it is not then a diffusion barrier layer has to be applied of another oxygen ion conductor material and it should be chemical compatible with this material)

c) It should have matched thermal expansion coefficient (If it does not match, to an extent it can be matched by the composite electrode approach)

d) Stability in oxidizing atmosphere in fabrication and as well in operation

e) Sufficient porosity to allow oxygen to diffuse through the cathode to the cathode/electrolyte interface

f) High catalytic activity of oxygen reduction reaction (ORR).

The electrochemical reaction in cathode of SOFC involves several surface and bulk processes such as adsorption, dissociation, reduction and incorporation of oxygen ions into the lattice of the cathode material. This is followed by ionic transportation through the cathode in the direction of electrolyte and ion jumping into the electrolyte lattice. Among these steps, oxygen reduction is the biggest contributor to the total cell resistance [11]. These electrochemical reaction takes place only at the triple phase boundary (TPB), where the gas, the electronic conduction phase and the oxide ion conducting phase meet together (Please see Fig. 3(a)). If there is discontinuity of any one of the above phases, then the electrochemical reaction cannot take place. If there is a hindrance of movement of gas, ions or electrons, then the site becomes inactive and known as 'dead TPBs'. This indicates that it is important to control the process parameters in order to get the right porosity and microstructure for the maximum of effective TPBs.

The oxygen electrodes may be either pure electronic conductor or a mixed ion-electronic conductor (MIEC). Sr doped lanthanum manganate (LSM), is an electronic conductor at high partial pressure of oxygen. In this case the electrochemical reaction takes place at only at the junction of the electrolyte and cathode, leading to in less numbers of active sites available for the electrochemical process. This has been explained in Fig 3(a). For a MIEC (e.g. $La_{1-x}Sr_xCo_{1-y}Fe_yO_{3-\delta}$) the whole surface of the cathode has both electronic and ionic conduction. Hence, the electrochemical reaction can take place at any place of the

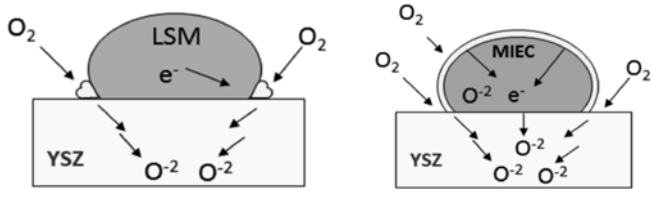

Fig. 3(a). Sites of Oxygen Reduction Reaction (ORR) in a (a) pure electronic conductor (b) mixed electronic ionic conductor (MIEC).

cathode and the ion can be carried to the electrolyte through the ionic conduction mechanism in the cathode. This has been explained in Fig 3(b).

As a single material cannot fulfill the requirement of an electrode, composite electrode approach has become an integral part of the SOFC/SOEC. The best example of composite electrode is Ni-YSZ as the hydrogen electrode which has been in use for a long time. Similar approach is also done for the oxygen electrode. LSM-YSZ composite is the most widely used oxygen electrode. Here the main objective is to increase the TBPs and the TBP length so that there will be higher number of sites available for electrochemical reaction. The other advantage is to minimize the thermal expansion coefficient (TEC). Higher the mismatch of TEC between electrolyte and electrode there is a chance of delamination at the electrode-electrolyte interface. It will lead to high resistance due to non-continuous ion conducting path/TPBs for electrochemical reaction. A cathode material can be mixed with suitably non-reactive electrolyte materials such as YSZ or GDC to form a composite cathode. The composite composition can be suitably adjusted to match the TEC with the electrolyte having sufficient percolation for the electron/ion conduction path without compromising its conductivity. In some cases it is essential to have the cathode to be very rigid. In this case the composite of the same with the electrolyte material makes it very robust. The electrodes should have high redox stability. This is especially for the SOEC application where the oxygen electrode must be stable upto +0.3V to assure high rate of oxygen evolution in this electrode. Similarly the hydrogen electrode should be stable down to -1.4 V in order to sustain a high H_2 evolution rate [12]. This indicates that the electrodes in SOEC mode are likely to more venerable/prone towards the delamination/damage than the SOFC mode in solid oxide cells [13]. A schematic of composite electrode is given in the Fig. 4.

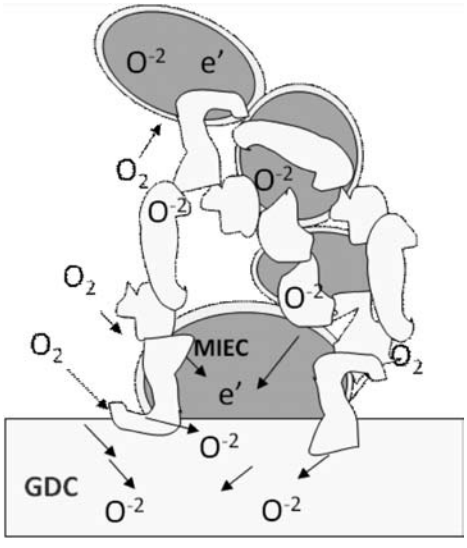

Fig. 4. Schematic of composite electrode of a MIEC with GDC.

Materials for Oxygen electrode

In this section we will be discussing about different materials which have recently been studied as oxygen electrodes. We understand that La doped Strontium Manganate (LSM) is the most widely used oxygen electrode material which has sufficient electronic conductivity, fairly matching TEC, chemically compatibility with electrolyte materials and good stability at high temperature (1350°C). However it being an electronic conductor, the absence of oxygen vacancies in LSM restricts the reductions of oxygen to the TPBs, a main reason for not having the acceptable performance at lower temperatures [14-16]. We will discuss about some selected materials which are gaining attention.

a) Co-Fe based perovskite electrode

The improvement of LSM performances has been done either by adding an ionic conducting secondary phase or by substituting A and/or B sites. A number of studies have indicated that when Mn is replaced by Co or Fe-Co, it shows enhanced electrocatalytical activity for oxygen reduction and increased ionic conductivity due to MIEC effect [17]. Literature indicates some noticeable materials in these directions which are mainly lanthande based iron cobaltites. Some pivotal materials in this directions are $La_{1-x}Sr_xFe_{1-y}Co_yO_{3-\delta}$, $Sm_{1-x}Sr_xFe_{1-y}Co_yO_{3-\delta}$, $Pr_{1-x}Sr_xFe_{1-y}Co_yO_3$ and more recent non-lanthanum based materials like $Ba_{1-x}Sr_xFe_{1-y}Co_yO_{3-\delta}$[18-26]. This is primarily due to the high electronic as well as ionic conductivity and high catalytic activity for oxygen reduction. The high conductivity of the material facilitates the migration of oxide ions through the bulk as well as on the surfaces of the electrode to the TPBs.

$(La_{0.6}Sr_{0.4})_{1-s}Fe_{0.8}Co_{0.2}O_{3-\delta}$ (LSCF) has been reported to have good electrocatalytic activity and its polarisation resistance (Rp) is lowest for A-site deficient (s=0.15) compounds (14.8 and 2.75 Ω.cm² at the temperatures 600°C and 700°C respectively) and it is 0.58 Ω.cm² at 800°C for s=0.10 [21]. The R_p value of $La_{0.58}Sr_{0.4}Fe_{0.8}Co_{0.2}O_{3-\delta}$ with 20 mol% of Sm doped ceria, has been reported to be of 0.23 Ω.cm² at 700°C and 0.067 Ω.cm² at 750°C respectively a value lower than LSM with YSZ [27]. LSCF also exhibits very good oxygen self diffusion coefficient between 600-800°C. The oxygen self diffusion coefficient of LSCF is 2.6 X 10^{-9} $cm^2\ s^{-1}$ at 500°C where as for $La_{0.8}Sr_{0.2}MnO_3$ it is 10^{-12} $cm^2\ s^{-1}$ at 1000°C [28,29]. $Ba_{0.5}Sr_{0.5}Fe_{0.2}Co_{0.8}O_{3-\delta}$ has been reported to have Rp of 0.1 Ω.cm² at a temperature as

low as 600°C. This is considerably much lower than other perovskite based electrode materials. However, it has also been reported that the electrodes of this compound are not stable over long period of time [26].

Large TEC of the Iron-Cobaltites ~ 20 X 10^{-6} K^{-1} compared to the manganites ~ 11 X 10^{-6} K^{-1} is due to the formation of oxygen vacancies, spin-state transitions associated with Co^{3+} and relatively weaker Co-O bond compared to that of Mn-O bond. $Ba_{0.5}Sr_{0.5}Fe_{0.2}Co_{0.8}O_{3-\delta}$ has TEC of more than 20 X 10^{-6} K^{-1} [30]. It has also been reported that the TEC of Co or Fe-Co based materials depends heavily on the extent of A-site deficiency. For $(La_{0.6}Sr_{0.2})_{1-s}Fe_{0.8}Co_{0.2}O_{3-\delta}$, the TEC value changed from 19.5 X 10^{-6} K^{-1} to 17.3 X 10^{-6} K^{-1} at 1000°C, when the A-site non-stoichiometry increased from s= 0.01 to 0.20 [21]. It has also been reported that in $La_{0.6}Sr_{0.2}Fe_{0.8}Co_{0.2}O_{3-\delta}$ (20% a site deficient) results in the TEC of 13.8 X 10^{-6} K^{-1} at 700°C [31]. This is quite comparable to most of the commonly used electrolyte materials.

b) Co based perovskite electrode

Perovskite cobaltites are reported to have better electro-catalytic activities for oxygen reduction reaction and higher electronic conductivities than other electrode materials [10,19,32-33]. However, the thermal expansion coefficient values of cobaltites remain on the higher side compared to ferrites or manganite based cathode materials. Thermal expansion coefficient of cobaltites is influenced by substituting 'A' sites or Co sites with suitable elements. Substitution of La sites in $LaCoO_3$ with aliovalent dopants, such as Sr, is reported to increase oxygen vacancy in the cobaltite structure. This results in increase in ionic conductivity and also increase in thermal expansion coefficient. The increase in ionic conductivity can have a beneficial effect on decreasing the electrode polarization resistance at the interface by way of enhancement of the triple phase boundary area. As the reaction at the cathode is heterogeneous in nature, larger triple phase boundary (TPB) area will lead to better reaction kinetics. However, the increase in thermal expansion coefficient is significant and is often balanced by doping Co sites with Fe, Mn etc. [10,19]. Among the different rare earths that form 'A' sites the thermal expansion coefficients of the cobaltites decrease in the order of La, Pr, Nd, Sm and Gd. $La_{0.8}Sr_{0.2}CoO_3$ and $Sm_{0.5}Sr_{0.5}CoO_3$ has TEC of 19.1 X 10^{-6} K^{-1} and 20 X 10^{-6} K^{-1}respectively [10].

c) $Ln_2NiO_{4+\delta}$ type Ruddlesden – Popper series materials

Recent studies have highlighted the potential of layered materials like Ruddlesden – Popper (RP) series for oxygen electrode applications in SOCs [34,35]. The main advantage of this type of materials is that it can accommodate oxygen excess by incorporation of oxygen interstitials which are mobile, apart from being MIEC conductors. The oxygen transport properties in layered structured compounds are better than that in non-ordered perovskites, resulting in lower activation energies and excellent oxygen surface exchange properties. Fig. 5, represents the structure of a typical RP series materials. The general formula for Ruddelsden – Popper series of materials can be written as $A_{n+1}B_nO_{3n+1}$ and consists of n ABO_3 perovskite layers sandwiched between two AO rock-salt layers. Commonly these materials consist of rare or alkaline earth metal at A site cations with transition metals on the B site, leading to the formation of an extensive series of compositions. However, for fuel cell applications, the particular interest is in some members of above series based on $Ln_2NiO_{4+\delta}$ (where Ln = La, Nd and Pr). These materials can accommodate moderate oxygen interstitials in the AO layers, giving rise to fast ion conduction and hence potential application as oxygen electrode in SOFCs/SOECs [36]. In these materials high oxygen mobility has been reported and in the case of $La_2NiO_{4+\delta}$ at a temperature as low as 450°C [37]. Another advantage of this kind of materials is matching thermal expansion coefficient with the commonly used electrolyte material like 8YSZ and GDC. For example, at operating temperature, it is 13×10^{-6}, 12.7×10^{-6} and 13.6×10^{-6} K^{-1} for $La_2NiO_{4+\delta}$, $Nd_2NiO_{4+\delta}$ and $Pr_2NiO_{4+\delta}$ respectively [38]. The oxygen excess content values for $La_2NiO_{4+\delta}$, $Nd_2NiO_{4+\delta}$

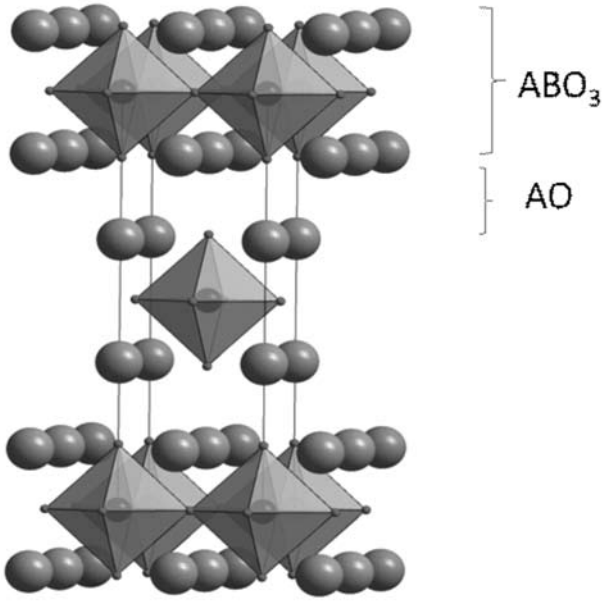

Fig. 5. Polyhedral view of Ruddlesden –Popper materials having general formula $A_{n+1}B_nO_{3n+1}$ consisting of nABO_3 perovskite layers sandwiched between two AO rock-salt layers.

and $Pr_2NiO_{4+\delta}$ are 0.17, 0.22 and 0.21 at room temperature and 0.07, 0.15 and 0.13 at 600°C respectively [39]. These indicate that compositions like $Nd_2NiO_{4+\delta}$ and $Pr_2NiO_{4+\delta}$ can be better candidates than $La_2NiO_{4+\delta}$. Further, these materials exhibit larger oxygen bulk diffusion (D*) and surface exchange (k) coefficients than classical perovskite compounds and electrical conductivity values σe ≈ 100 $S.cm^{-1}$. Chemical stability as a function of oxygen pressure (in the range of 1 to 10^{-5} atm) and under moist atmosphere, allows the use of these materials as air electrode in different systems such as IT-SOFC, PCFC or SOEC [40]. Further it has also been reported that these materials exhibit lower anodic polarization as in SOEC than the cathodic polarization in SOFC, which makes it more attractive for electrolysis applications.

d) Spinel Oxides

Spinel oxide materials have traditionally been explored in the field of SOFC as protective coating for ferritic steel interconnects to reduce the contact resistance between the electrode and interconnect. A coating of this material prohibits the diffusion of chromium from interconnect to the electrode material [41-42]. The added advantage of these materials is their high electronic conductivity and matching TEC, which makes them attractive as an electrode material. $Mn_{1.5}Co_{1.5}O_4$ which has been extensively used as a protective layer coating has practically been developed as an oxygen/air electrode material. The TEC of this material is 11.7 $X10^{-6}$ K^{-1} and electronic conductivity is 60 S/cm at 800°C. The TEC value matches with YSZ electrolyte and ferritic steels (e.g. Crofer 22APU) which is the commercial interconnect material. The electrode polarization of this material is reported to be 2.56 and 0.7 Ω.cm^2 at 700 and 800°C respectively [43]. These values are on the higher side of the conventional electrode materials but on suitable microstructural development the polarization resistance could be lowered to some extent. Above all, the spinels used in solid oxide cell application are mostly rare-earth free. This adds to a cost advantage compared to other oxygen electrode materials which are rare-earth based.

Development of Microstructure of certain cathode materials

a) Microstructural Development of $Pr_{0.6}Sr_{0.4}Fe_{0.8}Co_{0.2}O_{3-\delta}$

$Pr_{1-x}Sr_xFe_{1-y}Co_yO_3$ is one of the novel Fe-Co based electrode materials that have caught attention of many researchers in recent days. Electrode materials incorporating Pr^{3+} has been reported to have highest electrical conductivity and the lowest overpotential values due to additional contribution of Pr^{3+}/Pr^{4+} valency change[44]. A number of compositions have been attempted in this respect. Literature indicates that $Pr_{0.3}Sr_{0.7}Co_{0.3}Fe_{0.7}O_{3-\delta}$ has shown R_p value of 0.11 Ω.cm^2 at 700°C [25]. Similarly for A-site deficient $(Pr_{0.6}Sr_{0.4})_{1-s}Co0.2Fe_{0.8}O_{3-\delta}$ it has been reported to be varying between 0.017 to 0.05 Ω.cm^2 at 800°C for a range of composition where 's' varies from 0.01 to 0.2. This result indicates that, for s= 0.01 to 0.05, it gives lowest polarisation resistance [22]. However, the bottleneck problem in Co or Fe-Co based electrode materials including that of $Pr_{1-x}Sr_xFe_{1-y}Co_yO_3$, is the high

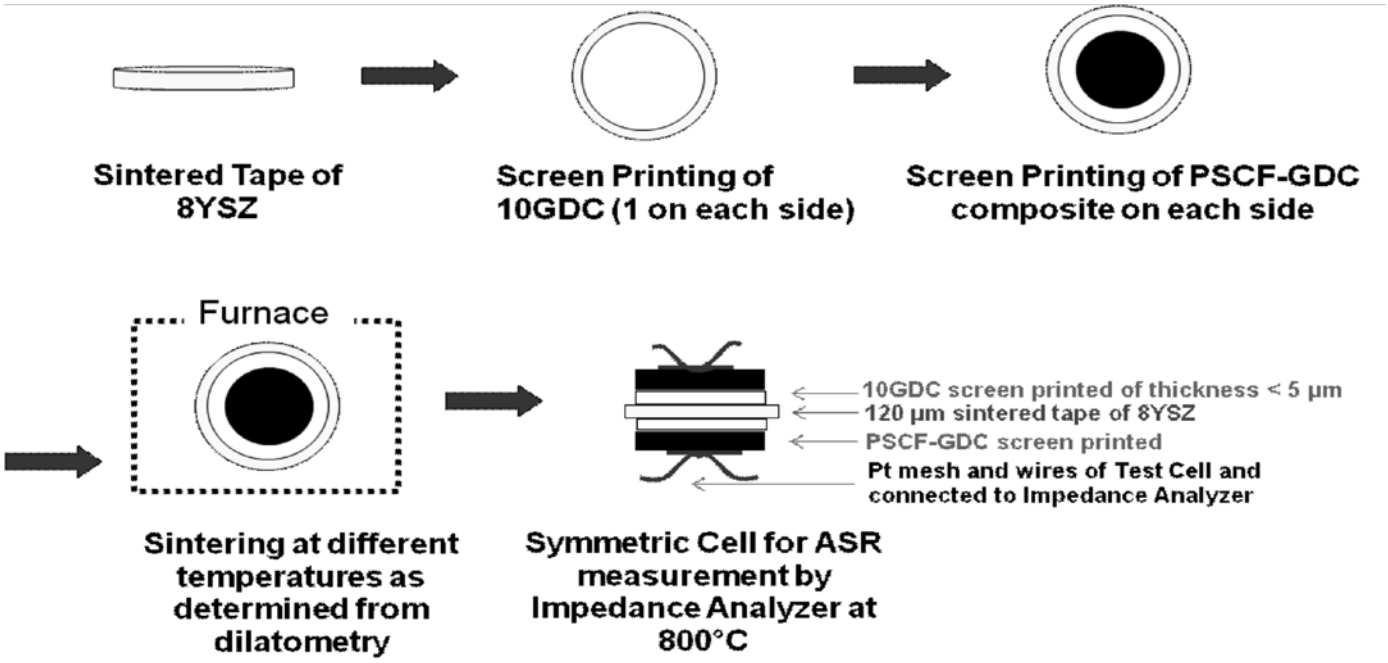

Fig. 6. Steps followed to fabricate the symmetric cells

Thermal Expansion Coefficient (TEC) mismatch of the material with the common electrolyte materials available and also in some cases the thermal stability of the electrode as well as chemical compatibility with electrolyte [45-46].

The findings of one particular composition of PSCF i.e. 2% Pr (A- site) deficient $Pr_{0.58}Sr_{0.4}Fe_{0.8}Co_{0.2}O_{3-\delta}$ has been presented here. In literature it has been reported that, $Pr_{0.6}Sr_{0.4}Fe_{0.8}Co_{0.2}O_{3-\delta}$, gives the highest electrical conductivity of 1040 S cm^{-1} at 300 °C and its TEC value is 19.69 X 10^{-6} K^{-1} when measured from 30°C to 850°C [24]. $Pr_{0.6}Sr_{0.4}Fe_{0.8}Co_{0.2}O_{3-\delta}$ with slight A-site deficient is expected to bring down the TEC value, without compromising the electrical conductivity. It has also been reported that, the A-site deficient $Pr_{0.6}Sr_{0.4}Fe_{0.8}Co_{0.2}O_{3-\delta}$, does not lead into formation of two perovskite phases with the Co-Fe spinel structure as in the case of A-site deficient $La_{0.6}Sr_{0.4}Fe_{0.8}Co_{0.2}O_{3-\delta}$ [22]. The current densities of the cells consisting of having A-site deficient LSCF electrode, CGO electrolyte and NiO-YSZ cermet anode were as high as 1.76 A cm^{-2} at 800°C, and 0.7 V. This is twice the current density of the cells with LSM/YSZ [10]. These factors make this material worthwhile to explore in details for the possible SOFC/SOEC applications.

Microstructure being one of the major factors for the performance of the cell, the optimization of the same on PSCF is briefed here. The optimizations were carried based on the polarization resistance measurements from the impedance study of symmetric cells. The steps followed to fabricate the symmetric cells are given in Fig. 6. To overcome the high thermal expansion coefficient of this material with the electrolyte, it is mixed with 10 mol% Gd doped ceria (GDC) and is used as the composite material. The choice of GDC as composite material was based on the chemical compatibility of PSCF with GDC.

Reactive phases were found when a mixture of PSCF with 8YSZ powder was calcined at 1200°C, whereas no reactive phase(s) at this temperature was found for GDC. For the electrolyte, 8YSZ discs of 100-120 µm thick was tape casted and then was laser cut to discs of 20 mm (16mm after sintering) and were sintered at 1500°C. Screen printing method was followed for electrode coating in the fabrication of symmetrical cells. To prevent the reaction between PSCF and YSZ one layer of GDC coating was given and above it required number of PSCF-GDC composite layer coating was given. The suitable range of sintering temperatures was chosen from the dilatometric shrinkage curve of PSCF-GDC composite. For this, PSCF-GDC composites with different weight ratio of the components were attempted. Initially the composite PSCF50-GDC50 (50 wt% of each components) was used and three layers of coating on each side of the electrolyte was applied and were sintered at the temperatures 1000, 1050, 1100, 1200 and 1250°C respectively for the identification of suitable sintering temperature. From the microstructural observation and electrochemical impedance study, the temperature 1100°C was chosen. For this temperature there were no delaminations at the interface and the microstructure was porous enough for gas diffusion and the polarisation resistance (Rp) of 0.14 Ω.cm² was observed, when measured in air at 800°C. Subsequently, the optimization of composition was carried out with compositions varying from 30 wt% to 70 wt% of PSCF rest GDC. Based on this it was observed that, PSCF50wt%-GDC50wt% composite resulted in the lowest polarisation resistance. Hence PSCF50-GDC50 was chosen as the optimized composition. Further to this, the optimization of the thickness of the coating was carried out by coating several layers of the material. It was found that the thickness of the electrode 7-9 µm, corresponding to two layers of coatings resulted in the lowest polarisation resistance of 0.12 Ω.cm² at 800°C. Figures 7(a) and (b) are the SEM micrograph of the surface and at the electrode-electrolyte interface respectively. The Nyquist plot for PSCF50-GDC50 having thickness of 7-9 µm corresponding to layers of screen printing is given in Fig. 8. In the Nyquist plot the low frequency arch corresponds to the gas transports phenomena and the high frequency arch represents TPBs, electrochemical reactions at the electrolyte-electrode interface. It was found that, from the SEM morphology that, the electrode-electrolyte interface improves with increase in the GDC content in the PSCF–GDC composite so the effect of intermediate layer was also investigated. However, it was observed that the intermediate layer did not reduce the polarisation resistance. Based on above findings, the optimized condition of PSCF electrode are a) sintering temperature

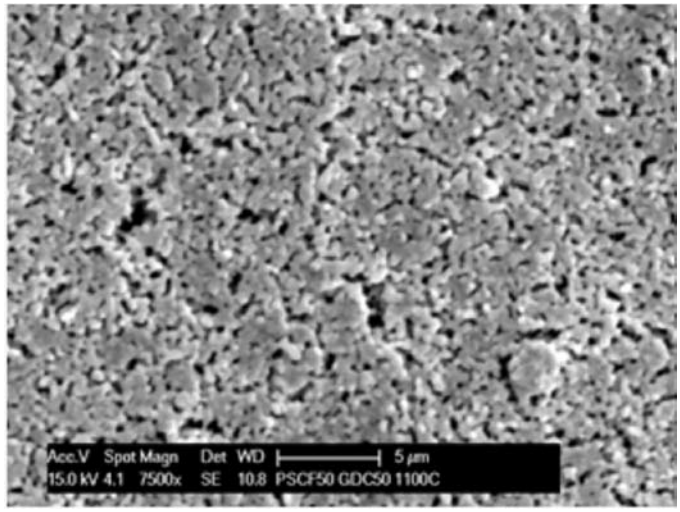

Fig 7 (a)

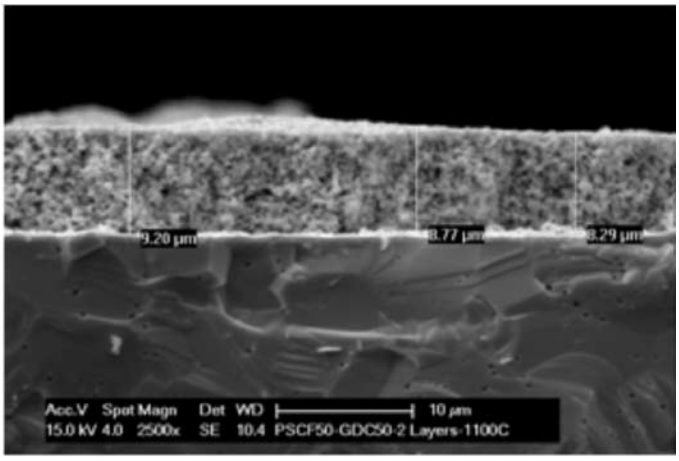

Fig 7 (b)

Fig. 7(a) and (b). SEM Micrographs of the PSCF50-GDC50 electrode surface and crossection of the symmetric cell

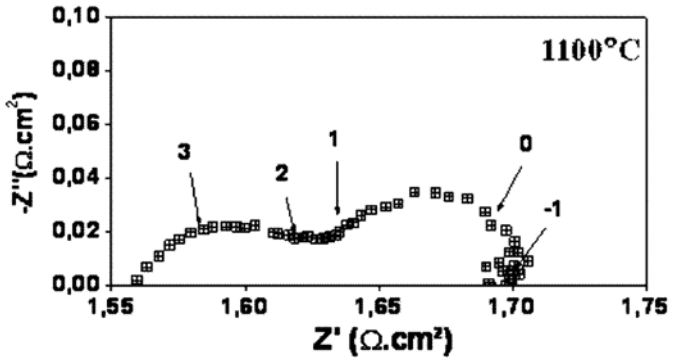

Fig. 8. Nyquist plot for PSCF50-GDC50 electrode measured at 800°C. (sintering temp 1100°C)

1100°C b) composite composition of PSCF50-GDC50 c) thickness of 7-9 µm corresponding to 2 layers of coating as observed from the microstructure and symmetric cell measurement in air at 800°C.

b) Microstructural Development of $GdCoO_3$ as an electrode material

$GdCoO_3$ is considered to be a potential oxygen electrode material. As the high TEC of cobaltites is the most detrimental, it can be further tuned to closely match with the conventional electrolyte material by the composite electrode approach [47-49]. The experimental findings in developing $GdCoO_3$ as a potential electrode material are discussed here. The average TEC was calculated to be 16 $\times 10^{-6}$ K^{-1} in the temperature range from ambient to 1000 °C. For the composite of this with GDC (50 wt% each), the TEC was found to be 12.9×10^{-6} K^{-1}. This is close to the GDC electrolyte material with nominal composition $Ce_{0.8}Gd_{0.2}O_{1.9}$ of 12.5 $\times 10^{-6}$ K^{-1} [50]. The DC conductivity of $GdCoO_3$ sintered at 1200°C measured by four probe technique was found to be around 580 $S.cm^{-1}$ at 800 °C . This value is in between the conductivity of $La_{1-x}Sr_xCoO_3$ (~1200 S/cm) [51] and $La_{1-x}Sr_xMnO_3$ (~130 S/cm) [52]. This higher value of conductivity is sufficient for current collection for SOC oxygen electrode applications. The Arrhenious plot of conductivity is shown in Fig. 9 and in this figure it can be observed that at around 400°C there is a change in slope indicating the change of conduction mechanism. At low temperature the conductivity is associated with Mott type hopping conduction i.e. small polaron hopping between Co^{2+} and Co^{3+}. However, at high temperature the conductivity is associated with activation mechanism. The ASR value for the symmetric cells obtained for the $GdCoO_3$-GDC composite are 1.1, 0.55 and 0.2 Ω.cm^{-1} at 800, 850 and 900 °C respectively. The Nyquist plot of the ASR measurement is given in Fig 10.

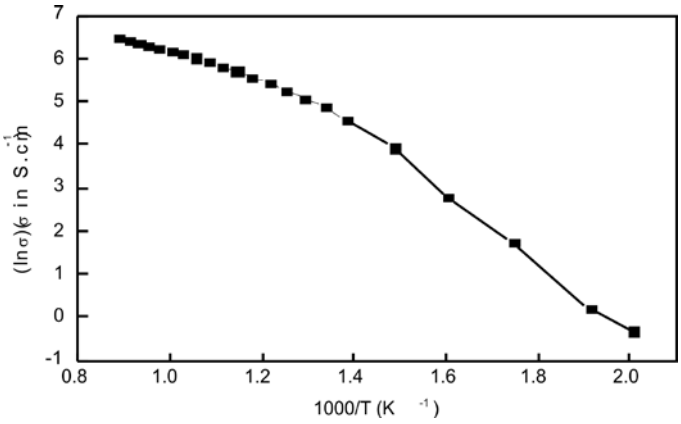

Fig. 9. Conductivity of dense $GdCoO_3$ pellet sintered at1200 °C

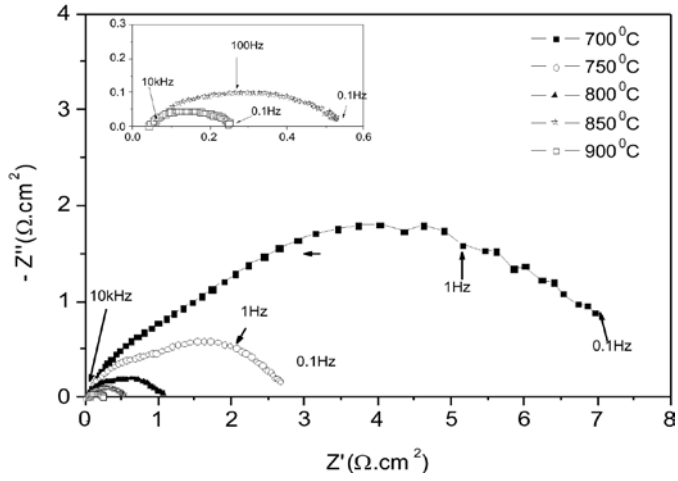

Fig. 10. Nyquist plot for symmetric cell prepared using pure $GdCoO_3$-GDC composite electrode at different temperatures (Inset shows the Nyquist plot for the temperatures of 850°C and 900°C)

Fig. 11 is the micrograph of fractured surface of the symmetric cell. A porous electrode layer of about 30 µm thick is found to be deposited over the dense GDC electrolyte.

There is a good adherence between the electrolyte and porous electrode layer. Apart from electrode composition the interfacial microstructure plays an important role in deciding the ASR value. The microstructure is influenced by ceramic processing parameters involved in integration of electrode with the electrolyte. Hence, there remains further scope in decreasing the ASR values through optimization of fabrication parameters. Mixed ionic electronic conductors (MIEC) are reported to be very effective in lowering the ASR by way of providing extended triple phase boundary area. With doping of suitable aliovalent ions, $GdCoO_3$ can be made an effective more MIEC material.

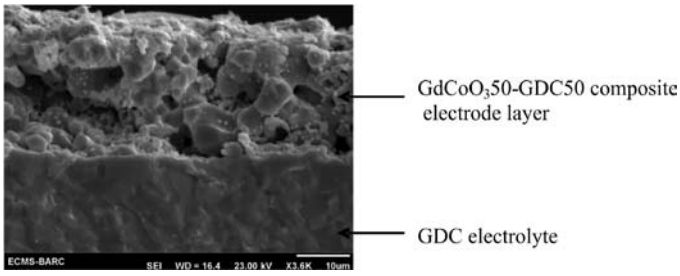

Fig. 11 SEM micrograph of the symmetric cell prepared using $GdCoO_3$-GDC composite electrode

c) Microstructural Development of Nd_2NiO_4

Among the nickelate based RP series materials, Nd_2NiO_4 seems to be a promising material for the SOFC/SOEC applications. The preliminary work carried out for the suitable development of microstructure for application in Solid Oxide Cells is briefly discussed here. Nd_2NiO_4 is chemically not compatible with YSZ but was compatible with GDC and YDC as determined from the XRD of the mixed powder after calcinations at 1200°C. Fig. 12 shows the XRD of the mixture of Nd_2NiO_4 and GDC, calcined at 1200°C and it clearly indicates that there is no reactivity of the powders. Hence for the symmetrical cell fabrication, application GDC /YDC layer before the electrode printing is essential on YSZ electrolyte to prohibit the reaction between Nd_2NiO_4 and YSZ. From the impedance measurements of the symmetrical cells, lowest electrode polarization resistance occurs at a sintering temperature of 1050°C and seems to be the most suitable sintering temperature.

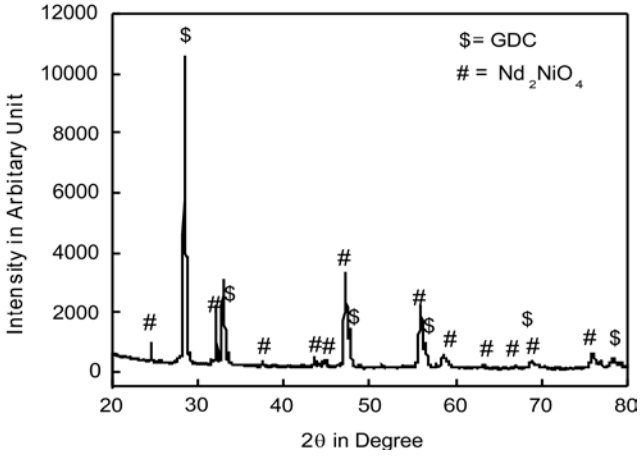

Fig. 12. XRD of the mixed (Nd_2NiO_4 and GDC) calcined at 1200°C

The corresponding microstructure of the sample also indicated the strong adherence between the electrode and the electrolyte and sufficient porosity for the gas transportation. The SEM micrograph of Nd_2NiO_4 based symmetric cell having GDC diffusion barrier layer is shown in Fig. 13. The Nyquist plot for the sample measured at 750°C temperatures is shown in Fig. 14. From the plot the area specific polarization resistance was calculated to be 0.142 Ω.cm^2 at 750°C. This indicates that Nd_2NiO_4 is one of the most promising materials for air/oxygen electrode applications in solid oxide cells.

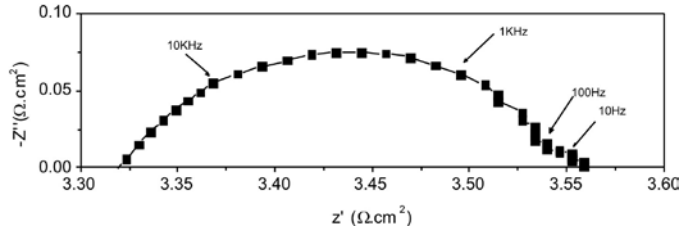

Fig. 13. Nyquist plot for Nd_2NiO_4 based symmetric cells measured at 750°C.

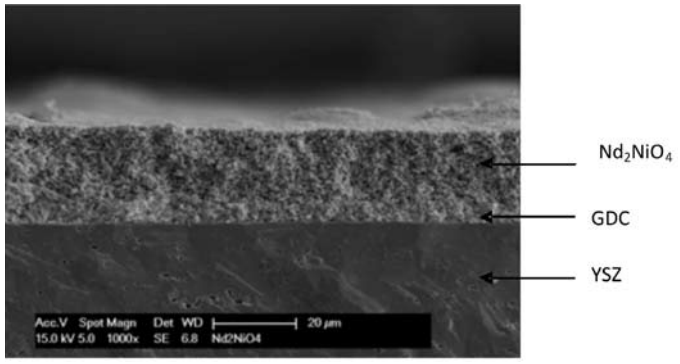

Fig 14. SEM Micrograph of a symmetric cell having GDC diffusion barrier layer and Nd_2NiO_4 electrode.

Conclusions

We have discussed about novel materials which are in the fore-front of air/oxygen electrode applications in solid oxide cells. The MIEC conductors have taken over completely the pure electronic conductors in this respect. However, the main issue lies with thermal expansion, stability and rate of degradation of these materials. Composite electrode approach to an extent is likely to minimize the thermal expansion coefficient mismatch issue. Careful processing technique should be adopted to avoid lowering of the overall conductivity. Most of the

Co, Co-Fe perovskites and the novel layered perovskites are susceptible to react with YSZ, which is one of the most well studied and commercially viable electrolyte materials. This poses a challenge to develop new materials which can match ionic conductivity, stability, strength and cost effectiveness etc. with YSZ so that novel materials can be easily be practically be used. Co and Co-Fe based perovskites are also unstable above 1250°C resulting in restriction in certain processing conditions. The long-term performance and rate of degradation of these materials is not well reported. These materials may need special processing parameters to control the microstructures so that they undergo least degradation during the prolonged use of the solid oxide cells. The novel materials discussed in this article have immense potential of the actual commercial application in Solid Oxide Cells.

References

1. H. Kawamoto, Science and Technology Trends (2008) 26, 52-70.
2. A. B. Stambouli, E. Traversa, Renewable and Sustainable Energy Reviews (2002) 6, 433-455.
3. A. Brisse, J. Schefold, M. Zahid, International J. of Hydrogen Energy (2008) 33, 5375-5382.
4. J. S. Herring, J. E. O'Brien, C. M. Stoots, G. W. Hawkes, J. J. Hartvigsen, M. Shahnam, International J. of Hydrogen Energy (2007) 32, 440-450.
5. J. D. Holladay, J. Hu, D.L. King, Y. Wang, Catalysis Today (2009) 139, 244-260.
6. S. Fujiwara, S. Kasai, H.Yamauchi , K. Yamada, S. Makino, K. Matsunaga, M. Yoshino, T. Kameda, T. Ogawa, S. Momma, E. Hoashi, Progress in Nuclear Energy (2008) 50, 422-426.
7. E. A. Harvego, M. G. McKellar, J. E. O'Brien, J. S. Herring, Nuclear Engineering and Design (2009) 239, 1571-1580.
8. K. Huang and J.B. Goodenough, Solid oxide fuel cell technology, Principles, performance and operation, Wood Head Publishing Limited, ISBN 978-1-84569-628-3.
9. A. J. Jacobson, Chem. Mater., (2010) 22, 660–674.
10. C. Sun, R. Hui, J. Roller, J. Solid State Electrochemistry (2010) 14, 1125-1144.
11. E. Siebert, A. Hammouche, M. Kleitz, Electrochimica Acta, (1995) 40,1741-1743.
12. M. Mogensen, S. Primdahl, M. J. Jérgensen, C. Bagger.J. Electroceramics (2000) 5, 141-152.
13. A. Virkar, I. J. Hydrogen Energy, (2010) 35, 9527-9543.
14. J. H. Kim, S. W. Baek, C. Lee, K. Park, J. Bae, Solid State Ionic (2008) 179, 1490-1496.
15. J. M. Ralph, A. C. Schoeler, M. Krumplet, J. Mat. Sc. (2001) 36, 1161-1172.
16. E. P. Murray, S. A. Barnett, Solid State Ionics (2001) 143, 265-273.
17. Y. Takeda, R. Kanno, M. Noda, Y. Tomida, O. Yamamoto, J. Electrochem. Soc. (1987) 134, 2656-2661.
18. 18. X. Meng, S. Lu, Y. Ji, Y Zhang, J. Power Sources (2008) 183, 581-585.
19. E. Tspis, V. V. Kharton, J. Solid State Electrochemistry (2008) 12, 1367-1391.
20. S. J. Skinner, J. Inorganic Materials (2001) 3, 113-121.
21. K.K. Hansen, K. V. Hansen, Solid State Ionics (2007) 178, 1379-1384.
22. 22. K.K. Hansen, J. Electrochemical Soc. (2009)156, B1257-B1260.
23. H. Y. Tu, Y. Takeda, N. Imanishi, O. Yamamoto, Solid State Ionics (1999) 117, 277-281.
24. X. Meng, S. Lu, Y. Ji, T. Wei, Y Zhang, J. Power Sources (2008) 183, 581-585.
25. K. Park, C. lee, J Bae, Y Yoo, International J. of Hydrogen Energy (2009) 34, 6852-6860.
26. Z. Shao, S. M. Haile, Nature, (2004) 431, 170-173.
27. C. J. Fu, K. Sun, N. Q. Zhang, X. b. Chen, D. R. Zhou, Electrochim Acta (2007) 52, 4589-4594.
28. V. Dusastre, J. A. Kilner,, Solid Stae Ionics, (1999) 126, 163-174.
29. B. C. H. Steele, Solid State Ionics, (2000) 129, 95-110.
30. B. Wei, Z. Lü, X. Huang, J. Miao, X. Sha, X. Xin, W. Su, J. Euro. Ceram. Soc. (2006)26, 2827- 2832.
31. G. Ch. Kostogloudis, Ch. Ftikos, Solid State Ionics, (1999)126, 143-151.
32. H. Ullmann, N. Trofimenko, F. Tiez, D. Stover, A. A.Khanlou, Solid State Ionics (2000)138, 79-90.
33. H. Uchida, S. Arisaka, M. Watanabe, J. Electrochemical Soc. (2002)149, A13-A18.
34. C. N. Munnings, S. J. Skinner, G. Amow, P. S. Whitfield, I. J. Davidson, Solid State Ionics, (2005)176, 1895-1901.
35. R. Sayers, J. Liu, B. Rustumji, S. J. Skinner, Fuel Cells, (2008)8, 338–343.
36. A. Tarancon, M. Burriel, J. Santiso, S. J. Skinner, J. A. Kilner, J. Mater. Chem. (2010) 20, 3799-3813.
37. S. J. Skinner, J. A. Kilner, Solid State Ionics (2000) 135, 709-712.
38. E. Boehm, J.M. Bassat, P. Dordor, F. Mauvy, J.C. Grenier, P. Stevens, Solid State Ionics (2005) 176, 2717–2725.
39. J. Dailly, S. Fourcade, A. Largeteau, F. Mauvy, J. C. Grenier, M. Marrony, Electrochimica Acta (2010) 55, 5847–5853.
40. J.C. Grenier, F. Chauveau, J. Dailly, C. Lalanne, M. Marrony, F. Mauvy, J. Mougin and J-M. Bassat, 216th ECS Meeting transaction, Abstract No1476 (2009).
41. P. Wei, X. H. Deng, M. R. Bateni and A. Petric, Corrosion (2007) 63, 529-536.
42. N. Shaigan, W. Qu, D. G. Ivey and W. X. Chen, J. Power Sources (2010) 195, 1529-1552.
43. H. Liu,X. Zhu, M. Cheng, Y.Cong and W. Yang, Chem. Comm. (2011) 47, 2378–2380.
44. T. Ishihara, T. Kudo, H. Matsuda, Y. Takita, J Electrochem Society (1995) 142, 1519-1524
45. L.W. Tai, M. M. Nasrallah, H. U. Anderson, D. M. Sparlin, S. R. Sehlin, Solid State Ionics (1995)76, 259-271.

46. A. Yan, M. Cheng, Y. Dong, W. Yang, V. Maragou, S. Song, P. Tsiakaras, Applied Catalysis B: Environmental (2006) 66, 64-71.
47. C. Xia, W. Rauch, F. Chen, M. Liu, Solid State Ionics (2002)149, 11-19.
48. K. Imahara, C.P. Jacobson, S.J. Visco, L.C. De Jonghe, (2005)176, 451-456.
49. H. Zhao, L. Huo, S. Gao, J. Power Sources (2004) 125, 149-154.
50. M. Mogensen, T. Lindegaard, U.R. Hansen, G. Mogensen J. Electrochem. Soc. (1994) 141, 2122-2128.
51. F. Tietz, I. Arul Raj, M. Zahid, D. Stover, Solid State Ionics (2006) 177, 1753-1756.
52. T. Kenjo, M. Nashiya, Solid State Ionics (1992) 57, 295-302.

Dr. P. K. Patro *obtained M.Sc. in Chemistry from Berhampur University, Odisha and Ph.D. in Materials Sc. from IIT-Bombay. He joined Energy Conversion Materials Section, Bhabha Atomic Research Centre Mumbai after completion of Dr. K. S. Krishnan Research Associateship (11th Batch) in 2007. He did a post-doctorate in Laboratory for Innovation in New Energy Technologies and Nanomaterials, French Atomic and Alternative Energy Department, Grenoble, France. His research interest is in synthesis and processing of advanced materials for solid oxide electrochemical cells and ferroelectric/ piezoelectric application, fabrication and electrical characterization of SOFCs, microstructure - property correlations in ceramics.*

Mr R. K. Lenka*: M.Sc in chemistry from Utkal University, Bhubaneswar, joined Energy Conversion Materials Section, Bhabha Atomic Research Centre in 2004 after completing one year orientation course from BARC training school. His research areas include synthesis and characterization of electroceramics and development of solid oxide fuel cell. Recently he submitted his thesis entitled "Nano Electroceramics for Intermediate Temperature Solid Oxide Fuel Cell" at HBNI, Mumbai.*

Dr. Tarasankar Mahata *obtained his B.E. (Metallurgy) from Bengal Engineering College (Calcutta University) in 1990, M.E. (Metallurgy) from Indian Institute of Science, Bangalore, in 1992 and Ph.D. (Materials Science) from Indian Institute of Technology (Bombay), Mumbai, in 2006. He joined BARC in 1993 after completing one year orientation course in Nuclear Science & Engineering at BARC Training School. Since then he is working as Scientific Officer in BARC in the field of Ceramic Processing, Ceramic Science and Powder Metallurgy. His current research interest: processing of oxide and non-oxide ceramics, characterisation of powder metallurgy products, fabrication and testing of solid oxide electrochemical cells, impedance spectroscopy. Dr. Mahata is life member of Indian Institute of Metals, Powder Metallurgy Association of India and Indian Nuclear Society.*

Shri P.K. Sinha *graduated in Chemical Engineering from Ranchi University, Bihar and joined Beryllium Pilot Plant, BARC in 1985. He has worked in development of beryllium technology in India and made outstanding contributions in powder metallurgy of Beryllium. He is recipient of DAE's Special Contribution Award 2008. He is currently heading Energy Conversion Material Section, Materials Group, BARC. His areas of interest involve the development of composite materials and shape forming through powder metallurgy route. He is a life member of Powder Metallurgy Association of India.*

Perovskite based electrolyte materials for proton conducting SOFCs

Pooja Sawant, S Varma, B N Wani, S R Bharadwaj
Chemistry Division, Bhabha Atomic Research Centre, Trombay Mumbai 400085
**Email:bnwani@barc.gov.in*

Abstract

This review focuses on the materials requirement, their structural properties, stability, conductivity behavior and electrochemical performance prerequisite as electrolyte materials used in proton conducting solid oxide fuel cells (SOFCs). The properties of ABO_3 type perovkite based ceramic electrolytes are briefly discussed, with emphasis on the approaches and findings reported during the last 15–20 years. Role of A- and B- site cations in the perovskite structures on electrical properties and their corresponding chemical stability in different atmospheres have been studied. Also, proton incorporation and transport phenomenon have been given in order to understand proton conductivity through these oxides.

Introduction

Limited natural fuel resources and an increase in energy demand, rising CO_2 emissions and the threat of global climate change have motivated researchers all over the world to deliver more efficient ways of extracting energy from already limited supplies, and to find more environmentally conscience energy sources. Fuel cells which is an alternative energy technology, have received growing attention in recent years since they have been one of the most promising energy production systems to reduce pollutant emissions. They are electrochemical devices that directly convert the chemical energy into electrical energy. Among the different types of fuel cells, the Solid Oxide Fuel Cell (SOFC) appears to be the most promising with regard to its fuel flexibility, efficient power generation and also provides significant environmental benefits [1-3]. Conventional SOFCs are based on oxygen ion-conducting electrolyte (SOFC-O), with state of art electrolyte, i.e., yttria-stabilized zirconia (YSZ) [4,5]. However, their high temperature operation (800-1000 °C), creates problems associated with the lack of stability and compatibility with other cell components. Recently SOFCs using ceramic proton conductors as a solid electrolyte (SOFC-H) have attracted the attention of researchers as compared to traditional oxide ion conductors due to their capability for low temperature operation [6-8]. Additionally, in contrast to oxide-ion-conducting fuel cells, the protonic fuel cells form water at the cathode side, hence the fuel at the anode remains pure and requires no treatment during recirculation. Fig. 1 shows the schematic mechanism of operation of oxide ion conducting and proton conducting SOFC.

In case of conventional ceramic oxygen ion conducting SOFCs, oxygen ions react with the hydrogen at the anode to produce water and liberate electrons in the external circuit. The oxygen ions are formed at the cathode by

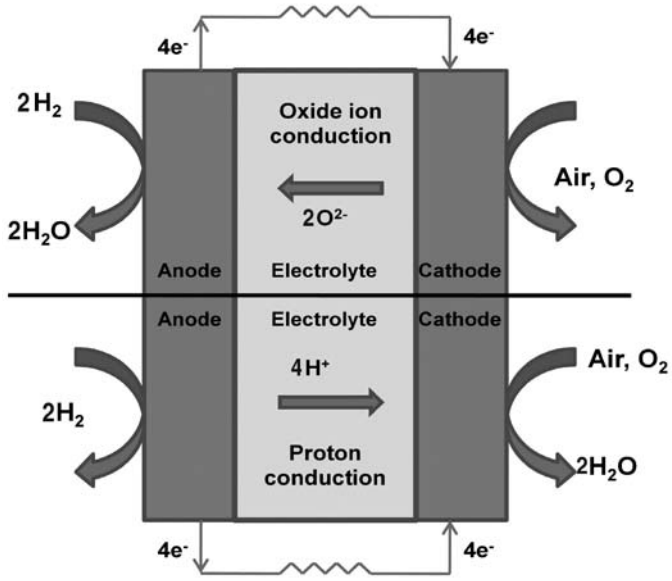

Fig.1. Diagram displaying the operation of oxide ion conducting and proton conducting SOFCs

reaction of oxygen from air with electrons recycled from the external circuit:

$$\text{Cathode} : O_2 + 4e^- \rightarrow 2O^{2-}$$
$$\text{Anode} : 2O^{2-} + 2H_2 \rightarrow 2H_2O + 4e^-$$
$$\text{Overall} : 2H_2 + O_2 \rightarrow 2H_2O + \Delta E$$

In case of proton conducting SOFCs, hydrogen is dissociated at the anode to form protons in the electrolyte and electrons in the external circuit. The protons are joined again with the electrons as well as oxygen at the cathode to produce water:

$$\text{Anode} : 2H_2 \rightarrow 4H^+ + 4e^-$$
$$\text{Cathode} : O_2 + 4H^+ + 4e^- \rightarrow 2H_2O$$
$$\text{Overall} : 2H_2 + O_2 \rightarrow 2H_2O + \Delta E$$

In early 1980s, Iwahara et al [9,10] found several perovskite-type oxides exhibiting high proton conductivity

at elevated temperatures, above 450 °C. Some non-perovskite type oxides or salts like $Ln_2Zr_2O_7$, $LaPO_4$ and α-alumina ceramics exhibit protonic conduction at elevated temperatures, but their conductivities are low compared to perovskite-oxides [11].

Perovskite based oxide Materials for Proton conduction

Several approaches have been reported in literature for the development of suitable proton conducting material. Among the various compounds investigated, perovskite oxides exhibit higher proton conductivity [12,13]. In addition to perovskites, binary rare earth oxides with fluorite-related structures and ternary oxides with the pyrochlore structure have been examined. Proton conductivities have been calculated from available data on proton concentrations and mobilities by Norby and Larring [14] for an extended temperature range and these have been summarized by Kreuer [15] as shown in Fig. 2.

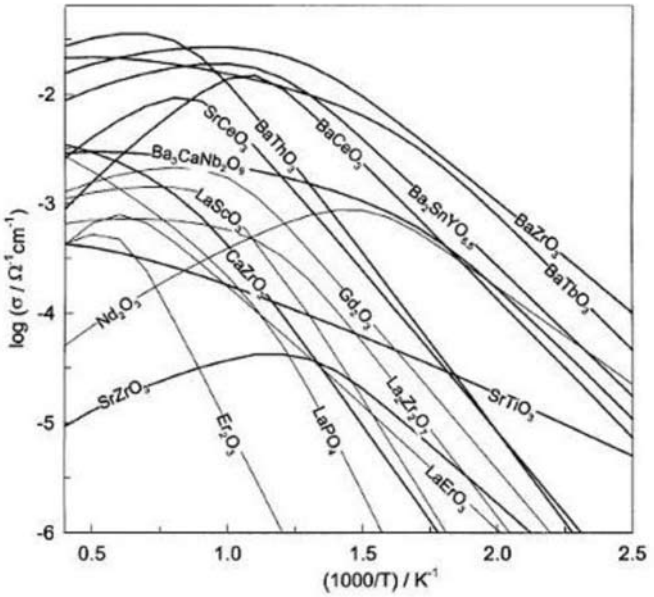

Fig. 2. Proton conductivities of various oxides as calculated from data on proton concentrations and mobilities, [14,15]

Many ABO_3 type perovskite doped with rare earth oxide exhibit protonic conduction when exposed to hydrogen and/or water vapour containing atmospheres over a wide range of temperatures. They have an alkaline earth element, such as Ba, Sr, and Ca in the A-site, while the B-site is occupied by a rare earth element, usually Ce and Zr. Proton conductivity of these electrolytes is dependent on the concentration of oxygen vacancies in the perovskites oxides. The oxygen vacancies in these oxides can be considerably increased by acceptor doping i.e. doping on the B-site by lower valance elements (LVE), such as Y, Nd, Sm, Yb, In, Eu, Gd, [16]. Literature data clearly demonstrate that the highest proton conductivities are observed for perovskite-type oxides, with $BaCeO_3$-based materials among the best proton-conducting oxides.

When oxygen is introduced from the environment, the following two reactions can occur:

$$2Ce^{X}_{Ce} + O^{X}_{o} + M_2O_3 \rightarrow 2M'_{Ce} + V^{\bullet\bullet}_{o} + 2CeO_2 \qquad (1)$$

$$1/2\ O_2 + V^{\bullet\bullet}_{o} \rightarrow O^{x}_{o} + 2h\bullet \qquad (2)$$

Water from the gas-phase dissociates into a hydroxide ion and a proton. Oxygen vacancies are then replaced by hydroxide ions and protons form covalent bonds with lattice oxygen. The following mechanism was proposed for the incorporation of protons in a hydrogen/water rich atmosphere [17,18].

$$H_2O_{(g)} + V^{\bullet\bullet}_{o} + O^{X}_{o} \rightarrow 2OH^{\bullet}_{o} \qquad (3)$$

Fig. 3 shows the hopping mechanism proposed by H. Iwahara et al [16] for proton conduction in perovskite oxides,

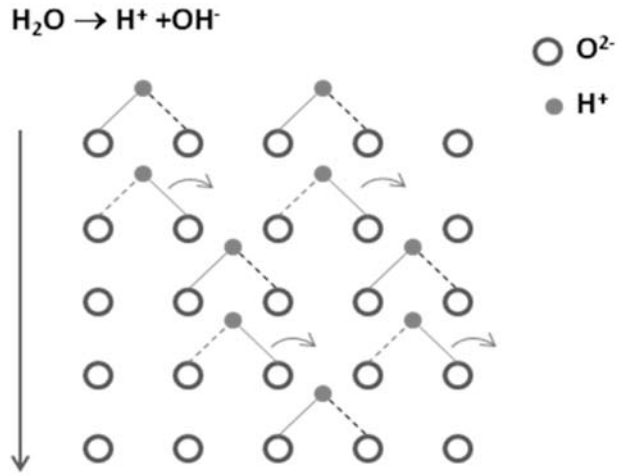

Fig. 3. Hopping mechanism of migration of proton from one oxygen ion to another nearest oxygen ion

Stability of proton conducting perovskite oxides

The most severe problem regarding both barium and strontium cerates based electrolytes is their low chemical stability. They react with acidic gases, e.g. CO_2, and with water vapour to form binary oxides and hydroxides, respectively. For example barium cerate reacts with CO_2 (equ.4) and with H_2O (equ.5) to form barium carbonate and bariun hydroxide respectively.

$$BaCeO_3 + CO_2 \rightarrow BaCO_3 + CeO_2 \qquad (4)$$

$$BaCeO_3 + H_2O \rightarrow Ba(OH)_2 + CeO_2 \qquad (5)$$

Since the use of hydrocarbon fuels (such as methane) can lead to the production of CO_2 and H_2O, the chemical instability of cerates in presence of these gases excludes

their application in fuel cell using hydrocarbon fuels. In comparison to the cerates, $BaZrO_3$-based oxides offer excellent chemical stability against reaction with CO_2 and H_2O. The stability of the perovskite structure has often been rationalized in terms of radii of the ions comprising the unit cell using a parameter known as the Goldschmidt tolerance factor (t), which is defined as:

$$t = \frac{r_A + r_O}{\sqrt{2}(r_B + r_O)}$$

where r_A, r_B and r_O are the ionic radius of A, B, and O ion, respectively. Virkar et al. [19,20] have successfully explained the stability of many perovskites in terms of the tolerance factor. The tolerance factor, which is a measure of ionic packing, is 1.0 for the ideal perovskite structure. Most perovskites deviate from this ideal value. However, it is known that the perovskite structure is stable, if the value of the tolerance factor (t) is close to unity. For example, in Table 1, Y doped $BaCeO_3$ has a tolerance factor over ~0.85 and it is unstable in CO_2 and H_2O atmosphere on the other hand Y doped $BaZrO_3$ has a tolerance factor of ~0.90, and is stable in both environments. While solid solutions of cerates and zirconates having high concentration of Zr are more stable as compared to compositions containing low concentration of Zr in these atmospheres.

Table 1 - Crystalline tolerance factors for different compounds and their stability under CO_2 and H_2O treatment [21]

Compound	Tolerance factor	Stability	
		in H_2O	in CO_2
$BaCe_{0.8}Y_{0.2}O_{3-\delta}$	0.85	Unstable	unstable
$BaCe_{0.6}Zr_{0.2}Y_{0.2}O_{3-\delta}$	0.86	unstable	unstable
$BaCe_{0.4}Zr_{0.4}Y_{0.2}O_{3-\delta}$	0.87	stable	quite stable
$BaCe_{0.2}Zr_{0.6}Y_{0.2}O_{3-\delta}$	0.88	stable	stable
$BaZr_{0.8}Y_{0.2}O_{3-\delta}$	0.90	stable	stable

Stability with respect to formation of carbonates and hydroxides in presence of CO_2 and H_2O respectively, increases from cerate to zirconate i.e. with increase of electronegativity of B-site cation [22].

The reaction of an ABO_3 perovskite with CO_2 (as per equ.5), where, A= Ba, Sr and B= Ce, Zr, can be broken into the following two reactions

$$ABO_3 \rightarrow AO + BO_2 \qquad (6)$$

$$AO + CO_2 \rightarrow ACO_3 \qquad (7)$$

Data on the formation enthalpy of the perovskite from the binary oxides (equ.6) and on the stability of the carbonate with respect to AO oxide (equ.7) help to understand the thermodynamics of the above reactions [23]. The formation enthalpies of different perovskite oxides, given in Table 2 [24,25] reflects the high chemical stability of $BaZrO_3$ compared to the other oxides. It has been observed that $\Delta H°$ for the formation of the perovskite from the individual oxides shows a correlation with the perovskite tolerance factor t [26] where stability increases with increasing perovskite tolerance factor from cerates to zirconates.

Table 2 – Enthalpy of formation (at 298.15 K) from oxides for some perovskite oxides

ABO_3	$\Delta H°$[kJ/mol]
$BaCeO_3$	-57
$SrCeO_3$	-6
$BaZrO_3$	-128
$SrZrO_3$	-74

Conductivity of perovskite oxides

Protonic conductivities of typical perovskite oxides in hydrogen atmosphere of the order of 10^{-2}–10^{-3} Scm^{-1} at 1000-600 °C are shown in Fig. 4.

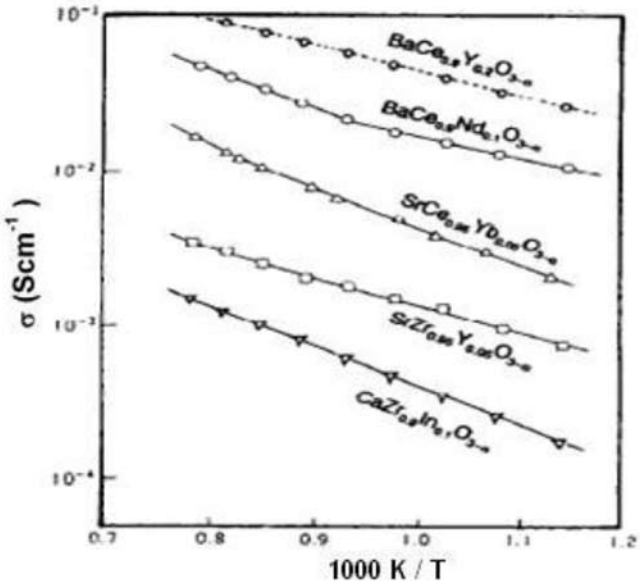

Fig. 4. Proton conductivity of some of perovskite oxides in H_2 gas atmosphere [16]

Research on proton conducting materials suggested doped $BaCeO_3$ based perovskite oxides shows the highest proton conductivity (about 10^{-2} Scm^{-1} at 600 °C). However, with increasing temperature their transport number of protons i.e. the ratio between proton conductivity and total electrical conductivity decreases and they become

oxygen ion conductors at high temperatures. Similarly, doped $SrCeO_3$ based oxides, show proton conductivity with a proton transport number higher than that of barium cerates however they have rather lower conductivity values than $BaCeO_3$ based oxides [16]. Therefore $BaCeO_3$ based oxides have became benchmark materials for high proton conductivity indicating that chemical and structural parameters play crucial role towards proton conductivity. Orthorhombic distortion from the ideal cubic perovskite structure is smaller in $BaCeO_3$ oxides as compared to $SrCeO_3$, due to their highest molar volume (lattice constants) than $SrCeO_3$. Deviations from the ideal cubic perovskite structure may lead to higher activation enthalpy for proton conduction. The activation energy for Y doped $BaCeO_3$ and Y doped $SrCeO_3$, obtained from the slope of the Arrhenius plot (Fig. 5) is 0.66 eV and 0.72 eV respectively [27].

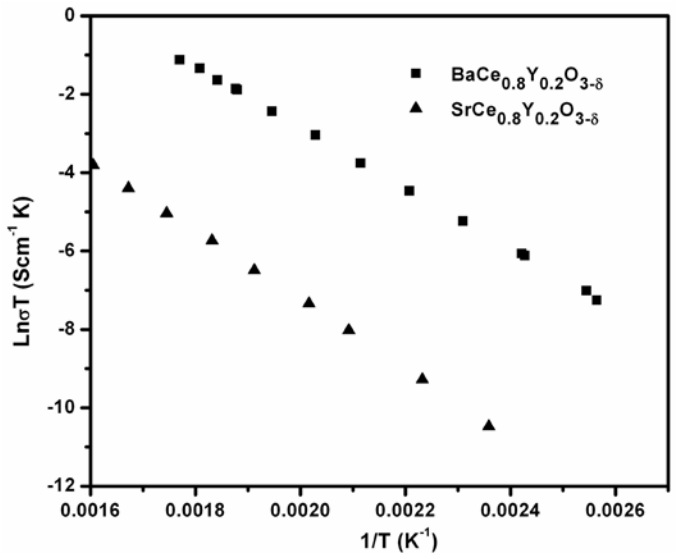

Fig. 5. Arrhenius plot for proton conduction in Y doped $BaCeO_3$ and Y doped $SrCeO_3$

In the distorted structure of Y doped $SrCeO_3$ the cubic oxygen site degenerates into two sites with probabilities of 1/3 for O1 and 2/3 for O2. These oxygen atoms show different chemical interactions with the cations, and therefore have different basicity which leads to different binding energies between protons and the oxygen on different sites. By contrast, in the high temperature phases of $BaCeO_3$ based oxides, these oxygen sites are crystallographically and energetically equivalent. The different crystal structure of $BaCeO_3$ and $SrCeO_3$ based oxides influence their proton conduction properties. Whereas in $SrCeO_3$ based oxides proton transport must involve transfer between chemically different O1 and O2 sites, in $BaCeO_3$ based oxides protons may show proton transport via the equivalent oxygen sites. This could explain the higher activation enthalpy and lower conductivity in $SrCeO_3$ compared with $BaCeO_3$ based oxides.

The protonic conduction in these oxides was confirmed by electrochemical hydrogen transport experiments in hydrogen or water vapor containing atmosphere at elevated temperatures. In contrast to cerates, zirconate-based protonic conductors have relatively low conductivity but good chemical stability. One way to achieve both excellent chemical stability and proton conductivity is to prepare a solid solution between cerate and zirconate by replacing desired fraction of the Ce with Zr. Fig. 6 shows the Arrhenius plot for proton conduction through solid solutions of cerates and zirconates where A- cation is Ba/Sr and B- site of Ce/Zr is doped with 20% Y [28]. The introduction of Zr into cerate clearly resulted in a reduction of the conductivity in the temperature range of 400 to 1000 K. Although any local ordering accompanying Zr/Ce mixing on the B-site is expected to reduce the proton mobility, the corresponding lattice expansion is anticipated to be advantageous with respect to the proton mobility provided that a close to cubic symmetry is maintained.

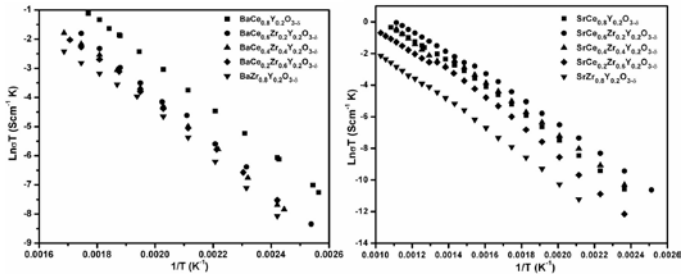

Fig. 6. Arrhenius plot for proton conduction in Y doped solid solutions of $BaCeO_3$- $BaZrO_3$ and $SrCeO_3$-$SrZrO_3$ [28]

Challenges and Future opportunities for Proton conducting SOFCs

The challenges for proton conducting SOFCs mainly concern their chemical stability in presence of water and CO_2 atmosphere for perovskite based electrolyte materials. The key is to obtain electrolyte material which is chemically inert in presence of moisture and have adequate protonic conductivity at intermediate temperatures. Secondly in spite of reduction in operating temperature selection of compatible electrode material is another issue that places constraints on proton conducting SOFCs commercialization. Development of suitable electrode materials for these proton conducting electrolytes will be the challenge for future material scientists.

References

1. A. B. Stambouli, E. Traversa, Renewable and Sustainable Energy Reviews, 6 (2002) 433.

2. S.C. Singhal, K. Kendall (2003) High temperature solid oxide fuel cells: fundamentals, design, and applications. Elsevier, Oxford, pp 1–22.
3. S.M. Haile, Acta Materialia, 51 (2003) 5981.
4. W. Vielstich, A. Lamm, H. Gasteiger, Handbook of Fuel Cells: Fundamentals, Technology, Applications, 4-Volume Set. New York. Wiley. 2003.
5. N.P. Brandon, S. Skinner and B.C.H. Steele, Annu. Rev. Mater. Res., 33 (2003) 183.
6. H.G. Bohn, T. Schober, J. Am. Ceram. Soc., 83 (2000) 768.
7. K. Katahira, Y. Kohchi, T. Shimura, H. Iwahara, Solid State Ionics, 138 (2000) 91.
8. K.D. Kreuer, St. Adams, W. Munch, A. Fuchs, U. Klock, J. Maier, Solid State Ionics, 145 (2001) 295.
9. H. Iwahara, H. Uchida, S. Tanaka, Solid State Ionics, 9-10 (1983) 1021.
10. H. Iwahara, H. Uchida, K. Ono and K. Ogaki, J. Electrochem. Soc., 135 (1988) 529.
11. H. Iwahara, Y. Asakurab, K. Katahirac, M. Tanakad, Solid State Ionics, 168 (2004) 299.
12. R. Haugsrud, Y. Larring, T. Norby, Solid State Ionics, 176 (2005) 2957.
13. K. Amezawa, Y. Kitajima, Y. Tomii, N. Yamamoto, M. Widerøe, T. Norby, Solid State Ionics, 176 (2005) 2867.
14. T. Norby, Y. Larring, Curr. Opin. Solid State Mater. Sci., 2 (1997) 593.
15. K.D. Kreuer, Annu. Rev. Mater. Res., 33 (2003) 333.
16. H. Iwahara, Solid state Ionics, 86-88 (1996) 9.
17. N.V. Sharova, V.P. Gorelov, Russ. J. Electrochem. 39 (2003) 461.
18. R. Glockner, M. Islam, T. Norby, Solid State Ionics 122 (1999) 145.
19. W. Meng, A.V. Virkar, J. Solid State Chem. 148 (1999) 492.
20. S. Bhide, A. Virkar, J. Electrochem. Soc. 146 (1999) 4386.
21. P. Sawant, S. Varma, B.N. Wani and S.R. Bharadwaj, Int. J. Hydrogen Energy, 37 (2012) 3848.
22. K.D. Kreuer,. Solid State Ionics, 125 (1999) 285.
23. W. Münch, K.D. Kreuer, G. Seifert, J. Maier, Solid State Ionics 136-137 (2000) 183.
24. E.H.P. Cordfunke, A.S. Booij, M.E. Huntelaar, J. Chem. Themodynam., 30 (1998) 437.
25. K.T. Jacob, Y. Waseda, Met. Mat. Trans., 26B (1995) 775.
26. S.M. Haile, G. Staneff, K.H. Ryu, J. Mater. Sci., 36 (2001) 1149.
27. P. Sawant, S. Varma, B.N. Wani, S.R. Bharadwaj, Unpublished work, (2012).
28. P. Sawant, D. Jain, S. Varma, B.N. Wani, S.R. Bharadwaj, Unpublished work, (2012).

Ms. Pooja P. Sawant, *is pursuing her Ph.D in Chemistry at Bhabha Atomic Research Centre (BARC) Mumbai under the guidance of Dr. Shyamala Bharadwaj. She obtained her M.Sc. degree in Chemistry from University of Mumbai in 2008. Her research work involves the development of various cell components for Proton Conducting Solid Oxide Fuel Cell (SOFC-H) and study various properties of these materials.*

Dr. Salil Varma *joined Bhabha Atomic Research Centre through 40th batch of Training School in 1996 after completing M.Sc. (Analytical Chemistry) from Mumbai University. He has been involved in research related to development of catalysts for DAE related applications. He completed his PhD in 2004, followed by post-doctoral research at University of Leipzig, Germany, on substituted rare earth orthovanadates for environmental applications. Currently, He has been involved in development of noble metal based catalysts for mitigation of hydrogen in nuclear reactor containment under LOCA conditions and production of hydrogen by sulphur-iodine thermochemical cycle and materials for application in solid oxide fuel cell. He has about 35 publications in international journals and has been recipient of DAE Group achievement award 2010 and Alexander von Humboldt fellowship 2004.*

Dr (Ms) Bina Wani*, working as a Scientific Officer at Chemistry Division, Bhabha Atomic Research Center (BARC). She obtained her M. Sc. degree from Bombay University in the year 1982 and awarded Ph. D degree in Chemistry in the year 1986 from the same University. Her research interest lies in the development of various cell components in Solid Oxide Fuel Cell at intermediate temperature (IT-SOFC). Recently she is involved in exploring various materials used in proton conducting SOFCs. She is also involved in developing mixed oxide based catalyst for pollution abetment. She has 64 publications in a various reputed international journals to her credit. She is a recipient of DAE Group Achievement Award 2010.*

Dr. Shyamala Bharadwaj *is presently Head, Fuel Cell Materials & Catalysis Section, Chemistry Division, Bhabha Atomic Research Centre, Mumbai, India. She obtained her M.Sc. in Chemistry in 1981 and her Ph.D. in Physical Chemistry in 1991 from Mumbai University. Her main area of work during the past 35 years has been determination of thermodynamic properties of nuclear materials using various techniques such as vapour pressure measurements, thermogravimetry, isoperibol calorimeter etc. During 2000-2001, she worked as guest scientist at Juelich Research Centre, Juelich, Germany on Solid Oxide Fuel Cell (SOFC) materials. Her current interests are in the fields of Intermediate Temperature Solid Oxide Fuel Cells (ITSOFC) and Sulphur – Iodine thermochemical cycle for generation of hydrogen from water. She was awarded the NETZSCH –ITAS Award (2006) by the Indian Thermal Analysis Society in the year 2006 for her contributions in the field of thermal analysis. DAE Group Achievement Award for the year 2010 was awarded to her Group for their work on catalysis. She is the Regional Editor for the Journal of Thermal Analysis and Calorimetry. She has been Hon. Treasurer and Hon. Secretary of Indian Thermal Analysis Society during the period of 1998 to 2005 and was involved in organizing several National Symposia and Workshops on Thermal Analysis in various parts of India. She has played active role in organizing the previous ISMC conferences (2006 to 2010) and also the current one (ISMC 2012). She has more than 120 papers in refereed international journals and more than 150 papers in National and International Symposia.*

Materials for IT-SOFC by Spray Pyrolysis

L.D. Jadhav

Rajaram College, Kolhapur- 416 004.
E-mail: ldjadhav.phy@gmail.com

Introduction

Thin films have proved their importance in almost every field of research and have become an integral part of several technologies. Numerous materials have been prepared in the form of thin films in the past century because of their potential technical value and scientific curiosity. in their properties. Thin films have many advantages over the bulk such as high surface to volume ratio; geometrical control (dictated by substrate); compactness; single crystal like properties. Thin films can be made amorphous, single crystalline, polycrystalline or epitaxial to tune with the end application. Thin film materials have been used in microelectronic devices, telecommunication devices, wear resistant coatings, decorative coatings, optical coatings (windows, solar cells, etc.), sensors, catalysts etc. Many reviews on thin film solar cells are available [1].

Several investigations have been made in search of the most suitable technique of producing thin films. Broadly, the techniques can be grouped into the vacuum-based and chemical techniques. The chemical techniques include dip coating, spin coating, spray pyrolysis etc [1]. Of these, spray pyrolysis have been known since 1966 when it was first used in CdS for solar cells. The technique has very widely been employed to prepare thin and thick films, ceramic coatings etc. using powders of noble metals, metal oxides, spinel oxides, chalcogenides and superconducting compounds [1-2]. Unlike other techniques, spray pyrolysis uses simple apparatus and hence represents a cost effective deposition method. It does not require high quality substrates or chemicals and can be used for preparing multi-layered films of any composition. It offers an extremely easy way to dope films with any element in any proportion.

Appraisal of spray pyrolysis for the SOFC materials

Solid oxide fuel cell (SOFC) is a well-known and highly efficient power generation device. SOFC converts gaseous fuel electrochemically into electricity in a highly efficient (~60%) and eco-friendly (virtually zero pollution) manner. However, the commercialization of SOFCs has not been fully demonstrated due to its initial cost of fabrication and degradation during its prolonged operation. All these problems have originated from its high operating temperature of the order of 1000 °C. Therefore, reducing the operating temperature of the SOFCs is desirable. This gives intermediate temperature SOFCs (IT-SOFCs). Although a reduction in the operating temperature is more favorable for less degradation, it is associated with a drop in electrochemical performance of the integrated ceramic materials. This performance reduction at intermediate temperatures can be tackled by different strategies [3].

A solid electrolyte is the heart of the SOFC and its conductivity inevitably decides the operating temperature. The first approach is replacing the conventional solid electrolyte e.g. yttria stabilized zirconia (YSZ) with an alternate solid electrolyte materials, which have high ionic conductivity at relatively low temperatures. A second approach is to identify the losses that are responsible for the drop in the electrochemical performance. Anodic and cathodic losses are attributed to the reduced surface exchange and diffusion kinetics. The reduction in the conductivity of an electrolyte due to ohmic loss also degrades electrochemical performance. Since the ohmic loss increases with the thickness of the electrolyte, thin electrolyte of few tenths of micron can significantly reduce the loss of electrochemical performance.

In addition to these approaches, a concept of thin film SOFCs has emerged wherein all SOFC components are essentially in thin film leading to μ-SOFCs. These are most suitable for portable electronic devices. μ-SOFCs operate at operating temperatures of 400–600 °C. Very recently, use of an anode functional layer (AFL) between the anode substrate and electrolyte of thickness of 10– 40 μm has been suggested to enhance the cell performance and to prevent the quick cell degradation [4].

In view of these, in recent past, use of thin films in SOFC has been envisaged and several research groups around the world are working on spray pyrolysis. The processing parameters of the spray pyrolysis can be tailored to control deposition microstructure and to deposit dense or porous films on polycrystalline, single crystalline or textured substrates. The spray pyrolysis technique is very attractive for the planar SOFC industry because it allows the deposition of a wide variety of ceramic films over large areas. Additionally, the technique is probably the cheapest and simplest of all the processes. SOFC electrolytes, interconnects, anodes and cathodes have been successfully prepared by spray pyrolysis.

Spray Pyrolysis: Apparatus and processing parameters

Fig. 1 shows the schematic diagram of the experimental setup of spray pyrolysis technique. The apparatus consists of an atomizing chamber producing the droplets of the starting materials. Droplets are conducted to a reactor, with air as the carrier gas. Thin film deposition using spray pyrolysis can be divided into three main steps: atomization of the precursor solution, transport of the resultant aerosol and decomposition of the precursor on the substrate.

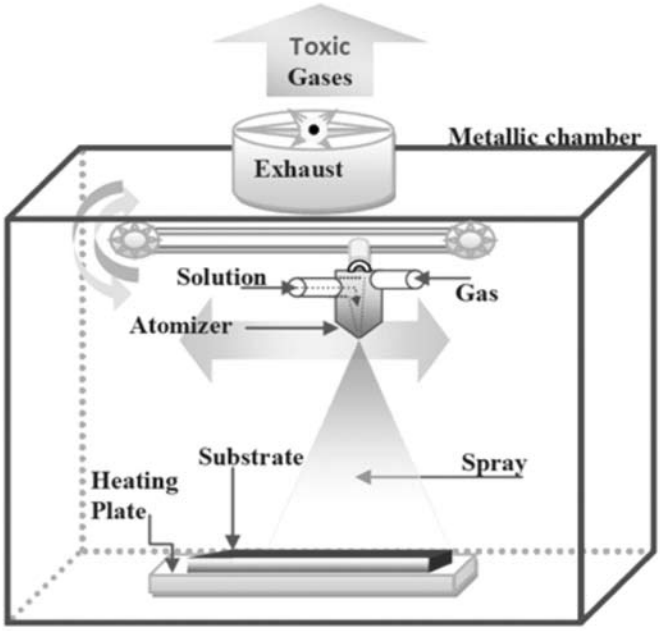

Fig. 1. The schematic diagram of the experimental setup of spray pyrolysis technique.

Several types of spray pyrolysis methods are available, based upon the atomizer such as electrostatic, gas pressurized, ultrasonic or air atomized. The method of atomization mainly determines the droplet size of the generated aerosol, which in turn determines the film quality. Each atomization type has advantages and drawbacks in terms of the complexity and quality of the deposit. Air atomized spray pyrolysis has been used in all our work.

The main process parameters of the spray deposition are the deposition (i.e. substrate) temperature, the solution flow rate, the composition and concentration of precursor compound, the solvent properties and the droplet size distribution. In addition to the above parameters, optimization of nozzle to substrate distance, and speed of nozzle is required. Once optimized, for the set up shown in the Fig. 1, the other parameters can be varied to see their effects on the film properties. Also the nature of the substrate surface can influence the film nucleation and growth. The substrate temperature is usually held at 150-550 °C. A typical solution flow rate is 5- 20 ml/minute. Various precursors (halides, acetates, nitrates and organo-metallic compounds) and solvents, e.g., water, butanol, butyl acetate and butyl carbitol, are used.

SOFC components by Spray Pyrolysis

Spray pyrolysis is versatile method and up till now it has been used to deposit porous electrodes and at the same time very dense electrolyte materials. The different materials deposited on to different substrates by spray pyrolysis are summarized in sections below.

The precursor solutions were prepared by dissolving appropriate amounts of metal nitrates in double distilled water. The solution was then sprayed using glass nozzle with air as carrier gas onto different substrates kept at optimized temperature. The crystallization of the material was achieved by subsequent annealing. The details of experiments can be found elsewhere [5]. In general, one of the processing parameters was varied keeping the others constant.

Gd doped Ceria

The high ionic conductivity of 10 mol % Gd doped Ceria (GDC-10) at 773- 923K compared to conventional solid electrolyte, Yttria stabilized Zirconia (YSZ), make it appropriate to implement in IT-SOFCs. Further, if GDC is fabricated in thin film, it would keep the ohmic loss at minimum level and allow the SOFC to operate at still lower temperature. Various thin film deposition methods have been applied so far e.g. electrochemical vapor deposition (EVD) [6], physical vapor deposition (PVD) [7], vacuum plasma spraying [8], tape casting [9], screen printing [10], slurry dip coating technique [11], chemical spray technique [12], aerosol-assisted metal-organic chemical vapor deposition (AA-MOCVD) technique [13], etc.

Figure 2 shows XRD patterns of the thin films of GDC-10 deposited at different substrate temperatures. XRD reveals polycrystalline film for substrate temperature of 300°C, and the crystallinity decreased for further rise in substrate temperature. Films have preferred orientation along (200) for the substrate temperatures in the range 325-375°C while it is amorphous for 400°C. The SEM of the film deposited at 300 °C is as shown in Fig. 3.

Films with variable thicknesses were obtained by spraying different amounts of solutions for different lengths of time. The dependence of electrical properties over the film thickness was studied using two-probe dc conductivity measurement technique. Two silver electrodes separated by 1cm were marked on GDC10 thin films using silver paste and were heat treated at 500°C for 2h. Two

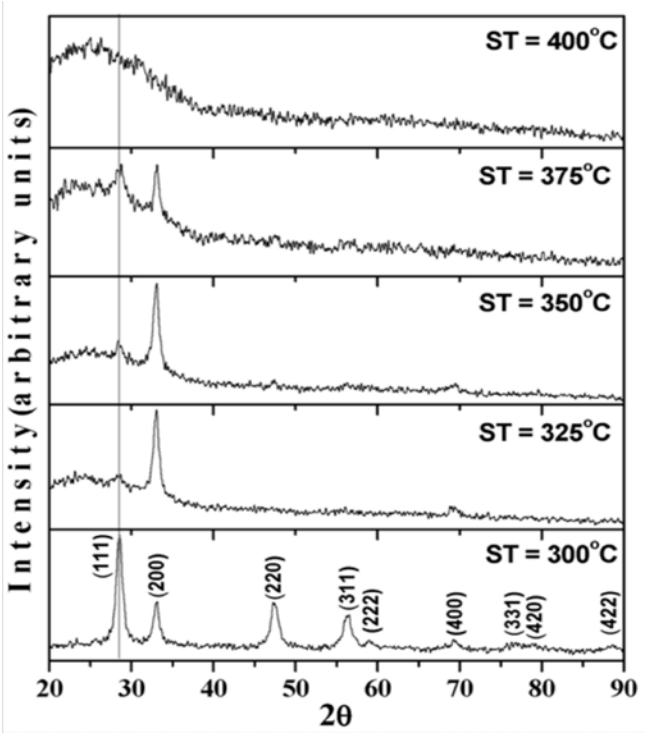

Fig. 2. XRD patterns of the thin films of GDC-10 deposited at different substrate temperatures

pressure point contacts were made from these two silver strips onto films, to apply the voltage bias and to measure the current. The current and voltage were used to calculate the resistance of the thin film, which was further used to determine its resistivity and conductivity. Fig. 4 shows the variation of conductivity values measured at 555°C and 450°C, for different film thickness. The dc conductivity was observed to be ~0.3 S/cm at 450°C, which is three times than that of YSZ at 1000°C (0.1S/cm). The conductivity for 3.3µm thick film is 0.03S/cm at 450°C and 0.12 S/cm at 555°C. On the contrary, GDC10 bulk sample (thickness = 1.78mm) sintered at 1500°C showed conductivity of 0.0011 S/cm at 555°C [14].

A stable chemical composition obtained from the spray pyrolysed films helps in a constant oxygen ion vacancy migration over the film thickness. The activation energy for oxygen ion transport increased with the film thickness as shown in Table 1.

Table 1. Estimated activation energies (>480°C) of GDC10 thin films.

Film thickness (µm)	Ea (eV)
3.30	0.98
1.40	0.79
0.93	0.73
0.50	0.71
0.45	0.61

However, measuring the bulk density of these films was a bit difficult. So films were deposited on to GDC10 pellets prepared by solid state route having more than 95 % of the theoretical density. The SEM shown in Fig. 5 reveals that the films have almost same density as that of the pellet. In addition to this, GDC 10 films of ~13 µm have also been deposited on to NiO-GDC 10 composites, which were used to form anode supported cell with thin electrolyte [15-16].

Yttria stabilized Zirconia (YSZ)

Yttrium stabilized zirconia (YSZ) is an attractive material because of high chemical and thermal stability, and good ionic conductivity. YSZ is the most popular electrolyte material for solid oxide fuel cells (SOFCs) because it conducts only oxygen ions over a wide range of oxygen partial pressures. SOFCs based on bulk (200–500 µm thick) YSZ membranes are normally operated at temperatures above 800 °C in order to achieve sufficiently high oxygen ion conductivity [17]. Although it is disregarded due to high operating temperature, its importance compared to its counterparts cannot be overlooked. Very recently, resurgence of interest in the YSZ films has developed. The

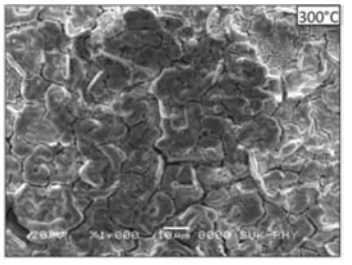

Fig. 3. The SEM of the GDC 10 film deposited at 300 oC.

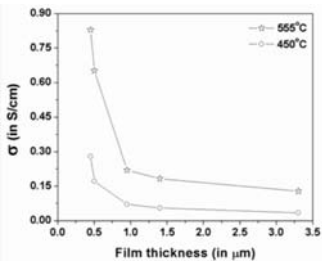

Fig. 4. The variation of conductivity with film thickness at 555°C and 450°C.

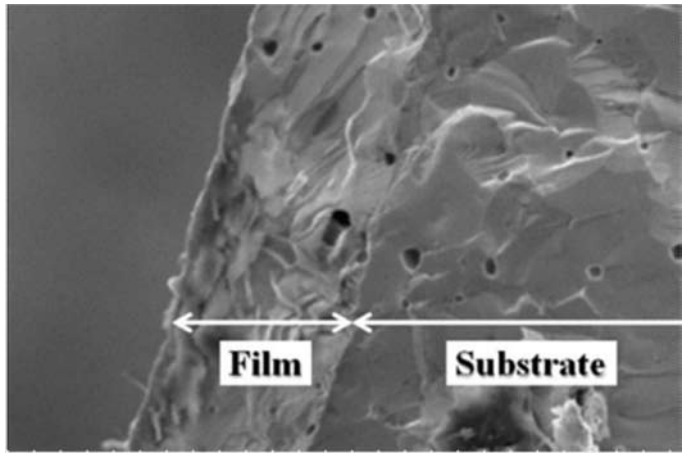

Fig. 5. SEM of GDC10 film deposited on GDC10 pellet.

YSZ film electrolyte were fabricated using pressing-heating technique [18], aqueous tape casting [19], chemical vapor deposition (CVD) [20], flame assisted vapor deposition [21], and physical vapor deposition (PVD) techniques (arc discharge deposition, DC sputtering, DC/pulsed DC magnetron sputtering, and e-beam deposition) [22,23].

In spray pyrolysis, the YSZ films were deposited from the precursor solution of zirconyl nitrate (ZrN_2O_7) and yttrium nitrate hexahydrate ($Y(NO_3)_3 \cdot 6H_2O$) taken in the stoichiometric amounts. The deposition was carried at substrate temperature of 400 ± 5 ◦C with the assistance of pressurized air sustained at the pressure of 1.5 kg cm^{-2} [24].

XRD pattern of YSZ film is shown in Fig.6. It shows a highly oriented (101) peak. The sharpness of (101) peak exhibits the high degree of texture with texture coefficient of 1.11. The crystallite size was about 26 nm. The film crystallized in tetragonal structure with no secondary phase. The lattice parameters were a = 3.596 ˚A and c = 5.199 ˚A with the c/a ratio of 1.44.

Impedance spectra of YSZ showed in Fig. 7 have only one semi-circle. This may be due to the negligibly small resistance offered by the electrode and relatively clean grain boundary in comparison to YSZ grains [24] and hence no contribution of electrode and grain boundary conductivity. Further the absence of grain boundary contribution reveals the purity and high density of the films. The total impedance decreases with rise of temperature. This may be due to the concentration of thermally activated oxygen ion vacancies, which results in the increase of diffusion coefficient for oxygen ion and hence the oxygen ionic conductivity.

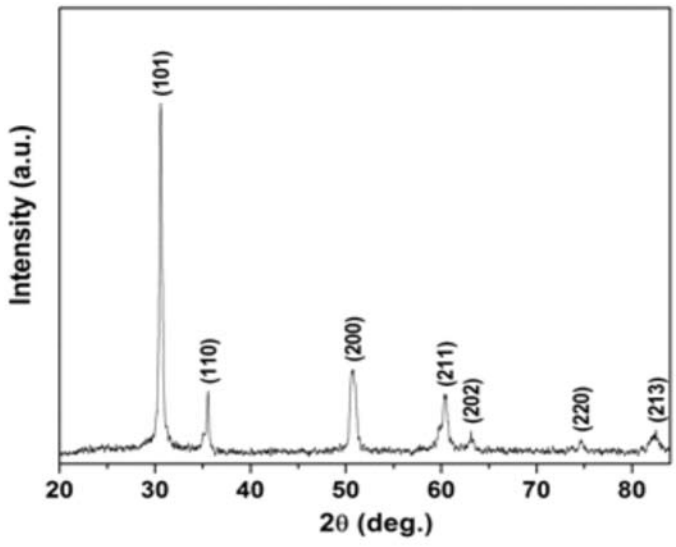

Fig. 6. XRD pattern of YSZ film.

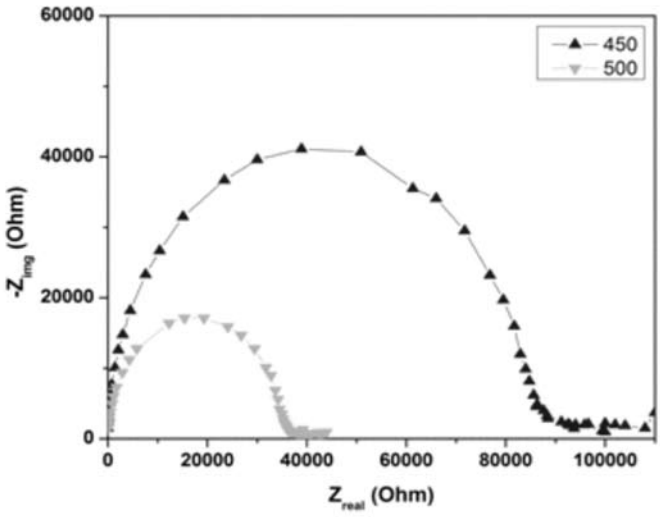

Fig. 7. Impedance spectra of YSZ at 450 and 550 °C

Electrode Materials

Electrodes, (both anode and cathode) should have favorable catalytic activity and high electronic conductivity. But often anodic and cathodic losses degrade the cell performance. Hence much attention has been focused on minimizing these losses. One way is to increase the number of reaction sites on the electrodes. The electrochemical reactions are known to occur at triple phase boundary (TPB) sites, where the reactant gas phase comes into contact with the electronic conductor and ionic conductor. Increasing the extent of TPBs in the electrode thereby can be used to increase the reaction sites and produce better electrochemical performance. Also, a highly porous electrode is required to efficiently supply fuel gas to the TPB sites. Therefore, designing and controlling the microstructure of the electrode is critical in improving cell performance [25]. Spray pyrolysis has proved its importance in controlling the microstructure and hence can be used to prepare suitable electrode materials.

References

1. P.S. Patil, *Materials Chemistry and Physics* 59 (1999) 185±198.
2. Z. Shao, W. Zhou, Z. Zhu, *Progress in Materials Science* 57 (2012) 804–874.
3. N. I. Karageorgakis, A. Heel, T. Graule, L. J. Gauckler, *Solid State Ionics* 192 (2011) 464–471.
4. M. Morales, M. E. Navarro, X. G. Capdevila, J. J. Roa, M. Segarra, *Ceramics International* 38 (2012) 3713–3722.
5. M.G. Chourashiya, S.H. Pawar, L.D. Jadhav, *Applied Surface Science* 254 (2008) 3431–3435.
6. M. F. Carolan, J. N. Michaels, *Solid State Ionics* 37 (1990) 189.
7. K. Honegger, E. Batawi, C. Sprecher, R. Diethelm, in: *U. Stimming, S.C. Singhal, H. Tagawa, W. Lehnert (Eds.), Proc. 5th Int. Symp. Solid Oxide Fuel Cells, Electrochemical Society,*

Pennington, NJ, 97 (1997) 321.

8. M. Lang, R. Henne, S. Schaper, G. Schiller, *J. Therm. Spray Technol.* 10 (2001) 618.
9. N.Q. Minh, K. Montgomery, *in: U. Stimming, S.C. Singhal, H. Tagawa, W. Lehnert (Eds.), Proc. 5th Int. Symp. Solid Oxide Fuel Cells, Electrochemical Society, Pennington, NJ,* 97 (1997) 153.
10. J. Herle, R. Ihringer, R.V. Cavieres, L. Constantin, O. Bucheli, *J. Eur.Ceram. Soc.* 21 (2001) 1855.
11. T. L. Nguyen, K. Kobayashi, T. Honda, Y. Iimura, K. Kato, A. Neghisi, K. Nozaki, F. Tappero, K. Sasaki, H. Shirahama, K. Ota, M. Dokiya, T. Kato, *Solid State Ionics* 174 (2004) 163.
12. P. Bohac, L. Gauckler, *Solid State Ionics* 119 (1999) 317.
13. Y.J. Leng, S.H. Chan, S.P. Jiang, K.A. Khor, *Solid State Ionics* 170 (2004) 9.
14. M.G. Chourashiya, J.Y. Patil, S.H. Pawar, L.D. Jadhav, *Materials Chemistry and Physics* 109 (2008) 39–44.
15. L. A. Ekal, D. D. Shivagan, P. M. Shirage, N. V. Desai, S. B. Mane, S. H. Pawar, *Thin Solid Films* 397 (2001) 249–254.
16. M. G. Chourashiya, L. D. Jadhav, *International Journal of Hydrogen Energy* 36 (2011) 14984-14995.
17. G. Laukaitis, J. Dudonis, D. Milcius, *Thin Solid Films* 515 (2006) 678–682.
18. J. Larminie, A. Dicks, *Fuel Cells Systems Explained,* JohnWiley and Sons Ltd., 2003.
19. F. Snijkers, A. de Wilde, S. Mullens, J. Luyten, *J. Eur. Ceram. Soc.* 24 (2004) 1107.
20. H. B. Wang, C. R. Xia, G. Y. Meng, D. K. Peng, *Mater. Lett.* 44 (2000) 23.
21. S. Charojrochkul, K.L. Choy, B.C. H.Steele, *J. Eur. Ceram. Soc.* 24 (2004) 2515.
22. E. Wanzenberg, F. Tietz, D. Kek, P. Panjan, D. Stover, *Solid State Ionics* 164 (2003) 121.
23. J. H. Suh, S. H. Oh, H. S. Kim, S. Y. Choi, C.-G. Chan-Gyung Park, *Vacuum* 74 (3–4) (2004) 423.
24. L. D. Jadhav, A. P. Jamale, S. R. Bharadwaj, S. Varma, C. H. Bhosale,, *Appl. Surf. Sci.* http://dx.doi.org/10.1016/j.apsusc.2012.04.078
25. L. Liu, G.Y. Kim, A. C. Hillier, A. Chandra, *Journal of Power Sources* 196 (2011) 3026–3032.

Dr. L.D. Jadhav *joined the Dept. of Physics, Shivaji University, Kolhapur as Assistant Professor in 1999 and completed her Ph.D. in Physics (High Temperature Superconductivity) in 2002. Presently she is working as Assistant Professor in Department of Physics, Rajaram College, (Govt. of Maharashtra) Kolhapur. She is also a visiting Professor to Dept. of Technology, Shivaji University since 2006. Dr. Jadhav specializes in the area of thin films and Nanomaterials for IT-SOFC. She has supervised two Ph.D. and two M. Tech. theses and presently supervising four Ph.D. students. She has carried out two sponsored research projects (plus two ongoing research projects). She has to her credit more than 25 publications in peer reviewed high impact International Journals and edited one book. She is life member of Society for Materials Chemistry, BARC, Mumbai, Indian Society of Fuel Cell Technologists (ISOFT), Materials Research Society, India, and Indian Association of Physics Teacher.*

Metal Oxides as Efficient Anode Catalysts for Methanol Electrooxidation

Sumanta Kumar Meher, P. Justin and G. Ranga Rao*

Department of Chemistry, Indian Institute of Technology Madras, Chennai 600036, INDIA

**E-mail: grrao@iitm.ac.in;*

Abstract

In the context of developing cheaper and more poisoning resistant electrocatalysts for direct methanol fuel cell (DMFC) application, metal oxides which generate higher active interfacial regions have shown tremendous promise in promoting Pt/C for electrocatalysis. Commercial Pt catalysts promoted by various metal oxides show enhanced methanol electrooxidation activity and CO tolerance behavior. In our laboratory we explored Pt–MoO_3/C and Pt–Nb_2O_5/C electrocatalysts in acidic media, and Pt–V_2O_5/C electrocatalyst in alkaline media for direct electro-oxidation of methanol. A fast and efficient intermittent microwave heating (IMH) method was employed to load metal oxides on carbon black (Vulcan XC-72). The oxide promoted electrocatalysts were found to be more active and stable as compared to the commercial Pt/C electrocatalyst for electrooxidation of methanol. Our work clearly shows the possibility of developing low Pt and/or non-Pt electrocalytic materials for alcohol fuel cells.

Key-words: *electrocatalysis, methanol fuel cell, electrocatalyst, oxides, microwave method*

Introduction

Fuel cells are static energy conversion devices that directly convert the heat of combustion of a fuel (hydrogen, natural gas, methanol, ethanol, hydrocarbons, etc.) into electrical energy without producing any pollutants [1-3]. The fuel is electrochemically oxidized at the anode and produces water and/or carbon dioxide, whereas the oxidant (oxygen from the air) is reduced at the cathode. A critical comparison of fuel cell with other distributed generation technologies shows that, the fuel cells offer tremendous advantages like high energy conversion efficiency (50–80%) which is not limited by the Carnot cycle, zero emission, modularity and scalability for bulk use [4]. Fuel cells can be categorized based on either electrolyte employed or operating temperature of the cell. Among these arrays of fuel cells, DMFC is of particular interest, due to higher energy density, use of liquid fuel (methanol), low operating cost and compact design which is greatly promising for practical application in transport and portable device applications [5,6]. The use of methanol (MeOH) as a fuel is essentially based on its high net energy density (5.26 kWh kg^{-1}) which is more than that of pure H_2 and comparable to gasoline. Essentially, the complete oxidation of MeOH in an acid or alkaline media is a $6e^-$ process which is presented in eqn. 1 and 2, respectively [7,8]:

$$CH_3OH(l) + H_2O(l) \rightarrow CO_2(g) + 6H^+ + 6e^- \quad (1)$$

$E^0 = 0.016$ V vs. SHE at pH = 0

$$CH_3OH(l) + 6OH^- \rightarrow CO_2(g) + 5H_2O(l) + 6e^- \quad (2)$$

$E^0 = -0.810$ V vs. SHE at pH = 14

During the oxidation process, numerous intermediates are formed depending on the reaction conditions, which are prone to poison the active catalyst sites for further reaction. Among all those intermediates, CO is the most stable and has a tendency to poison the active Pt sites, due to its high binding energy of 1.5 eV [9], which hinders further methanol adsorption and oxidation. Although, the electrochemical oxidation of CO

$$(CO + H_2O \rightarrow CO_2 + 2H^+ + 2e^-;\ E^0 = -0.10\ V\ vs.\ RHE)$$

is thermodynamically feasible, in practice a large overpotential is required on pure Pt surfaces before the occurrence of oxidation. For example, on carbon supported Pt catalyst, the onset of CO oxidation is not observed until 0.5V at 80 °C. A catalyst for methanol oxidation should be able to (a) break C–H and O–H bonds of methanol and (b) facilitate the reaction of the resulting residue with some O–containing species to form CO_2. The first process (a) involving adsorption of methanol molecule can only begin near 0.2V vs. RHE (above this potential only enough Pt sites will be free from adsorbed H atoms) for a polycrystalline Pt electrode. In spite of the problem of being strongly poisoned by adsorption product, no better catalyst than Pt is known at present which can break the C–H and O–H bonds of MeOH. This is due to the optimal bonding affinity between Pt and MeOH. The initial adsorption and de-protonation of MeOH followed by some surface rearrangement results in linearly bonded CO to Pt (Pt−CO end-on type stable intermediate) which is schematically shown as [8]:

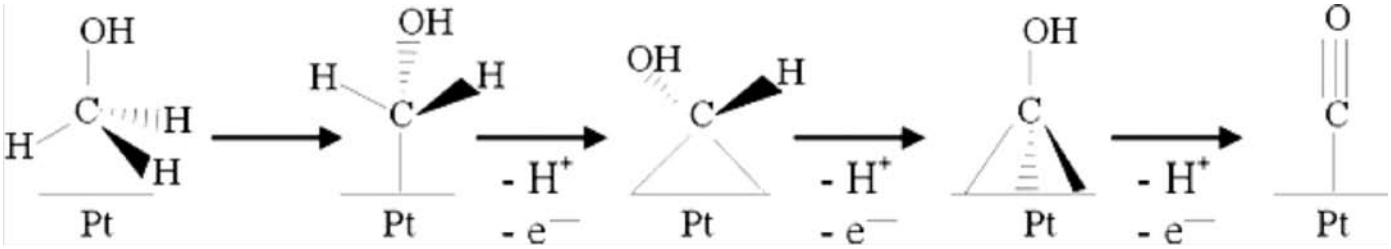

Afterwards, the dissociative adsorption of water (oxygen donor of the reaction) followed by oxidation of adsorbed CO to CO_2 generates free Pt sites for further adsorption and oxidation of MeOH [10].

$$Pt(s) + H_2O(l) \rightarrow Pt - OH_{ads} + H^+ + e^- \quad (3)$$

$$Pt - CO_{ads} + Pt - OH_{ads} \rightarrow 2Pt(s) + CO_2(g) + H^+ + e^- \quad (4)$$

Studies show that, the removal of the CO_{ads} is the rate determining step during methanol oxidation, not the dissociation of the C–H bond during the initial MeOH adsorption [11]. On pure Pt, the dissociative adsorption of water (oxygen transfer) is very slow at normal operating potentials of DMFC (i.e., 0.0 - 0.2V). The sufficient interaction of water with catalyst surface is only possible at potentials above 0.4–0.45V vs. RHE [10]. Thus, on pure Pt, the complete oxidation of methanol cannot begin below 0.45V and hence, the surface of pure Pt remains poisoned throughout its useful potential range. This difficulty has led to the exploration of catalyst that can dissociate water at relatively lower potentials than Pt and show a high reactivity for CO oxidation [12] In the presence of a second metal like Ru, water adsorption starts at lower potential with the formation of Ru−OH species at the catalyst surface which reduce the anodic overpotential by 0.4V [13]. The Ru−OH reacts with the bound CO species to produce CO_2 and H^+ species, which in essence removes the poisoning CO species (Eq. 5 and 6).

$$Ru(s) + H_2O(l) \rightarrow Ru - OH_{ads} + H^+ + e^- \quad (5)$$

$$Pt - CO_{ads} + Ru - OH_{ads} \rightarrow PtRu(s) + CO_2(g) + H^+ + e^- \quad (6)$$

The enhanced activity of the Pt–Ru catalyst when compared with Pt for the methanol electro-oxidation has been explained as bi-functional mechanism [14] as well as the ligand (electronic) effect [11]. The bi-functional mechanism involves the dissociative adsorption of water at lower potentials of 0.2−0.3V vs. RHE on Ru atoms which promote the oxidation of adsorbed CO to CO_2 with the regeneration of free Pt sites for further oxidation of methanol. The ligand effect assumes that the alloy component changes the electronic properties of Pt atoms in its vicinity. In the bulk alloy, Pt and Ru form a stronger bond than Pt–Pt and Ru–Ru. The bonding interaction between Pt and Ru, and the accompanying charge-transfer result in the weakening of Pt–CO bond and the strengthening of Ru–CO bond [11]. This means that Ru donates electrons to Pt and reduces the Pt–adsorbate bond strength, which results in a lowering of the oxidation potential of the adsorbate. According to both bi-functional and electronic theories, the role of the second element is to increase OH adsorption on the catalyst surface at lower potentials adjacent to the poisoned Pt sites and to reduce the adsorption strength of the poisoning methanolic residues (e.g., CO). Based on this assumption, the Pt alloyed with co-catalysts such as Ru, Rh, Sn, Ir, Os, Re, Mo, V, Cr, Co, Ni, Cu etc., in binary, ternary as well as quaternary fashion have been employed as methanol oxidation catalysts in DMFC [15-18]. However, most of the added metals, which promote antipoisoning and enhance the kinetics of methanol electro-oxidation, are also noble and commercially non-feasible. As alternate to these, in recent years metal oxides which allow activation of water at low potentials and can efficiently undergo bifunctional mechanism have shown immense promise for promoting electrocatalytic and antipoisoning activity of Pt, to be effectively utilized for DMFC applications [19-24]. In this context, various metal oxides such as RuO_2, WO_3, ZrO_2, MgO, MoO_2, TiO_2, and CeO_2 in combination with carbon have been exploited for methanol electrooxidation reactions [25-31]. These composites are reported as highly promising active electrocatalysts and show significant tolerance to CO poisoning. Metal oxides also stabilize the dispersion of Pt particles which favors the increase in active surface per weight of the catalyst. Further, most of the metal oxides possess a good capacity for storing and releasing oxygen, which plays an important role in CO_{ads} electrooxidation. In this context, we explored the promoting activities of MoO_3, Nb_2O_5 and V_2O_5 for methanol electrooxidation reactions in acidic as well as alkaline media.

Experimental

The Pt-oxide/C composite electrocatalysts were prepared by solid-state reaction under intermittent microwave heating. The appropriate amount of oxides (MoO_3, Nb_2O_5 and V_2O_5) were dispersed in 40 mg of carbon black (Vulcan XC-72) using 2-propanol as solvent, and the mixtures were dried in an oven at 80 °C. The products were then subjected to microwave irradiation in a domestic microwave oven (Sharp NN-S327 WF, 2,450

MHz, and 1,100 W) for 6 cycles, each cycle for 20 s with a pause of 60 s between heating cycles. In the second step, Pt was loaded on the oxide/C composites by a modified microwave-assisted polyol process [20-23, 32].

The working electrodes for electrochemical measurements were fabricated by dispersing the electrocatalyst powders in 1.0 mL of distilled water and 0.1 mL of 5 wt% Nafion solution. Ultrasonic treatment was applied for 15 min to achieve uniform dispersion of the mixture at room temperature. A known amount of suspension was dispersed on a glassy carbon electrode (6 mm dia) and the solvent was slowly evaporated. For comparative studies, commercial Pt–Ru(2:1)/C catalyst (Johnson Matthey, India) and Pt(20 wt%)/C were used. The amounts of carbon black (Vulcan XC-72) and Pt in each sample were fixed at 40 and 10 mg, respectively.

Results and discussion

The reduction of H_2PtCl_6 to Pt in ethylene glycol under microwave irradiation is presented as:

$$PtCl_6^{2-} + CH_2OH - CH_2OH \rightarrow Pt^0 + CHO - CHO + 4H^+ + 6Cl^- \quad (7)$$

Here, ethylene glycol acts as a reducing agent and microwave irradiation speeds up the reaction to produce nanosized metal particles from metal ions [33]. The microwave also provides gradient less heating for nucleation and growth of uniform sized metal nanoparticles. The transmission electron microscopic (TEM) images of Pt–V_2O_5/C, Pt–MoO_3/C and Pt–Nb_2O_5/C composites are shown in Fig. 1, which confirm the homogeneous dispersion of small and uniformly dispersed spherical Pt particles (dark spots) with size of about 2–3 nm.

Methanol oxidation on V_2O_5 promoted Pt/C electrocatalyst in alkaline media

The cyclic voltammograms of Pt/C and Pt-V_2O_5(4:3)/C electrocatalysts recorded at a scan rate of 50 mV s^{-1} in 1.0 M CH_3OH + 1.0 M KOH electrolyte are shown in Fig. 2A. Although both the electrocatalysts show large methanol oxidation currents between –0.1 and 0.2 V (vs Hg/HgO), the Pt–V_2O_5/C catalyst exhibits nearly twofold increment in peak current density (~200 mA cm^{-2}) as compared to the Pt/C catalyst (~102 mA cm^{-2}). Further, the observed onset potentials for methanol oxidation for Pt/C and Pt–V_2O_5/C catalysts are about –0.39 V and –0.49 V, respectively. The enhanced methanol oxidation current and negative shift in the onset oxidation potential for Pt–V_2O_5/C catalyst clearly indicates the promotional activity of V_2O_5 to Pt/C. These results also suggest the faster removal of adsorbed poisoning species such as CO and regeneration of fresh Pt sites in the presence of V_2O_5 [34, 35]. Since the amount of oxide in the Pt–oxide/C composite plays a significant role in its overall catalytic activity, the optimum amount of V_2O_5 loading for maximum oxidation efficiency of Pt–V_2O_5/C catalyst was verified by studying the methanol electrooxidation reactions on catalysts prepared with different weight ratios of Pt and V_2O_5. The linear sweep voltammetry curves at a scan rate of 50 mV s^{-1} on the Pt–V_2O_5/C catalysts with different weight ratios of Pt and V_2O_5 (fixed Pt loading of 0.30 mg cm^{-2}) are shown in Fig. 2B. It is observed that with increase in the V_2O_5 content under a fixed amount of Pt, the peak current density increases and the onset of oxidation potential decreases. The best performance is observed for the catalyst with the weight ratio of Pt and V_2O_5 at 4:3. Hence, it is inferred that, V_2O_5 actually promotes Pt/C for methanol electrooxidation reaction. However, increase in the V_2O_5 content beyond the weight ratio of Pt and V_2O_5 at 4:3 reduces the conductivity of the catalyst, which in effect inhibits the performance of the composite.

The chronopotentiometry profiles of Pt/C and Pt-V_2O_5/C sample electrodes recorded at a bias current density of 5 mA cm^{-2} are shown in Fig. 2C. In chronopotentiometry,

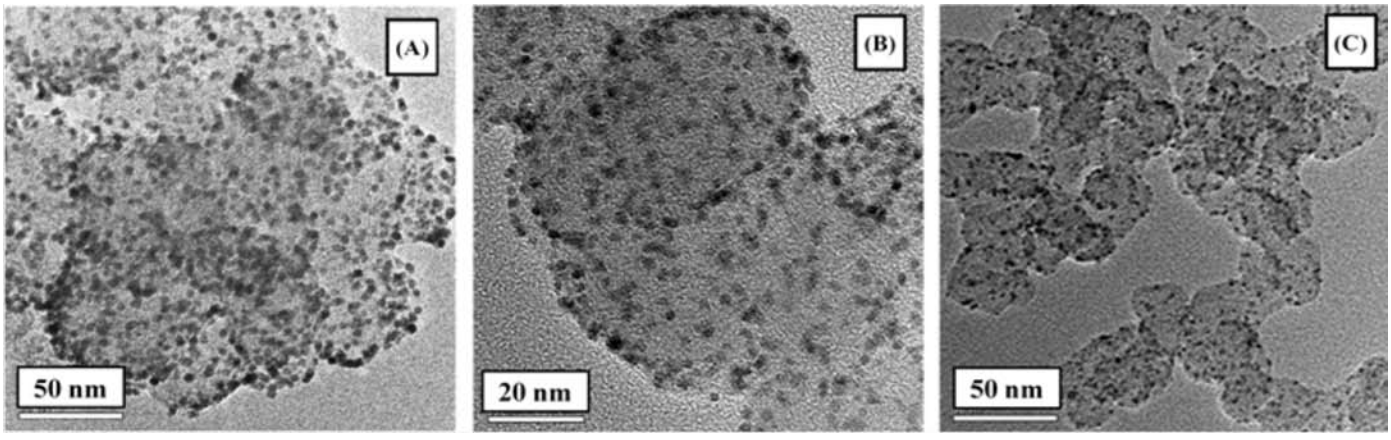

Fig. 1. TEM images of (A) Pt–V_2O_5/C, (B) Pt–MoO_3/C and (C) Pt–Nb_2O_5/C composites

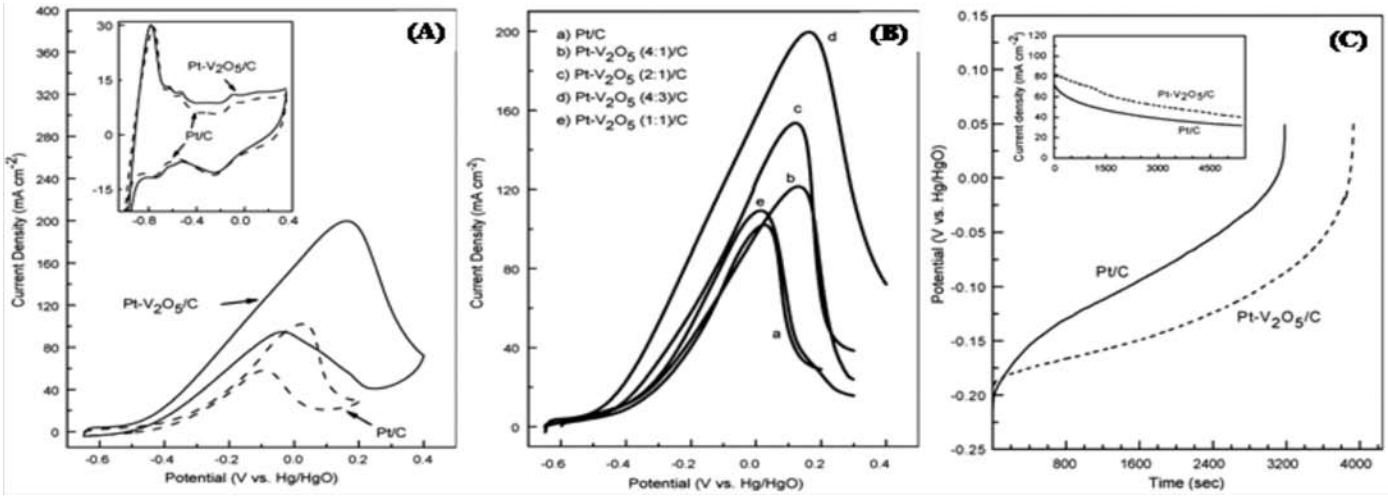

Fig. 2. (A) Cyclic voltammograms of Pt/C and Pt-V2O5 (4:3)/C sample electrodes at a scan rate of 50 mV s–1 in 1.0 M KOH + 1.0 M CH3OH solution. Inset shows the hydrogen electrosorption voltammetric profiles of the sample electrodes in 1.0 M KOH; (B) The linear sweep voltammograms at a scan rate of 50 mV s¬–1 on the Pt/C and Pt–V2O5/C catalysts with different weight ratios of Pt and V2O5 (fixed Pt loading of 0.30 mg cm–2); (C) Chronopotentiometry profiles of Pt/C and Pt–V2O5/C sample electrodes measured at a current density of 5 mA cm–., Inset shows the corresponding chronoamperometry profiles of the samples measured at a bias potential of 0.1 V

the potential increases with polarization time due to surface accumulation of poisoning species such as CO, and finally the potential shifts to a limiting value indicating oxygen evolution and poisoning of the catalyst [25]. From the chronopotentiometry profiles in Fig. 2C, it is observed that the polarization potentials of Pt–V_2O_5/C are lower for than the bare Pt/C electrocatalyst sample. This essentially indicates that the V_2O_5 promoted Pt/C electrocatalyst can withstand the poisoning species for longer time as compared to the bare Pt/C sample [34, 35]. It is possible that V_2O_5 assists in generating oxygen-containing species such as OH_{ads} at lower potential which oxidize CO-like poisoning species on Pt surface to CO_2.

The chronoamperometry behavior of Pt/C and Pt-V_2O_5/C electrocatalysts was measured at a bias potential of 0.1 V, and the corresponding profiles are shown in the inset of Fig. 2C. It is seen that the initial as well as limiting current densities of Pt-V_2O_5/C are higher than those for Pt/C electrocatalyst in the measured time range, which essentially shows that the presence of V_2O_5 improves the electrochemical methanol oxidation activity of Pt/C [20-22].

Methanol oxidation on Nb_2O_5 promoted Pt/C electrocatalyst in acidic media

The Pt-Nb_2O_5(2:2)/C sample was subjected to cyclic voltammetry analysis in 1.0 M CH_3OH + 0.5 M H_2SO_4 solution and the resultant CV profile is compared with that of Pt–Ru(2:1)/C sample, which are shown in Fig. 3A. It is seen that the oxidation peak current density for Pt-Nb_2O_5(2:2)/C sample is significantly higher than that for Pt–Ru(2:1)/C sample, which shows higher promoting activity of Nb_2O_5 as compared to Ru. Since surface oxygen of oxides helps oxidizing the adsorbed CO on Pt surface electrochemically, it appears that Nb_2O_5 provides more oxygen containing species as compared to Ru for the oxidation of adsorbed CO during methanol oxidation reaction. Further, from the CV profiles it is seen that, the onset of oxidation potential for Pt-Nb_2O_5(2:2)/C is lower than that for Pt–Ru(2:1)/C sample, which suggests that in the presence of Nb_2O_5, the adsorption of water followed by oxidation of CO like species occurs at lower over potential. This further implies that the Pt···Nb_2O_5 interface is largely involved during the methanol oxidation process.

Linear voltammetry studies were performed in order to determine the limiting amount of Nb_2O_5 needed to draw maximum activity from the Pt-Nb_2O_5/C composite for methanol electrooxidation reaction. The linear voltammograms of Pt-Nb_2O_5/C composites with different Nb_2O_5 content at a fixed Pt content of 0.21 mg cm^{-2} are shown in Fig. 3B. Essentially, with increase in the Nb_2O_5 content, the peak current density increases and the onset of oxidation potentials are shifted to lower potentials. However, the best performance is found for the catalyst with an optimal weight ratio of Nb_2O_5 and Pt at 2:2.

Chronopotentiometry studies on the Pt–Nb_2O_5(2:2)/C electrocatalyst was performed and its activity was compared with the Pt–Ru(2:1)/C sample to assess the promotional antipoisoning activity of Nb_2O_5 to Pt/C for methanol electrooxidation reaction. The chronopotentiometry

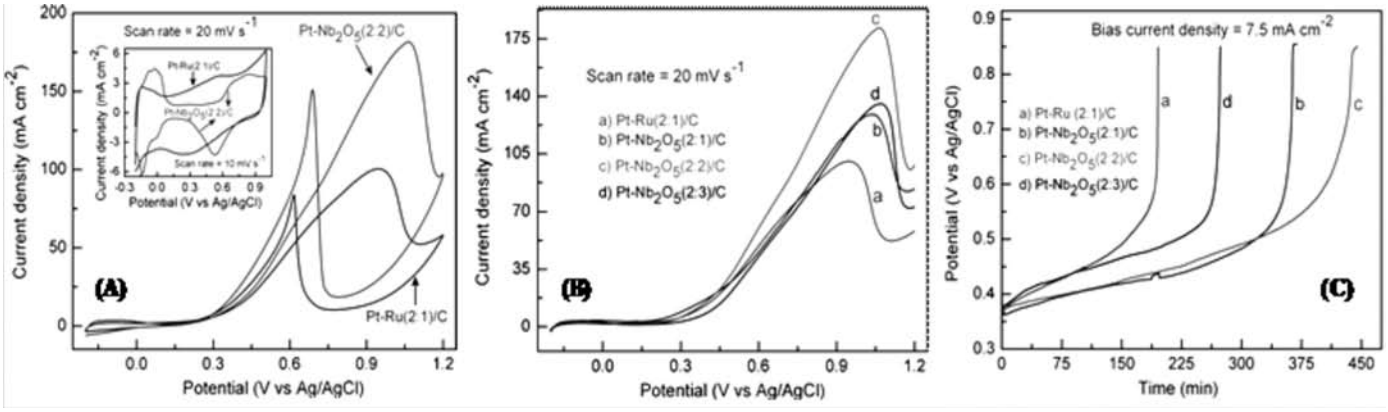

Fig. 3: (A) Cyclic voltammograms for the electrooxidation of methanol on Pt–Ru (2:1)/C and Pt–Nb_2O_5 (2:2)/C electrodes in 1.0 M CH_3OH + 0.5 M H_2SO_4 solution at a scan rate of 20 mVs^{-1}, inset shows the hydrogen electrosorption voltammetric profiles of the electrodes in 0.5 M H_2SO_4 at a scan rate of 10 mV s^{-1}; (B)Linear voltammograms at a scan rate of 20 mV s^{-1} on the Pt–Ru (2:1)/C and Pt–Nb_2O_5/C catalysts with different weight ratios of Pt and Nb_2O_5 (fixed Pt loading of 0.21 mg cm^{-2}); (C) Chronopotentiometry profiles of Pt–Ru (2:1)/C and Pt–Nb_2O_5/C catalysts measured at a current density of 7.5 mA cm^{-2}

measurements were performed at a bias current density of 7.5 mA cm^{-2} and the resultant profiles are presented in Fig. 3C. It is apparent that the polarization potentials for Pt–Nb_2O_5(2:2)/C are lower than the Pt–Ru(2:1)/C sample. Further, the Pt–Nb_2O_5(2:2)/C sample retains its electrocatalytic activity for longer period as compared to the Pt–Ru(2:1)/C sample. These results obviously indicate that Nb_2O_5 is a stronger promoter than Ru for electrooxidation of methanol in acidic medium.

Methanol oxidation on MoO_3 promoted Pt/C electrocatalyst in acidic media

To evaluate the promoting activity of MoO_3, the cyclic voltammetric response of Pt-MoO_3 (2:2)/C was recorded in 0.5 M H_2SO_4 solution at a scan rate of 10 mV s^{-1} and the corresponding profile was compared with the response from Pt/C sample in Fig. 4. The typical CV profiles show peaks due to hydrogen adsorption and desorption (–0.2V to 0.1 V), the double layer potential plateau, and formation (0.5 to 1.0 V) followed by reduction (1.0 to 0.25 V) of platinum surface oxides [36-38]. The redox peaks between 0.08 and 0.32 V observed for the Pt-MoO_3(2:2)/C sample (absent in the Pt/C sample) are attributable to the formation of hydrogen molybdenum bronzes (H_xMoO_3) due to the intercalation/de-intercalation of H into the MoO_3 lattice [22]. This is represented as:

$$xH^+ + xe^- + MoO_3 \rightleftharpoons H_xMoO_3 \qquad (8)$$

The prominent redox peaks due to H_xMoO_3 confirm significantly active interface between Pt and MoO_3 in the Pt-MoO_3/C electrocatalyst, which essentially provides transport paths for electrons as well as protons during methanol oxidation reaction [39, 40].

To assess the promoting efficiency of MoO_3 to Pt/C, cyclic voltammetry of the MoO_3 promoted Pt/C and bare Pt-Ru/C samples was carried out in 1.0 M CH_3OH + 0.5 M H_2SO_4 solution at a scan rate of 20 mV s^{-1}, and the corresponding CV profiles are shown in Fig. 4B. It is seen that the Pt-MoO_3(2:2)/C exhibits higher current response as compared to the Pt-Ru(2:1)/C sample electrode in methanol electrooxidation reaction. This is attributed to the formation of H_xMoO_3 species which plays a prominent role as a proton acceptor and in fact helps in the oxidation of adsorbed intermediates like CH_zO ($0 \le z \ge 4$) and CO on the Pt surface [39].

The anti-poisoning efficiency of MoO_3 for methanol electrooxidation was evaluated by chronopotentiometry study at a current density of 15 mA cm^{-2}, and the corresponding chronopotentiometry profiles of Pt-Ru(2:1)/C and Pt-MoO_3(2:2)/C samples are compared in Fig. 4C. It is seen that the polarization potentials are lower for Pt-MoO_3(2:2)/C sample as compared to the Pt-Ru(2:1)/C sample electrode. Further, the time taken by Pt-MoO_3(2:2)/C to reach the limiting potential is more as compared to that by Pt-Ru(2:1)/C sample electrode. This essentially demonstrates the higher promoting activity and stability of MoO_3 based Pt/C as compared to Ru based Pt/C for methanol oxidation in acidic medium. We propose that the close contact of the noble metal with MoO_3 changes the electronic and ensemble properties of Pt which plays a significant role in the adsorption of oxygen containing species to oxidize poisonous species on the catalysts during oxidation of methanol [22].

The long-term stability performance of the MoO_3 as well as Ru promoted Pt/C samples for methanol electrooxidation was evaluated by chronoamperometry

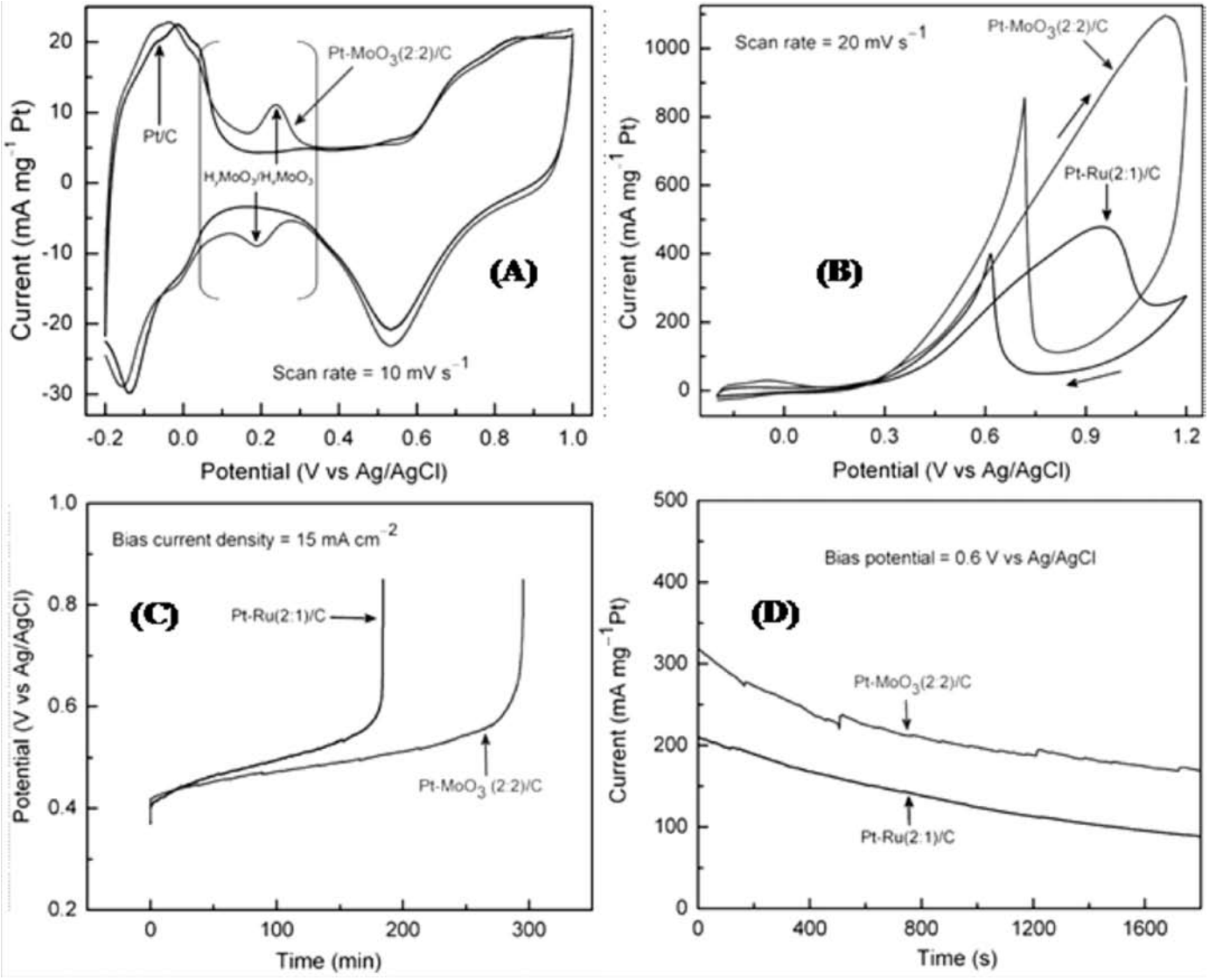

Fig. 4: (A) Hydrogen electrosorption voltammetric profiles of Pt/C and Pt-MoO_3(2:2)/C sample electrodes in 0.5 M H_2SO_4 solution at a scan rate of 10 mV s^{-1}; (B) Cyclic voltammograms of Pt-Ru(2:1)/C and Pt-MoO_3(2:2)/C sample electrodes in 1.0 M CH_3OH + 0.5 M H_2SO_4 at a scan rate of 20 mV s^{-1}; (C) Chronopotentiometric curves of Pt-Ru(2:1)/C and Pt-MoO_3/C sample electrodes at a current density of 15 mA cm^{-2}; (D) Chronoamperometry curves on Pt-Ru(2:1)/C and Pt-MoO_3/C electrodes at a bias potential of 0.6 V

analysis at a bias potential of 0.6 V (vs Ag/AgCl), and the corresponding profiles are presented in Fig. 4D. It is observed that the initial and limiting current densities of Pt-MoO_3(2:2)/C are higher than those of Pt-Ru/C sample electrodes, which clearly suggests higher catalytic activity and stability of MoO_3 promoted Pt/C as compared to Ru promoted Pt/C sample. The small current spikes observed in the amperometric curve of Pt-MoO_3(2:2)/C electrode are due to the detachment of the CO_2 bubbles formed on the electrode surface during methanol oxidation reaction, which is a signature of facile electrooxidation of CO on MoO_3 promoted Pt/C sample [22].

The above results suggest enhanced promoting activity of metal oxides (MO) to Pt/C for methanol oxidation, which is essentially due to facile adsorption of oxygen containing species such as OH on the oxide surface which assist in the oxidation of adsorbed poisoning species such as CO on Pt surface. This can be represented as [41]:

$$MO(s) + H_2O(l) \rightarrow MO - OH_{ads} + H^+ + e^-$$
$$Pt - CO_{ads} + MO - OH_{ads} \rightarrow Pt(s) + MO(s) + CO_2(g) + H^+ + e^- \quad (9)$$
and/or
$$Pt - MO(s) + xCO(g) \rightarrow Pt - MO_{1-x}(s) + xCO_2(g)$$

This phenomenon can also be represented schematically as:

Conclusions

Metal oxides can play a major role for addressing the challenges of electrode materials/catalyst systems in

widespread commercialization of DMFCs. In this context, we have shown the promoting activity of Nb_2O_5 and MoO_3 on Pt/C for electro-oxidation of methanol in acidic medium, and V_2O_5 playing a significant role in promoting Pt/C for methanol oxidation in alkaline medium. These oxides strongly interact with Pt to provide stability, and facilitate adsorption of oxygen containing species which oxidize the adsorbed poisoning species on the catalyst surface during methanol oxidation reaction. Hence, it is proposed that V_2O_5, Nb_2O_5 and MoO_3 based Pt/C electrocatalysts can be alternate to commercial Pt-Ru/C electrocatalysts for DMFC applications.

Acknowledgment: We thank MNRE and DRDO, Government of India, for financial support.

References

1. J. A. Turner, Science, 285 (1999) 687.
2. L. Carrette, K. A. Friedrich and U. Stimming, Fuel Cells, 1 (2001) 539.
3. D. J. L. Brett, , A. R. Kucernak, P. Aguiar, S. C. Atkins, N. P. Brandon, R. Clague, L. F. Cohen, G. Hinds, C. Kalyvas, G. J. Offer, B. Ladewig, R. Maher, A. Marquis, P. Shearing, N. Vasileiadis and V. Vesovic, ChemPhysChem, 11 (2010) 2714.
4. M. Winter and R. J. Brodd, Chem. Rev., 104 (2004) 4245.
5. C. Lamy, A. Lima, V. LeRhun, F. Delime, C. Coutanceau and J.-M Léger, J. Power Sources, 105 (2002) 283.
6. S. Song, V. Maragou, and P. Tsiakaras, J. Fuel Cell Sci. Technol., 4 (2007) 203.
7. A. Hamnett, Catal. Today, 38 (1997) 445–457.
8. J. L. Cohen, D. J. Volpe and H. D. Abruña, Phys. Chem. Chem. Phys. 9 (2007) 49.
9. S. Wasmus and A. Küver, J. Electroanal. Chem., 461 (1999) 14.
10. T. Iwasita, X. H. Xia, H.-D. Liess and W. Vielstich, J. Phys. Chem. B, 101 (1997) 7542.
11. Q. Ge, S. Desai, M. Neurock and K. Kourtakis, J. Phys. Chem. B, 105 (2001) 9533.
12. B.Beden, F.Kadirgan, C. Lamy, J.M. Legar, J Electroanal Chem. Int. Electrochem., 127 (1981)75-85
13. A. Crown, I. R. Moraes and A. Wieckowski, J. Electroanal. Chem., 500 (2001) 333.
14. M. Watanabe and S. Motoo, J. Electroanal. Chem. Interfacial Electrochem., 60 (1975) 267.
15. E. Reddington, A. Sapienza, B. Gurau, R. Viswanathan, S. Sarangapani, E. S. Smotkin and T. E. Mallouk, Science, 280 (1998) 1735.
16. B. Gurau, R. Viswanathan, R. Liu, T. J. Lafrenz, K. L. Ley, E. S. Smotkin, E. Reddington, A. Sapienza, B. C. Chan and T. E. Mallouk, J. Phys. Chem. B, 102 (1998) 9997.
17. E. Antolini, J. R. C. Salgado and E. R. Gonzalez, J. Power Sources, 160 (2006) 957.
18. Y. Zhang and P. J. McGinn, J. Power Sources, 206 (2012) 29.
19. H. Yuan, D. Guo, X. Qiu, W. Zhu and L. Chen, J. Power Sources, 188 (2009) 8.
20. P. Justin and G. Ranga Rao, Catal. Today, 141 (2009) 138.
21. P. Justin, P. H. K. Charan and G. Ranga Rao, Appl. Catal., B: Environmental, 100 (2010) 510.
22. P. Justin and G. Ranga Rao, Int. J. Hydrogen Energy, 36 (2011) 5875.
23. G. Ranga Rao, P. Justin and S. K. Meher, Catal. Surv. Asia, 15 (2011) 221.
24. D. R. M. Godoi and H. M. Villullas, Langmuir, 28 (2012) 1064.
25. C. Xu and P. K. Shen, Chem. Commun., (2004) 2238.
26. S. Jayaraman, T. F. Jaramillo, S.-H. Baeck and E. W. McFarland, J. Phys. Chem. B, 109 (2005) 22958.
27. N. Rajalakshmi, N. Lakshmi and K. S. Dhathathreyan, Int. J. Hydrogen Energy, 33 (2008) 7521.
28. F. Peng, C. Zhou, H. Wang, H. Yu, J. Liang and J. Yang, Catal. Commun., 10 (2009) 533.
29. H. Song, X. Qiu and F. Li, Appl. Catal., A, 364 (2009) 1.
30. S. V. Selvaganesh, G. Selvarani, P. Sridhar, S. Pitchumani and A. K. Shukla, J. Electrochem. Soc., 159 (2012) B463.
31. M. Tian, G. Wu and A. Chen, ACS Catal., 2 (2012) 425.
32. W. Yu, W. Tu, H. Liu, Langmuir, 15 (1999) 6.
33. E. A. Anumol, P. Kundu, P. A. Deshpande, G. Madras and N. Ravishankar, ACS Nano, 5 (2011) 8049.
34. G. García, M. T. M. Koper, ChemPhysChem, 12 (2011) 2064.
35. J. Zeng, J. Mater. Chem., 22 (2012) 3170.
36. R. P. Buck and L. R. Griffith, J. Electrochem. Soc., 109 (1962) 1005.
37. A. Zolfaghari, M. Chayer and G.Jerkiewicz, J. Electrochem. Soc., 144 (1997) 3034.
38. C.-C. Hu and K.-Y. Liu, Electrochim. Acta, 44 (1999) 2727.
39. W. Li, J. Lu, J. Du, D. Lu, H. Chen and H. Li, Electrochem. Commun., 7 (2005) 406.
40. Z. H. Zhou, W. S. Li, Z. Fu and X. D Xiang, Int. J. Hydrogen Energy, 35 (2010) 936.
41. U. Krewer, T. Vidakovic-Koch, L. Rihko-Struckmann, ChemPhysChem, 12 (2011) 2518.

Sumanta Kumar Meher *has received M. Sc. and M. Phil. degrees in Chemistry from Sambalpur University, Odisha, India. He obtained a PhD degree in Physical Chemistry from IIT Madras in 2012, under the guidance of Prof. G. Ranga Rao. His research area covers multidisciplinary area of chemistry and physics in designing and understanding the surface as well as interface science of novel functional nanomaterials for various applications. His major research thrusts are: Nanomaterials chemistry and nanotechnology, Electrochemical energy conversion and storage systems, Engineered nanomaterials for electronic and optical device applications, Heterogeneous catalysis, Nanoelectrochemistry, Electrochemical sensors, Electrocatalysis and nanocrystals for cleaner environment and sustainability.*	
P. Justin *has received M. Sc. degree in Chemistry from Madurai Kamaraj University, Tamil Nadu, India and M. Tech. Degree in Surface Science & Engineering from NIT Jamshedpur, India. He obtained PhD degree in Chemistry from IIT Madras in 2011, under the guidance of Prof. G. Ranga Rao. Currently, he is a Lecturer of Chemistry in Rajiv Gandhi University of Knowledge Technologies (RGUKT), Andhra Pradesh, India. His major research interests include Energy sciences and engineering (fuel cells, electrochemical capacitors and photo-splitting of water), Nanoscience and nanotechnology (electrochemical biosensor, magnetic materials and photochromism), and Surface science and engineering (electrochemical corrosion prevention and control).*	
G. Ranga Rao *obtained PhD from IISc, Bangalore, and worked as post-doc in Europe and Japan before joining as a faculty member in IIT Madras. He is currently a professor in the Department of Chemistry, IIT Madras. His research interest covers surface chemistry and spectroscopy, solid state electrochemistry, heterogeneous catalysis - new materials for catalysis and electrocatalysis, photocatalysis, environmental catalysis and energy storage applications, materials chemistry - synthesis and applications of new layered-, hybrid-, porous- and nanomaterials.*	

Biofuel Cells: A Promising Technology for Energy Generation

Shilpa N. Sawant* **and Sugosh Prabhu**

Chemistry Division, Bhabha Atomic Research Centre, Mumbai 400085
E-mail: stawde@barc.gov.in

Introduction

There is growing interest worldwide towards development of sustainable technology for power generation. The objective is to develop newer methods which will reduce dependency on fossil fuel as well as help in controlling the environmental pollution [1]. Biofuel cells (BFCs) have emerged as a promising alternative in this direction. BFCs provide a means for capturing the abundant energy present in organic matter in waste biomass with the help of biocatalyst.

There are different types or formats of fuel cells which utilize microorganisms and enzymes as the biological catalyst. The biocatalyst can be used for production of simple fuels such as hydrogen or methane from complex substrates or biomass. These simple fuels can then be used in conventional fuel cells with inorganic catalyst to produce electricity. These types of fuel cells are classified as secondary or indirect biofuel cells [1, 2]. These are actually a combination of a bioreactor and a fuel cell, hence are not true biofuel cells [1]. On the other hand, biocatalysts can also be used to directly convert organic fuel into electricity in a primary or direct biofuel cell. The present article focuses on the latter.

A biological fuel cell (abbreviated as biofuel cell), can thus be defined as a device capable of directly transforming chemical energy to electrical energy via electrochemical reactions involving biochemical pathways [3]. They utilize enzymes or microorganisms as biocatalyst to oxidize wide varieties of substrates (*eg.* glucose, alcohols, fatty acids, carbohydrates, inorganic ions etc.) as fuel. The first biofuel cell was demonstrated in 1911 by M. C. Potter, a professor of botany. Their fuel cell used yeast cells at the anode to oxidize glucose [4]. However, the research on BFC's got an impetus in 1960s when NASA showed interest in development of technology for generation of power from organic waste on space shuttles [2, 3].

MFC setup and design:

Biofuel cells are derived by amalgamation of two parent technologies, namely, fuel cells and biotechnology. Like conventional fuel cells, a typical biofuel cells comprise of an anode and a cathode separated by a cation selective membrane (Figure 1). Conventional fuel cells use precious metals as catalyst, whereas biofuel cells utilize enzymes or microorganism as catalyst which oxidizes the substrate/ fuel through various metabolic pathways. During this process, they pass on the electrons to the electrode leading to generation of current in the external circuit. Since biomolecules are used as the catalyst, BFCs have the advantage of operation at ambient temperature and physiological pH.

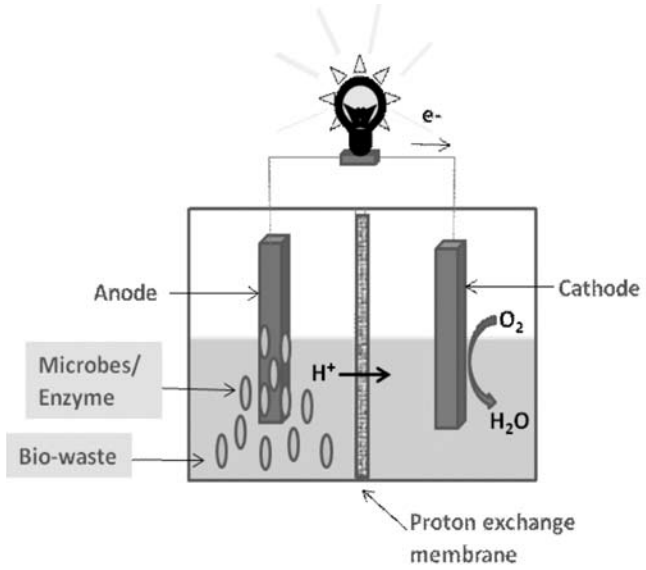

Fig. 1. Schematic representation of a biofuel cell utilizing enzyme/ microbes as the catalyst for conversion of the fuel present in waste into electricity.

Anode

The anode material should have good conductivity, chemical stability, mechanical strength and large surface area. Non corrosive metals and carbon materials like graphite rod, graphite fiber brush, carbon cloth, carbon paper, carbon felt, and reticulated vitreous carbon (RVC) are the most widely used anodes in BFC studies [5]. Since the anode is in contact with the biological species, it needs to have a good biocompatibility to allow immobilization/ adhesion of enzymes or microbes. Electrode modification is important in order to improve bacterial adhesion and electron transfer and has emerged as a new topic of interest in BFC research.

Cathode

The cathodic chamber consists of a high potential electron acceptor. Oxygen serves as an ideal electron

acceptor in most of the studies as it simplifies the BFC design. The cathode commonly consists of carbon electrode impregnated with oxygen reduction catalyst like platinum, metal complexes etc. Other standard redox couples like ferricyanide are also used as electrolyte in the cathode chamber due to its low overpotential and good performance [6]. Use of biocathodes immobilized with enzymes like laccase and billirubin oxidase have also been demonstrated [7]. The enzyme multi-copper oxidase, for example, which is capable of a four-electron reduction of O_2 to water, has been used as biocathode in a BFC working at physiological pH [8].

Single/double compartment BFC

The conventional BFC is a two chamber system, consisting of anode and cathode chambers that are separated by a proton exchange membrane like Nafion. However, due to their complex designs, two-compartment MFCs are difficult to scale-up for operation either in batch or continuous mode. Thus single chamber MFC are being developed which have structural simplicity, reduced cost and better adaptability for practical applications. But for running a single chamber BFC, the substrates and products of the two half reactions should not interfere with each other. Enzymes, being highly specific, can be better utilized for development of single chamber BFCs.

Catalyst and Fuel

Based on the type of catalyst used, biofuel cells can be classified as Enzymatic Fuel cells (EFC) and Microbial fuel cells (MFC) respectively.

Enzymatic fuel cells (EFC)

Enzymatic fuel cells use enzymes to catalyze the oxidation of substrate/ fuel at the anode surface thus releasing electrons in the external circuit. Since the enzymes have a high turnover rate, EFCs exhibit higher power densities (1.65–4.1 mW/cm^2) as compared to MFCs [9]. The redox active sites of the enzyme are generally embedded inside the insulating protein matrix. Hence the power output of an EFC is limited by the rate of electron transfer from the enzyme active site to the electrode surface in spite of the high biocatalysis rate of the enzymes. This problem has been solved to some extent by the advent of several materials and polymers which allow efficient immobilization of enzymes thus facilitating the transfer of electrons from the enzyme to the electrode [1]. The use of electron mediators (eg. organic dyes, organometallic complexes) has also helped to improve the efficiency of charge transfer [7].

The use of purified enzymes in fuel cells is derived as an extension of research on biosensors. EFCs utilize specific or defined biochemical reactions leading to potential application to power *in vivo* devices such as glucose sensor for use in diabetics or as an implantable power source for cardiac pacemaker [10].

The enzymes used in EFCs generally belong to the oxido-reductase family as these enzymes are capable of catalyzing redox reactions. They can be broadly classified into three groups based on the type of redox active centre [11]. The first group includes enzymes with a nicotinamide adenine dinucleotide (NADH/NAD+) or nicotinamide adenine dinucleotide phosphate (NADPH/ NADP+) cofactor, e.g. glucose dehydrogenase and alcohol dehydrogenase. The second group consists of enzymes with flavin adenine dinucleotide (FAD) redox cofactor (eg. glucose oxidase). The third group consists of enzymes with pyrroloquinoline quinine (PQQ) cofactor like alcohol dehydrogenases.

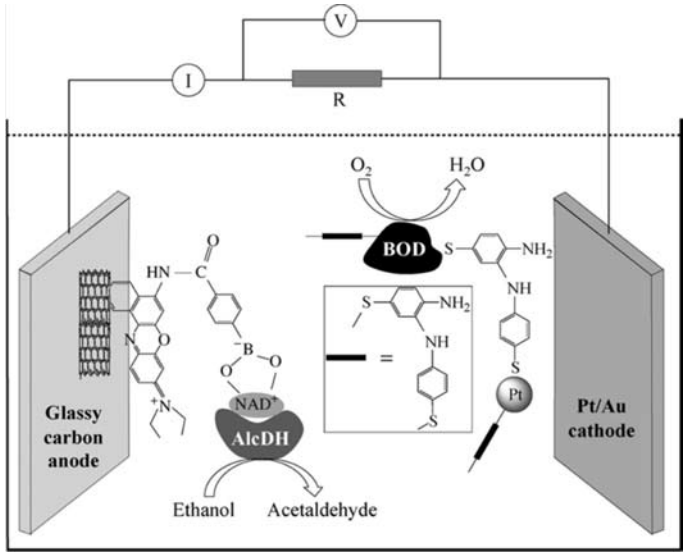

Fig. 2. Schematic presentation of the biofuel cell employing bioelectrocatalytic electrodes composed of electrically contacted alcoholdehydrogenase-SWCNTs (anode) and Platinum nanoparticle/ billirubin oxidase (cathode) [13]. Adapted with permission from Yan et al.[13].

A judicious selection of enzymes and electrodes can lead to EFCs with high power output. Kamitaka *et al.* [12] have reported a single chamber membrane-less fructose/O_2 fuel cell with fructose dehydrogenase immobilised carbon paper as the anode and multi-copper oxidases immobilized carbon paper cathode. Their fuel cell was capable of delivering power densities of the order of 1mWcm^{-2}. In another example, SWCNTs have been used to immobilize alcoholdehydrogenase enzyme on glassy carbon anode (Figure 2). Thioaniline-modified Pt nanoparticles were used at the cathode to immobilize billirubin oxidase. The open circuit voltage (OCV) of the cell was 0.62 V and the

maximum current density was found to be 370 $mAcm^{-2}$, which corresponded to 0.2 mW cm^{-2} [13].

Though EFCs exhibit higher power densities as compared to MFCs, they have the disadvantage of shorter lifetimes (~ 7-10 days) due to the sensitive nature of enzymes [14]. The purified enzymes are expensive and the fuel/substrate is also partially oxidized in an EFC leading to lower fuel efficiency. However, the enzymes have the added advantage of specificity, which can eliminate the need for a membrane separator in an EFC.

An alternative to redox enzymes is the use of microorganisms in biofuel cells. This eliminates the isolation and purification of individual enzymes and also permits the use of cheaper substrates as fuel.

Microbial Fuel Cell (MFC)

Microbial fuel cells make use of living cells to catalyze the oxidation of fuels at the anode surface. The advantage of using microorganisms is that they have better stability and are able to regenerate the required enzymes as a part of their natural functioning. MFCs can utilize a wide variety of natural substrates and waste biomass as fuel because the microbes are capable to grow and adapt to the environment [7].

Aerobic microbes generally survive and grow in oxygen rich environment and oxidize/metabolize organic matter through aerobic respiration. However, in a MFC, the microbes are forced to shift from aerobic respiration to anaerobic respiration so that the electrons produced during oxidation/metabolism of the fuel are passed on to the anode [15]. The electrons then flow through a resistor/load to the cathode, where the electron acceptor is reduced. The protons generated during oxidation of the substrate pass to the cathode chamber through the proton exchange membrane.

The output of the MFC thus depends on the rate of electron transfer from the microbes to the electrode. Direct electron transfer to the electrode can be facilitated via outer membrane protein. Kim *et. al*. observed direct electrochemical communication of *Shewanella putrefaciens* with an anode via cytochromes localized on the outer membrane [16]. Bacterial species like *Clostridium butyricum* and *Pseudomonas aeruginosa* are known to produce their own mediators which shuttle the electrons to the electrode [17]. Some microbes can achieve direct electrical contact with the electrode via the pili present on the cell surface. This method was established by Derek Lovley group, where they observed that no current is produced in the MFC on deletion of the gene responsible for the electrically conductive pili in *Geobacter sulfurreducens* [18]. On the other hand, mediated electron transfer can be achieved by using natural or artificial redox mediators as electron shuttle. The mediator should have the following characteristics; (a) redox potential matching that of the metabolite, (b) ability to penetrate the cell membrane so shuttle the electrons across the membrane, (c) should not interfere with the metabolism of the microbes, (d) fast kinetics for electron transfer at the anode as well as inside the organism [3]. Some of the commonly used redox mediators are methylene blue, neutral red, quinones, thionine, metal complexes etc.

The microbial culture can be used as a suspension in the anodic chamber, immobilized on the electrode or a biofilm can be grown on the anode surface. Each approach has its own merits and demerits. When the microbes are used as suspension, the MFC needs to be operated in batch mode. Immobilization on the electrode or biofilm formation allows the operation of MFC in continuous mode. The microorganisms are used either as pure culture or as mixed culture. Pure cultures are used to study the electrochemical performance of specific organism whereas mixed cultures are used for practical applications where complex substrates and waste biomass is used. Mixed cultures are reported to have higher power density, although, certain pure cultures like *Rhodopseudomonas palustris* strain and *Geobacter sulfurreducens* have current densities comparable to that of mixed culture [19]. Activated sludge, soil, marine sediment, waste water are all rich sources of microbial consortia and are extensively used in MFCs [20]. *Shewanella, Geobacter, Pseudomonas* and *Clostridium* are the most commonly reported species in MFC research [21]. The type and source of microbes determine the output of the MFC. Park *et. al.* carried out electrode modification by impregnating the anode with a redox mediator [22]. This leads to a thousand fold increase in the power density form 0.44 mWm^{-2} to 91 mWm^{-2} when pure *Escherichia coli* was used as the biocatalyst. However, when the pure culture was replaced by sewage sludge, they observed an increase in power density to 788 mWm^{-2}. This led them to conclude that the sewage sludge may contain efficient electrophilic organisms that transfer electrons more readily than *E. coli* [22].

The main advantage of MFCs is their capability to oxidise the substrate completely into carbon dioxide and water [3]. Hence they are more suitable for waste treatment. MFCs have long lifetimes of up to 5 years [4]. Their power densities are however limited by the slow transport of electrons and mediators across cellular membrane.

Principle and Performance

A MFC uses microorganisms to generate power from biodegradable organic/inorganic matter like glucose, ethanol, proteins, cellulose, carbohydrates etc. In a MFC utilizing glucose as the substrate, the microbes oxidize glucose in a series of metabolic reactions which can be described in the form of a simplified equation as [23]:

At anode: $C_6H_{12}O_6 + 6\,H_2O \rightarrow 6\,CO_2 + 24\,H^+ + 24\,e^-$ (1)

The anode potential is set by the potential of the respiratory enzymes present in the microbes and has a typical value of about -0.2 to -0.3 V (vs NHE) [24]. The release of electrons to the anode is accompanied by release of protons into solution.

The cathodic potential depends of the cathode material and the catholyte present. Oxygen is the most common electron acceptor used in MFCs. Oxygen in the atmosphere is reduced to water according to the equation:

At cathode: $6\,O_2 + 24\,H^+ + 24\,e^- \rightarrow 12\,H_2O$ (2)

The cathode potentials observed in MFCs with oxygen are ~ 0.3 V even with Pt-catalyzed electrodes, which is much lower than the theoretical value of ~0.8 V [25]. Thus the overall cell potential for MFC with above reactions is 0.5 V. Other electron acceptors like ferricyanide or manganese oxide generate higher cell voltages but are not sustainable and need to be replenished with time [24]. The low voltage obtained in MFC is due to the various overpotential losses occurring at the electrode [26].

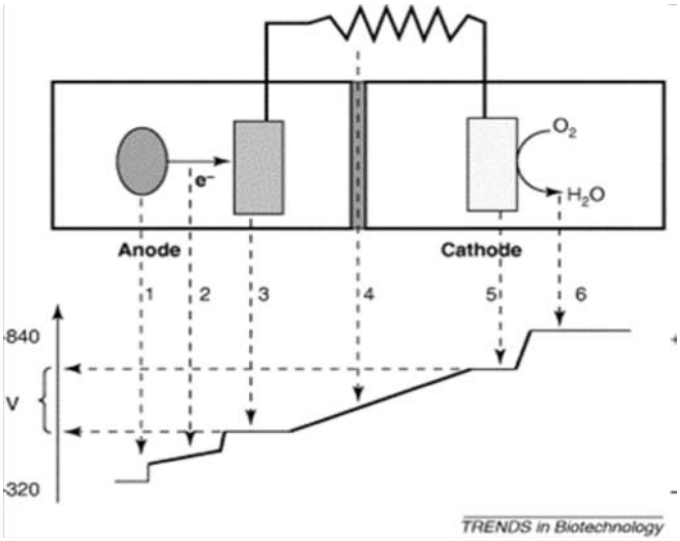

Fig. 3. Potential losses during electron transfer in a MFC. 1. Loss owing to bacterial electron transfer. 2. Losses owing to electrolyte resistance. 3 Losses at the anode. 4. Losses at the MFC resistance (useful potential difference) and membrane resistance losses. 5. Losses at the cathode. 6: Losses owing to electron acceptor reduction. Reproduced with permission from [26] Elsevier.

The power output of a BFC depends on the voltage (V) and current (I) according to the relation, P= V x I. The current is influenced by kinetics of electron transfer at the electrode, the internal cell resistance as well as external load resistance. On the other hand, the voltage of the cell can be described as $V = E^0 - \eta_a - \eta_c - IxR$, where E^0 is the maximum cell voltage, η_a is the activiation overpotential, η_c is the concentration overpotential, and IxR is the loss due to electrolyte resistance [26]. The various potential losses occurring during electron transfer in a MFC is depicted in Figure 3.

Challenges and the way ahead

Having understood the various factors responsible for the low current and potentials observed in BFCs, scientists around the world are working towards improving different parameters which could help to improve the overall power output. Some of the parameters are discussed in this section.

One of the main factors affecting the performance of a BFC is the efficient transfer of electrons from the enzymes/ microbes to the electrode. Immobilized or solution based mediators have helped to solve this problem to a certain extent. Use of electrode material with higher surface area such as highly porous structure can help to increase the current density by providing more sites for the electrode reaction [27, 28]. Novel electrode designs can be employed, such as graphite brush anode designed by Logan et al. by winding graphite fibers around a central conductive, non-corrosive metal rod [29]. The internal resistance of the graphite-bush fuel cell was lower than one with plain carbon paper electrode and could achieve power densities of $0.24 mWcm^{-2}$ [29].

The other method to improve electron transfer is by modifying the electrode surface with material which can facilitate efficient transfer of electrons. Conducting polymers, especially polyaniline is being extensively used in biosensors [30, 31] for this purpose. A ten times increase in current output was observed for the first time by Schröder *et al*. on coating the anode of a MFC with polyaniline [32]. Since then, conducting polymers are finding increasing application in BFCs.

As far as the biocatalyst is concerned, bacterial attachment and formation of a biofilm on the anode surface are essential for the efficient transfer of electrons in an MFC. Genetic manipulation in enzymes and microbes can also help to enhance electrode performance [33]. The electrode surface needs to be biocompatible so as to sustain the enzymes and microorganism. Conducting polymers like polyaniline are known to exhibit good biocompatibility [34]

and can help for efficient immobilization of the biocatalyst in addition to enhancing the electron transfer.

The geometric design of BFCs needs to be optimized so as to maximize the voltage output taking into account the electrode overpotential. The internal resistance can be minimized by proper design and positioning of the electrodes [6]. Use of proton exchange membrane is known to increase the internal cell resistance. Therefore it is of great significance to either develop efficient membranes or eliminate the use of membranes by ingenious designing of BFC.

The voltage output of individual BFC is generally low for any practical application. By connecting several MFCs in series to form a stack, it is possible to sustainably increase the net voltages produced. However, it is observed that the net voltage output of a stack in series is reduced due to the problem of voltage reversal [35]. Several approaches have been attempted to overcome this problem.It was demonstrated by Logan group that MFC voltages can be increased with continuous power production using an electronic circuit containing two sets of multiple capacitors that were alternately charged in parallel by the MFCs and discharged to the external load through capacitors linked in series. This way, they could produce up to 2.5 V using four capacitors [35].

Novel Biofuel cells

In recent years, there is a growing interest in combining several physical phenomena like photosynthesis, magnetism etc with BFCs. This has led to development of novel BFCs such as photo-microbial fuel cells (PMFC), benthic fuel cells etc. In PMFC, microbes capable of photosynthesis are used as the biocatalyst. These microbes utilize the photosynthetic cycle to generate electrons instead of respiratory cycle which is normally used in MFCs [3]. Benthic or sediment MFCs harvest energy from potential gradient at marine sediment-seawater interface. The anode is shallowly embedded in marine sediment and connected via a load to the cathode positioned in overlying water [36].

Applications

BFCs provide an environment friendly means to generate electricity from biomass and biofuels. They have typical power densities of ~2 to 3 W m^{-2}, under optimum conditions [25] which is much lower than those in hydrogen fuel cells (~1Wcm^{-2}) or liquid fuel cell such as one using methanol. However, BFCs have shown success in utilizing complex fuel molecules and waste biomass. Thus they can serve the dual purpose of energy generation and waste disposal. EFCs have shown potential to power implantable biomedical devices such as hearing aids, heart pacemakers using substances in body fluid (eg. glucose) as fuel. They can be used to power *in vivo* biosensors for continuous monitoring of metabolites like glucose, cholesterol etc. or for controlled drug delivery. EFC have been actually implanted in animals and operated in vivo. Cinquin et al. were the first group to demonstrate the operation of a BFC in the retroperitoneal space of freely moving rats [37]. Recently, Evgeny Katz and collaborators [38] have demonstrated successful operation of a BFC in living snail (Figure 4). The electrodes were suitably modified so as to facilitate direct transfer of electrons from the redox enzymes to the electrode.

In addition to in vivo applications, EFCs can be used to power electronic gadgets. Sony Corporation has demonstrated an EFC working on glucose which could give a power output of 50 mW (Figure 5). Four EFCs were connected to power a music play back on a Walkman. Sakai *et al.* have developed a BFC containing membrane electrode assembly which was constructed by combining the anode with a cellophane membrane and an air-breathing cathode [39]. Two cells connected in series could operate a small toy car for more than two hours continuously.

MFCs on the other hand are more suitable for power generation from waste streams with simultaneous bioremediation of the effluent. They are capable of exploiting the full gamut of biochemical reactions for power generation utilizing different types of microorganisms. MFCs of different size, from microlitre capacity to several liters, have been demonstrated in literature. A large-scale MFC was first set up at Foster's brewery at Yatala in Australia (Figure 6). The reactor consists of 12 modules and has a volume of approximately 1 m^3 with carbon fibre electrodes (www.microbialfuelcell.org).

Researchers at University of Connecticut have developed a pilot scale MFC running on water from local waste treatment plant. The MFC could remove up to 80% of the chemical oxygen demand present at 300–600 mg/L [6]. Using a continuous flow MFC, Logan Lab at the Penn State University could generate 15.5 Watts power per cubic meter of household wastewater flowing through it [40]. A mediator-less MFC was used as a biosensor for determination of biochemical oxygen demand (BOD) of wastewater. The BOD sensor has been operated for over 5 years in a stable manner without any servicing [41]. MFCs have also been used to power devices for environmental monitoring. A benthic MFC developed by Tender *et al*. was used to power a meteorological buoy deployed in the Potomac River in Washington DC, USA [36]. The bouy was deployed to measure temperature, relative humidity

(a)

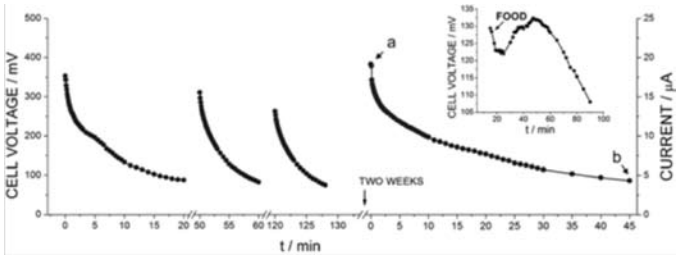

Fig.4. (a) Photograph of a snail with implanted biocatalytic electrodes connected with crocodile clips to the external circuitry. (b) Voltage generated by the implanted biofuel cell operated in vivo on a 20 kΩ load resistance as a function of time. Inset: Restoring the cell voltage in real time upon feeding the snail. Reproduced with permission from [38] Copyright (2012) Americal Chemical Society.

Fig. 5. Bio Batteries used by Sony Corporation to power a Walkman at a press event in August 2007 (http://www.sony.net/SonyInfo/News/Press/200708/07-074E/index.html).

Fig. 6. Tubular microbial fuel cells tested for power production using wastewater produced at Foster's brewery in Yatala, Australia (www.microbialfuelcell.org).

and some other environmental parameters. The anode was placed in the sediment while the cathodes were exposed to the overlying water. Their benthic MFC could supply power to the bouy for a period of seven months.

Conclusion

There is a growing interest in the field of BFCs which is evident from the large number citation on the topic. The present article gives an introduction to the field of biofuel cells providing a glimpse of the latest development in the field including the practical applications. Further efforts are required to improve the output of BFCs so as to meet the challenges faced in practical applications. It is hoped that with continuous efforts from various research labs around the world, BFC will certainly become a viable 'green' technology for power generation as well as waste management in the near future.

References:

1. F. Davis and S. P. J. Higson, Biosens. Bioelectron., 22 (2007) 1224.
2. J. Kim, H. Jia and P. Wang, Biotechnol. Adv., 24 (2006) 296.
3. R. A. Bullen, T. C. Arnot, J. B. Lakeman and F. C. Walsh, Biosens. Bioelectron., 21 (2006) 2015.
4. M. J. Cooney, V. Svoboda, C. Lau, G. Martin, and S. D. Minteer, Energy Environ. Sci.,1 (2008) 320.
5. J. Wei, P. Liang and X. Huang, Bioresour. Technol., 102 (2011) 9335.

6. B. E. Logan, Appl Microbiol Biotechnol, 85 (2010) 1665.
7. M.H. Osman, A.A. Shah and F.C. Walsh, Biosens. Bioelectron., 26 (2011) 3087.
8. F. Durand, C. H. Kjaergaard, E. Suraniti, S. Gounel, R. G. Hadt, E. I. Solomon, N. Mano, Biosens. Bioelectron., 35 (2012) 140.
9. X. Y. Yang, G. T. Nan Jiang and B.L. Su, Energy Environ. Sci., 5 (2012) 5540.
10. E. Katz, A.F. Buckmann, I. Willner, J. Am. Chem. Soc. 123 (2001) 10752.
11. A. Heller, J. Phys. Chem., 96 (1992) 3579.
12. Y. Kamitaka, S. Tsujimura, N. Setoyama, T. Kajino and K. Kano, Phys. Chem. Chem. Phys., 9 (2007) 1793.
13. Y. M. Yan, I. Baravik, R. T. Vered and I. Willner, Adv. Mater., 21 (2009) 4275.
14. S. D. Minteer, B. Y. Liaw and M. J. Cooney, Curr. Opin. Biotechnol., 18 (2007) 228.
15. B.E. Logan, Nat. Rev.: Microbiol.,7 (2009) 375.
16. H. J. Kim, H. S. Park, M. S. Hyun, I. S. Chang, M. Kim, B. H. Kim, Enzyme Microb. Technol., 30 (2002) 145.
17. M.H. Osman, A.A. Shah and F.C. Walsh, Biosens. Bioelectron., 26 (2010) 953.
18. H. Richter, K. McCarthy, K. Nevin, J. Johnson, V. Rotello, D. Lovley, Langmuir 24 (2008) 4376.
19. D. R. Lovley, Energy Environ. Sci., 4 (2011) 4896.
20. J. Niessen, F. Harnisch, M. Rosenbaum, U. Schröder and F. Scholz, Electrochem. Comm. 8 (2006) 869.
21. V. Sharma and P.P. Kundu, Enzyme Microb. Technol., 47 (2010) 179.
22. D. H. Park and J. G. Zeikus, Biotechnol. Bioeng. 81 (2003) 348.
23. S. K. Chaudhuri and D. R. Lovley, Nat. Biotechnol., 21 (2003) 1229.
24. B. E. Logan and J. Regan, Environ. Sci. Technol., 40 (2006) 5172.
25. B. E. Logan and K. Rabaey, Science 337 (2012) 686.
26. K. Rabaey and W. Verstraete, Trends Biotechnol. 23 (2005) 291.
27. F. Zhao, R. C. T. Slade and J. R. Varcoe, Chem. Soc. Rev., 38 (2009) 1926.
28. M.U. Anu Prathap, B. Thakur, S. N. Sawant and R. Srivastava, Colloids Surf. B: Biointerfaces 89 (2012) 108.
29. B.E. Logan, S. Cheng, V. Watson and G. Estadt, Environ. Sci. Technol. 41 (2007) 3341.
30. S. Cosnier and M. Holzinger, Chem. Soc. Rev., 40 (2011) 2146.
31. M. U. Anu Prathap, A. K. Chaurasia, S. N. Sawant and S. K. Apte, Anal. Chem. 84 (2012) 6672.
32. U. Schröder, J. Nießen, F. Scholz, Angew. Chem., Int. Ed. 2003, 42 (25), 2880
33. D. R. Lovley, Nat Rev Micro 4 (2006) 497.
34. P. K. Prabhakar, S. Raj, P.R. Anuradha, S. N. Sawant and M. Doble, Colloids Surf. B: Biointerfaces 86 (2011) 146.
35. Y. Kim, M. C. Hatzell, A. J. Hutchinson and B. E. Logan, Energy Environ. Sci., 4 (2011) 4662.
36. L. M. Tender, S. A. Gray, E. Groveman, D. A. Lowy, P. Kauffman, J. Melhado, R.C. Tyce, D. Flynn, R. Petrecca, J. Dobarro, J Power Sources 179 (2008) 571.
37. P. Cinquin, C. Gondran, F. Giroud, S. Mazabrard, A. Pellissier, F. Boucher, J.-P. Alcaraz, K. Gorgy, F. Lenouvel, S. Mathe, P. Porcu and S. Cosnier, PLoS One, 5 (2010) 10476.
38. L. Halámková, J. Halámek, V. Bocharova, A. Szczupak, L. Alfonta, E. Katz, J. Am. Chem. Soc., 134 (2012) 5040.
39. H. Sakai, T. Nakagawa, Y. Tokita, T. Hatazawa, T. Ikeda, S. Tsujimura and K. Kano, Energy Environ. Sci., 2 (2009) 133.
40. S. Cheng, H. Liu, B. E. Logan, Environ. Sci. Technol., 40 (2006) 2426.
41. B. H. Kim, I. S. Chang, G. C. Gil, H. S. Park and H. J. Kim, Biotechnol. Lett., 25 (2003) 541.

Dr Shilpa N. Sawant *joined Chemistry Division, BARC in the year 1997 through 40th batch of Training School after completing her MSc. in chemistry from Indian Institute of Technology, Bombay. Since then she has been working in the field of conducting polymer, self assembled monolayers, Langmuir–Blodgett films and electrochemical biosensors. She received her PhD from Tokyo Institute of Technology under the JSPS RONPAKU Fellowship. Her current research interest is in the field of polymer based biosensors for detection of metabolites of importance in clinical diagnostics and development of microbial fuel cells. She has presented her findings as invited talks at international conferences and has published several papers in reputed international journals.*

Mr Sugosh Prabhu *obtained his MSc degree from Fergusson College, Pune University. He is currently pursuing PhD at the Bhabha Atomic Research Centre (BARC) under the CSIR-UGC scheme. Major objective of his research work includes development of modified electrodes and membrane materials for microbial fuel cells.*

News and Forthcoming Events

International Conference in 2013

1. Electrochemistry 2013, Canary Islands (Spain) February 25-28, 2013. http://www.zingconferences.com/index.cfm?page=conference&intConferencence
2. 2nd Annual International Conference on Sustainable Energy and Environmental Sciences SEES 2013, Singapore, February 25-26, 2013, e-mail:info_at_env-energy.org, http://www.env-energy.org
3. 11th International Conference on Materials Chemistry (MC11), Coventry, U.K., July 8-11, 2013, http://www.rsc.org
4. Challenges in Chemical Renewable Energy (ISACS12), Cambridge, U.K., September 3-6, 2013, http://www.rsc.org
5. Thermodynamics 2013, Manchester, U. K., September 3-6, 2013, e-mail:mcc.reg_at_manchester.ac.uk , http://www.thermodynamics2013.org
6. 7th Euro Mediterranean Symposium on Laser Induced Breakdown Spectroscopy Bari, Italy, 16th -20th Sept. 2013.

National Conferences in 2013

1. National Conference on Nanomaterials - (NCN-2012), 3rd to 4th December 2012, Coimbatore, Tamilnadu, India. Website: http://www.karunya.edu/sh/physics/NCN-2012
2. 5th ISAEC Triennial International Conference on Advances and recent trends in Electrochemistry. Hyderabad, India, Jan. 16-20, 2013. website:http://www.iseac.org/elac2013
3. ISAEST-10 International Advances in Electrochemical Sciences and Technology, Chennai, India, Jan 28-30, 2013.
4. Nuclear and Radiochemistry, NUCAR 2013, Jabalpur, India, Feb. 19-23 2013 website:http//www.barc.gov.in/sympo/nucar2013

Achievments, Honours and Awards received by the SMC members

Name of the member & Affiliation	Name of the award/honour	Comferred by
Dr. S. N. Achary BARC, Mumbai	Science and Technology Award	Department of Atomic Energy
	Fellow- Maharashtra Academy of Sciences	Maharashtra Academy of Sciences
Dr. Niharendu Choudhury BARC, Mumbai	Fellow- Maharashtra Academy of Sciences	Maharashtra Academy of Sciences
Dr. Vinita Grover Gupta BARC, Mumbai	INS Young Scientist Award	Indian Nuclear Society
Ram Avtar Jat BARC, Mumbai	Mettler Toledo Award	Thermal Analysis Society during THERMANS-2012
Dr. S. Kannan BARC, Mumbai	Science and Technology Award	Department of Atomic Energy
Dr. R. Mittal BARC, Mumbai	Fellow- Maharashtra Academy of Sciences	Maharashtra Academy of Sciences
Dr. T. Mukherjee BARC, Mumbai	Special Contribution Award	Department of Atomic Energy
Prof. Arun Pratap M S University, Vadodara	Kishore Kumar Memorial Award	Indian Institute of Metals (Baroda Chapter)
Dr. Archana Sharma BARC, Mumbai	Science and Technology Award	Department of Atomic Energy
Dr. R. K. Vatsa BARC, Mumbai	Science and Technology Award	Department of Atomic Energy
Prof. Sandeep Verma Indian Institute of Technology, Kanpur	DAE-SRC Outstanding Investigator Award	Department of Atomic Energy

Printed by:
Ebenezer Printing House
Unit No. 5 & 11, 2nd Floor, Hind Service Industries
Veer Savarkar Marg, Shivaji Park Sea-Face, Dadar (W), Mumbai - 400 028
Tel.: 2446 2632 / 2446 3872 Tel Fax: 2444 9765 Email : eph@vsnl.com / outworkeph@gmail.com

In this issue

Feature articles

Published by

Society for Materials Chemistry

C/o. Chemistry Division Bhabha Atomic Research Centre, Trombay, Mumbai, 400 085 (India)

E-mail: socmatchem@gmail.com,

Tel: +91-22-25592001